RF cavities for ultrafast electron microscopy

Nohlmans, J.R.

Award date:
2007

RF cavities for ultrafast electron microscopy

J.R. Nohlmans

December 2007
CQT 2007-14

Supervisor:
dr. ir. O.J. Luiten

Committee:
dr. ir. M. Kemerink
dr. ing. F.B. Kiewiet
dr. ir. O.J. Luiten
ir. T.v. Oudheusden
dr. ir. L. Pel
dr. ir. E.J.D. Vredenbregt

TU/e Technische Universiteit Eindhoven University of Technology

Department of Applied Physics
Research group Coherence and Quantum Technology

Abstract

Electron microscopy is a powerful tool for many research areas in physics, chemistry and biology. Current state-of-the-art microscopes enable the study of individual atoms in samples (better than 0.1 nm spatial resolution). Research is now aimed at viewing the ultrafast motion of these atoms. This requires ultrashort electron pulses of 100 femtosecond duration.

A radio frequency (RF) cavity has been designed for use as a streak camera to measure the duration of ultrashort, 100 keV electron pulses. Analytical calculations and particle tracking simulations show it should be able to measure electron pulses with 100 femtosecond temporal resolution. In order to enable operation of the cavity with a compact 1 kW RF source the design has been optimized for low power consumption. The cavity has been manufactured by high-precision machining with better than 10 μm accuracy. Characterisation measurements show that the resonant frequency and on-axis field profile are in good agreement with the design. The cavity has been driven with 1 kW RF power without breakdown and is now ready for implementation.

In addition, other applications of RF cavities for electron microscopy have been investigated. The streak camera cavity can also be used to create ultrashort electron pulses in an existing electron microscope: by placing a small aperture behind the cavity a continuous electron beam is chopped into short pulses. Furthermore a similar RF cavity can be used as a time dependent, axially symmetric charged particle lens with negative focal length. This is not possible with the regular axially symmetric electrostatic and magnetostatic lenses and could provide a new way for correcting spherical and chromatic aberrations.

Contents

Chapter 1

Introduction

1.1 Electron microscopy

1.1.1 Spatial resolution

Microscopes allow the study of objects or details that are too small to be observed with the unaided eye. Microscopes that use visible light have a resolution limit however, since they can not resolve details with dimensions smaller than the wavelength of the light used. This means a resolution limit of approximately 0.1 μm.

To overcome this limitation electrons are used instead of light. The wavelength λ of an electron depends on its energy E as

$$\lambda \approx \frac{h}{\sqrt{2mE}} \tag{1.1}$$

for non-relativistic energies, where h is Planck's constant and m the electron mass. An electron energy commonly applied in electron microscopy is 100 keV, which yields a wavelength of 0.004 nm. Current electron microscopes are not yet near this wavelength limit in resolution, because they are limited by other aspects such as spherical and chromatic aberrations of their lenses. The state of the art in electron microscopes can achieve a resolution down to 0.05 nm [6]. This spatial resolution is enough to show individual atoms in a sample. This is the smallest dimension of interest in most applications.

1.1.2 Basics of electron microscopy

Basically two types of electron microscopes exist, the Transmission Electron Microscope (TEM) and the Scanning Electron Microscope (SEM). Only the former will be considered here. A TEM works somewhat like a slide projector, Its basic layout is shown in figure 1.1. A beam of electrons is emitted by a source. A magnetic condenser lens collimates the beam, before it passes through the object under investigation, which must be a thin sample. With an objective lens an enlarged image of the sample is projected onto a fluorescent screen or digital camera. Generally, the electron source consists of a sharp metal needle cathode and an anode. A high voltage, typically 50 - 300 kV, is applied between them to extract electrons from the needle and subsequently accelerate them towards the anode. Passing through a hole in the anode, the beam enters the microscope column. Besides the 'imaging' mode the microscope can be used in 'diffraction' mode. Diffraction measurements reveal a pattern of bright spots

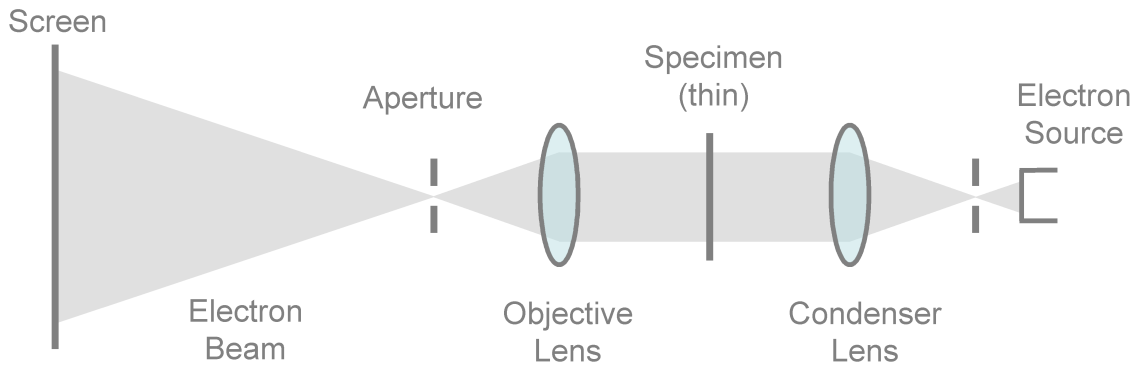

Figure 1.1: *Schematic of a Transmission Electron Microscope (TEM)*

from which properties of the sample such as lattice spacing, shape and orientation can be derived.

1.2 Ultrafast electron microscopy

1.2.1 Temporal resolution

The time needed to take a picture can be considered as a temporal resolution. For current electron microscopes this is in the order of a second. Many interesting processes however, happen much faster than this. The fastest process of interest is the motion of atoms, the ultimate goal for the temporal resolution. This timescale of atomic motion is of the order of 100 fs, $100 \cdot 10^{-15}$ s. Atoms at room temperature move about 0.1 nm in this time.

Because electronics for image capturing are not that fast, the way to study these processes is to illuminate the sample with a short pulse of electrons.

To make a film of a process in which you can see individual atoms move the following procedure can be adopted. The atomic motion in a sample is initiated by something (pump), usually an ultrashort laser pulse, in order to define the zero of time of the process. Now the process is in action a picture is taken with an electron pulse of typically 100 fs duration (probe). This pump-probe sequence is repeated many times with different probe delay times.

1.2.2 Single shot measurements

For a 1000 x 1000 pixel image about 10^8 electrons are required (100 per pixel), whereas for diffraction measurements 10^5 will suffice. To take an image in a single shot the electron bunch of 100 fs duration has to contain 10^8 electrons i.e. 10 pC, which results in a peak current of 100 A. Such electron bunches can be made by photo-emission of electrons with a fs laser pulse. Current electron microscopes however, deliver electron currents of nA to μA. This means that the electrons are separated by enough distance to neglect the repulsive Coulomb force between them. If instead a bunch with many electrons passes through the column, the electrons will interact. This deteriorates the spatial resolution. In reference [4] it is shown that at 200 keV electron energy a 1 pC bunch of 30 ns duration can give an image with about 20 nm spatial resolution. For shorter bunches the interaction between electrons will be stronger

thus decreasing spatial resolution. To get both the desired temporal and spatial resolution in a single shot, the electron microscope has to be redesigned, perhaps with implementation of radio-frequency lenses to correct aberrations.

1.2.3 Stroboscopic imaging

Even without large changes to the microscope images can be made with high spatial and temporal resolution. This is done by so-called stroboscopic imaging, which was first applied in 1977 [5]. In this imaging mode, 100 fs bunches are used which contain only one or a few electrons. To build up one image, many ($\sim 10^8$) pump-probe sequences are required with the same delay time. To produce an image within a reasonable amount of time, the sequence should be repeated with a frequency of at least a MHz, but preferably several GHz. Therefore this method is limited to processes that are rapidly repeatable, such as electronic phase transitions and gas reaction dynamics. It should be noted that the limitation to repeatable processes also applies, to some extent, to the single shot imaging. Although it allows an image to be taken in one shot, several shots are needed to study the temporal behavior of the sample under investigation.

Perhaps the most elegant method to do stroboscopic imaging is to free electrons from the electron source within 100 fs (with a fs laser pulse). This method has been used by [10] to create bunches that contain on average one electron per pulse, with which nm resolution could be achieved. However, the desired temporal and spatial resolution have not yet been reached with this method. Although it looks promising, it requires more investigation.

A more straightforward method is to operate the microscope as usual but with a relatively small extra component which interrupts the electron beam most of the time but lets pulses of 100 fs through. This way the electron beam is chopped into pulses. This method gives the freedom to choose the electron source independent from the temporal resolution requirement; the source does not have to be optimized for the laser. A continuous beam with a current of 1 μA chopped into 100 fs pulses will have on average about 1 electron per pulse.

1.3 RF cavities for ultrafast microscopy

In the work described in this thesis time-varying, radio frequency (RF) fields are employed. They are used to manipulate electrons at timescales of the order of 100 fs. Therefore GHz frequencies are used, at these frequencies the fields can be considered linear over a time span of 100 fs, since the oscillation period is of the order of 100 ps. The electromagnetic fields are contained in a resonant cavity, a hollow metal object of some shape with dimensions such that the fields are resonant inside it at the desired frequency. In the cavity the fields will oscillate harmonically. This makes it easy to synchronize the fields with electron bunches created with either a femtosecond laser pulse or an RF chopper. That means the fields can be used at one specific phase every time, which is essential for proper functioning. Besides, in a cavity a higher field strength can be obtained more easily than in some non-resonant setup. Out of the available common frequencies the S-band around 3 GHz, with a wavelength of 10 cm is chosen. This gives a cavity size of the order of this wavelength and thus a manageable size.

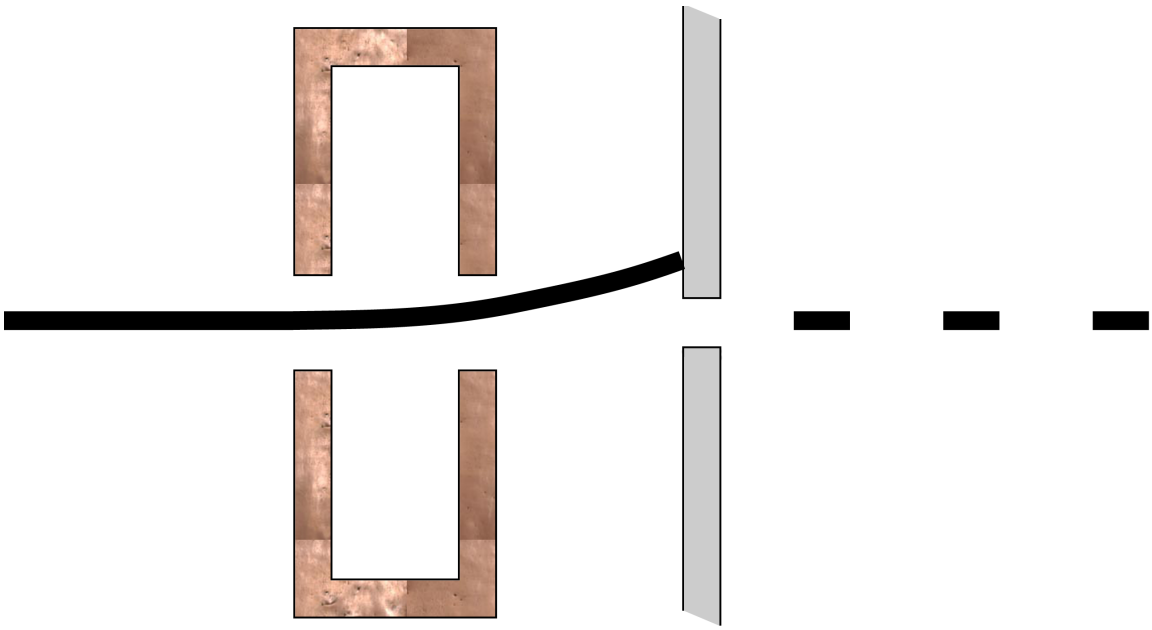

Figure 1.2: *Electron beam chopping with an aperture behind a resonant cavity.*

1.3.1 RF chopper

In this section we investigate the possibility of chopping the electron beam with a resonant cavity, which has a hole in the bottom and top surface, allowing the electrons to pass through. The electromagnetic fields form a standing wave such that on the axis along which the electrons pass, the main field component is a magnetic field perpendicular to the electron motion. The direction of motion of the electrons is defined as the z-direction. Then if we take the magnetic field direction as the y-direction, the electrons are deflected in the x-direction. The magnitude of the deflecting force depends on the phase of the field at the moment when the electron passes through. The electron beam is then chopped by a small aperture placed at some distance behind the cavity. Electrons can only pass through this aperture if they arrived in the cavity at the proper phase. This is illustrated in figure 1.2. By changing the aperture diameter, the distance from cavity to aperture or the field amplitude in the cavity, the pulse duration can be varied. The cavity described in this thesis is resonant at a frequency of 3 GHz, and pulses can be formed twice per period, so in principle $6 \cdot 10^9$ measurements per second can be done with this setup, which means that an image can be taken in 0.01 s. The sample has to be pumped at the same rate, so a laser used for this purpose needs to have this frequency as well. Furthermore the sample has to be able to recover to its original status within the 150 ps between pulses.

1.3.2 RF charged particle lenses

In both electron and light optics, the paths of the electrons or photons are often described with their first order approximation, the paraxial approximation. In this approximation, a point source is imaged by a lens into a point and a parallel beam is focussed to a point in the lens focus. A point source at a distance r from the axis is imaged to a point at a distance $M \cdot r$

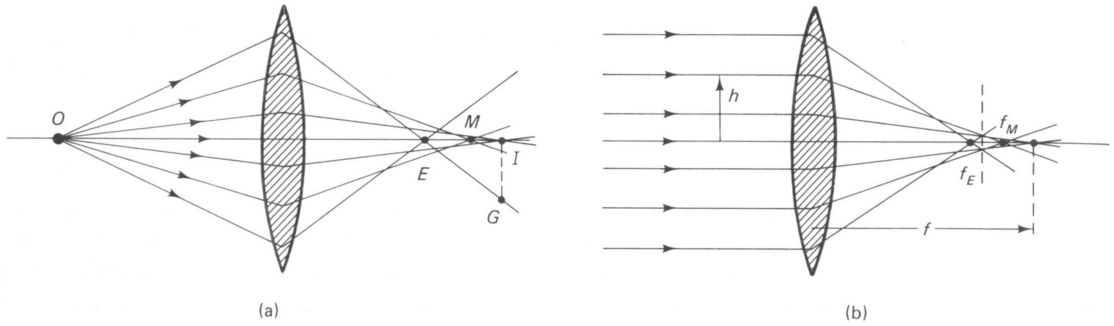

Figure 1.3: *A lens with spherical aberration.*

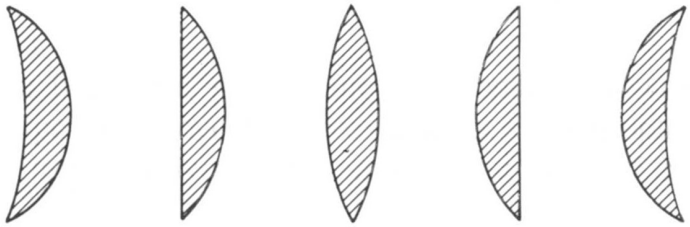

Figure 1.4: *Different lens shapes*

from the axis, with M the magnification. The image position is thus linear in r, the object position. However, to describe the paths properly higher order terms have to be taken into account. These terms are called higher order terms because the image positions depends not linearly on r but to higher orders of r. These terms are often called aberrations, because they describe the aberration from the paraxial description. The aberrations have several causes. One has to do with geometry; the sine of the angle θ of the path with the optical axis is approximated in first order by θ itself. The other cause is non-linearity of the lenses. The effect of spherical aberration is that particles farther from the axis are focussed at a different position than particles near the axis. As is illustrated in figure 1.3, this results in a spot being formed instead of a point, so that details smaller than the spot can not be imaged properly. This limits the resolution of the microscope.

Another aberration that deteriorates the resolution is chromatic aberration. This aberration is due to energy spread in an electron beam. Because faster electrons are deflected less than slower electrons, a beam with energy spread is imaged as a spot of a point. In optical microscopes most aberrations can be corrected for. One way to do this is to change the shape of the lens. Figure 1.4 shows several possible shapes for glass lenses. These lenses have the same strength and so the same focal distance, but differ in aberration. A similar effect can be reached by using different types of glass. By cleverly combining lenses a microscope can be made which has very little aberration. For optical microscopes this can be done so well that the resolution is limited more by the wavelength of the light than by aberrations.

In electron microscopes electrostatic and magnetostatic lenses are used. These lenses mostly have positive focal length and furthermore Scherzer has shown that for electrostatic and magnetostatic axially symmetric lenses aberration coefficients are always positive [12].

So whereas in optical microscopes lenses can be combined to reduce aberrations, in electron microscopes this is not possible with electrostatic and magnetostatic lenses. Other types of lenses exist to correct aberrations such as quadrupole and octupole lenses but these are very complex and have not done much to push the limit of resolution towards the wavelength of the electrons.

One type of lens not yet much explored is a high frequency lens. This lens uses an electromagnetic field which varies in time at up to GHz frequencies. The calculation done by Scherzer does not hold for time-dependent fields, so it is possible to design a lens with a negative aberration coefficient. Because the fields reverse direction every half period the lens has a positive focal length half the time and negative focal length the other half. Since the shape of the field does not change in time the aberration coefficient changes sign together with the focal length. Thus the lens has a negative aberration coefficient half the time, which can be used to correct the aberration of the static lenses in the microscope.The properties of this lens are described in more detail in section 2.4.3.

1.3.3 RF streak camera

In order to do ultrafast microscopy, one does not only need a method for producing ultrashort pulses or bunches, but also a way of measuring the bunch length and thus establish the temporal resolution. While it is a challenge to make these bunches as short as possible, it is also a challenge to measure the actual duration that has been achieved. One way to measure the bunch duration is with a streak camera. The deflecting cavity described in section 1.3.1 for beam chopping can also be used as a streak camera. Similar to a beam, an incoming bunch is deflected sideways by the rapidly varying field, in such a way that the front of the bunch is deflected more than the back, or vice versa. This gives the bunch a lateral size which depends on its original duration. This lateral size can easily be measured by impinging the bunch on a phosphor screen and measuring the streak produced by the bunch with a CCD-camera. When the deflecting force is known by properly characterizing the cavity, the original bunch duration can be calculated. This will be described thoroughly in chapter 3.

1.4 Scope

As described in this chapter, microwave cavities containing radio frequency electromagnetic fields have many interesting possible applications. Starting from a 'simple' cylinder shaped cavity, two different field modes are described in chapter 2, with their respective possible applications in electron microscopy and elsewhere. One interesting application is the use of a cavity in a streak camera setup. We have a setup at hand where a very fast streak camera would be most useful for measuring electron bunch durations from 10 fs to 10 ps. Therefore the remainder of this report is dedicated to this application. Chapter 3 investigates the influence of all input parameters on the streaking process. To operate the streaking cavity with only 1 kW of power an energy-efficient shape has been designed, which is described in chapter 4. Based on this design a cavity has been manufactured by high-precision machining. Chapter 5 describes the measurements that have been performed on this cavity to characterize it and to verify that it is in agreement with the design. Finally, conclusions are drawn in chapter 6.

Chapter 2

RF cavity theory

The fields within such a resonant cavity can be calculated using Maxwell's equations. This is derived in appendix A. Within any shape of resonant cavity several field arrangements are possible. These are called 'modes' and they each have a specific frequency at which they are resonant in the cavity. In this thesis the shape of the cavity basically is a hollow cylinder. Although the exact shape of the cavity will not simply be a cylinder, it is convenient to describe them in cylindrical coordinates (r, ϕ, z) as is depicted in figure 2.1. In such a coordinate system two types of modes can be distinguished. The Transverse Magnetic (TM) modes have only transverse magnetic fields, so no magnetic field component in the z-direction. The electric fields can then have any direction. The Transverse Electric (TE) modes have only transverse electric field, so no electric field component in the z-direction. The magnetic fields can then have any direction.

The different modes are distinguished by an index added to the mode type. In this chapter two modes will be described. Firstly the TM_{010} mode in section 2.1 and secondly the TM_{110} mode in section 2.2. In section 2.3 the effects of energy losses will be considered, which is the same for both modes. Next, some possible applications of the TM_{010} mode will be described in section 2.4: acceleration, bunch compression and focusing. The application of the TM_{110} mode as an electron beam chopper will be described in section 2.5 and chapter 3 will be fully devoted to the application as a streak camera.

2.1 The TM_{010} mode

The TM_{010} mode is the lowest TM-mode. The fields of this mode will be described below for a cylinder-shaped cavity or 'pillbox-cavity' with length d and radius R as depicted in figure 2.2. The derivation can be found in appendix A.

By definition of a TM-mode, $B_z = 0$. For perfectly conducting material E must be perpendicular to the wall, so that for $r = R$, $E_z = 0$. With this boundary condition and considering the mode index, E_z becomes

$$E_z = E_0 J_0(kr) \cos \omega t \tag{2.1}$$

Where E_0 is the field amplitude, J_0 is the zeroth order Bessel function of the first kind, ω is the angular frequency of the mode and k is the corresponding wave number, according $k = \frac{\omega}{c}$ with c the speed of light. Because for $r = R$ the electric field has to be zero, the argument kR

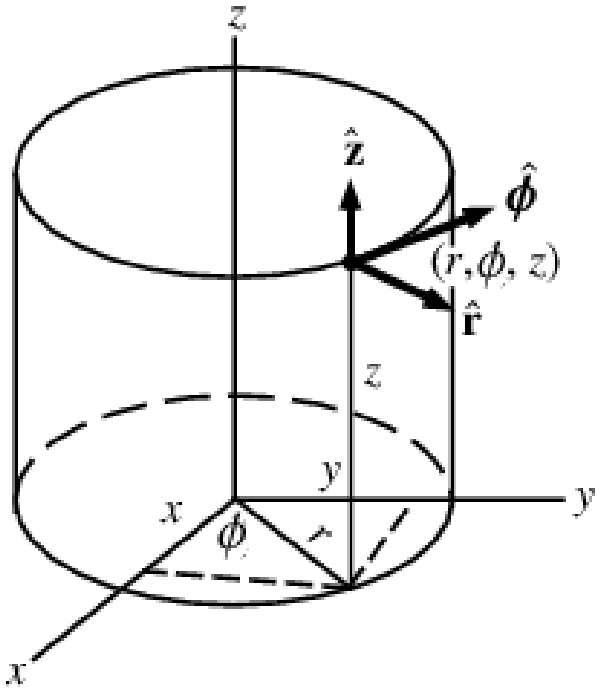

Figure 2.1: *Cylinder coordinate system.*

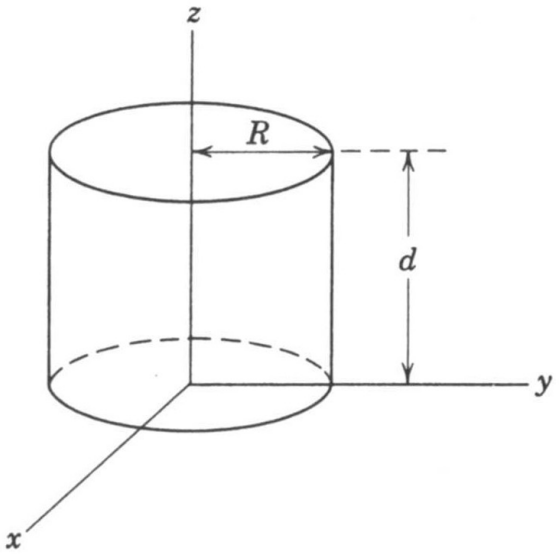

Figure 2.2: *Pillbox cavity dimensions.*

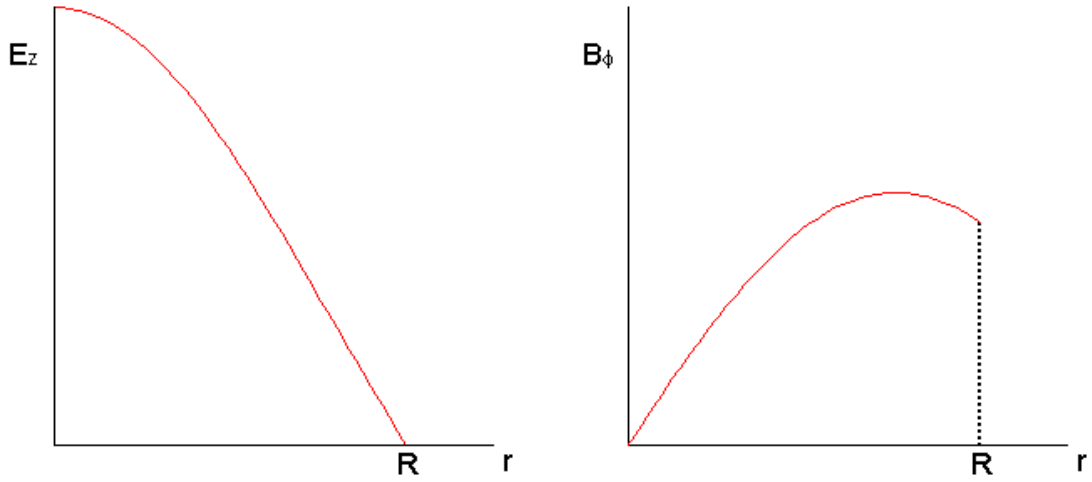

Figure 2.3: *The field amplitude as a function of radius for the electric field (left) and the magnetic field (right) of the TM_{010} mode.*

has to be equal to the first node of the Bessel function, $kR = 2.405$. For an applied frequency of 2.9985 GHz the required radius R is 38 mm. With E_z known the other field components in the cavity can be calculated which results in

$$B_\phi = -\frac{1}{c} E_0 J_1(kr) \sin \omega t \tag{2.2}$$

All other components, B_r, E_ϕ, E_r are 0 for this mode. Figure 2.3 shows E_z and B_ϕ as a function of the radius, figure 2.4 shows E_z in a plane of the cavity and a vector representation of B_ϕ.

We want to use the cavity fields to manipulate the trajectories of accelerated electrons. Therefore two small holes have to be made in the cylinder at the center of the top and bottom surface to let the electrons enter and exit. This will off course alter the fields in the cavity, but for now this will be neglected.

2.2 The TM_{110} mode

Another field mode that has been applied in this research is the TM_{110} mode. The "110" means that the longitudinal electric field E_z has one node in the ϕ-direction, one in the radial or r-direction viz. at the wall and no node in the z-direction, implying the field is constant in that direction. The electric field is then

$$E_z = E_0 J_1(kr) \cos(\phi) \cos(\omega t) \tag{2.3}$$

Where $J_1(x)$ is the first order Bessel function. For r equal to the cylinder radius R the field has to be zero, so $kR = 3.832$, the first node of $J_1(x)$. This yields $R = 61$ mm for a

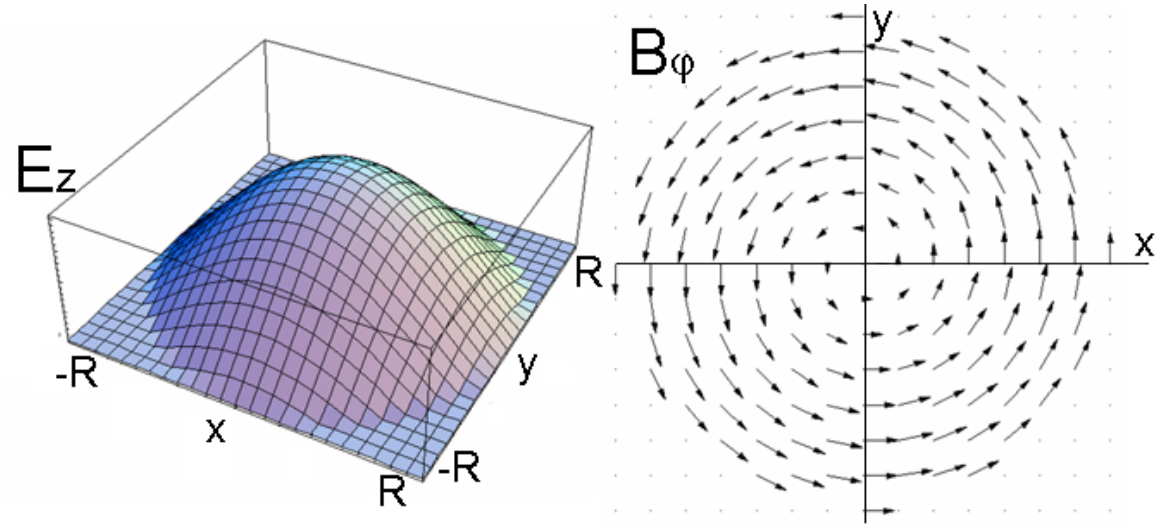

Figure 2.4: *Field distribution of a TM_{010} mode. The electric field magnitude in a plane with constant z is plotted on the left. The magnetic field is plotted as vectors in a plane (right). For different values of z the fields are the same.*

frequency of 2.9985 GHz. The other field components in the pillbox-cavity are

$$B_r = \frac{E_0}{\omega}\frac{1}{r}J_1(kr)\sin(\phi)\sin(\omega t) \tag{2.4}$$

$$B_\phi = \frac{E_0}{\omega}\frac{\partial}{\partial r}J_1(kr)\cos(\phi)\sin(\omega t) \tag{2.5}$$

The electric and magnetic fields are depicted in figure 2.5 and 2.6. Two small holes in the center of the top and bottom surface allow electrons to pass through the cavity. At the center of the cavity the electric field is almost zero while the magnetic field is large. For small radius it is convenient to describe the magnetic field in cartesian coordinates.

$$B_x = B_r\cos\phi - B_\phi\sin\phi \tag{2.6}$$

$$B_y = B_r\sin\phi + B_\phi\cos\phi \tag{2.7}$$

For $r = \sqrt{x^2+y^2} \ll R$, $\frac{1}{r}J_1(kr)$ and $\frac{\partial}{\partial r}J_1(kr)$ are approximately $\frac{k}{2}$. Therefore on the z-axis

$$B_x = 0 \tag{2.8}$$

$$B_y = \frac{E_0}{2c}\sin\omega t \tag{2.9}$$

The magnetic field in the (arbitrarily defined) y-direction working on electrons moving in the z-direction results in a deflection in the x-direction.

2.3 Energy dissipation

In the derivation of the fields it has been assumed that the cavity walls are perfect conductors. In practice, materials are used with a high but finite conductivity. The fields will therefore extend a bit into the walls and induce electric currents in the wall which cause energy dissipation.

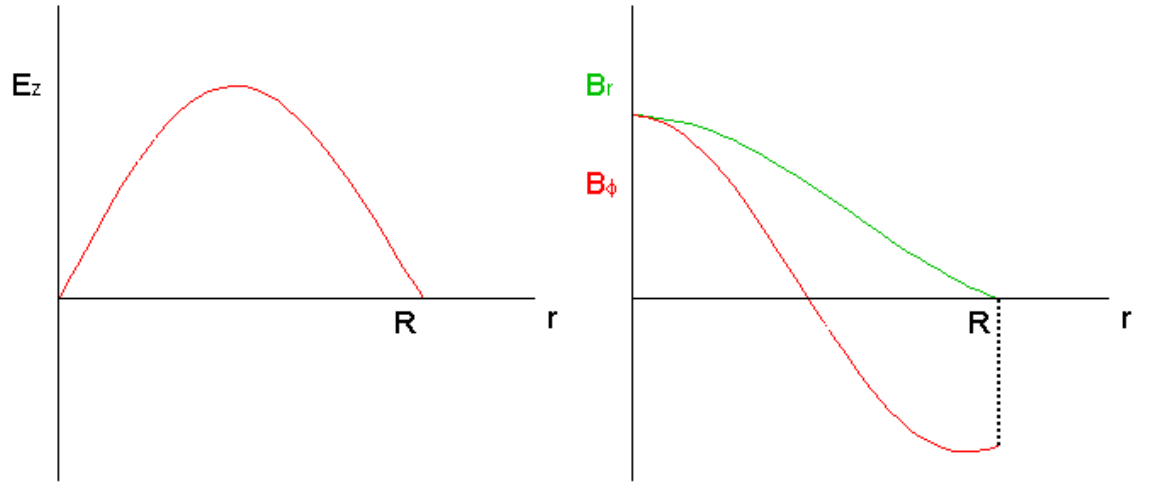

Figure 2.5: *The field amplitude as a function of radius for the electric field (left) and the magnetic field (right) of the* TM_{110} *mode.*

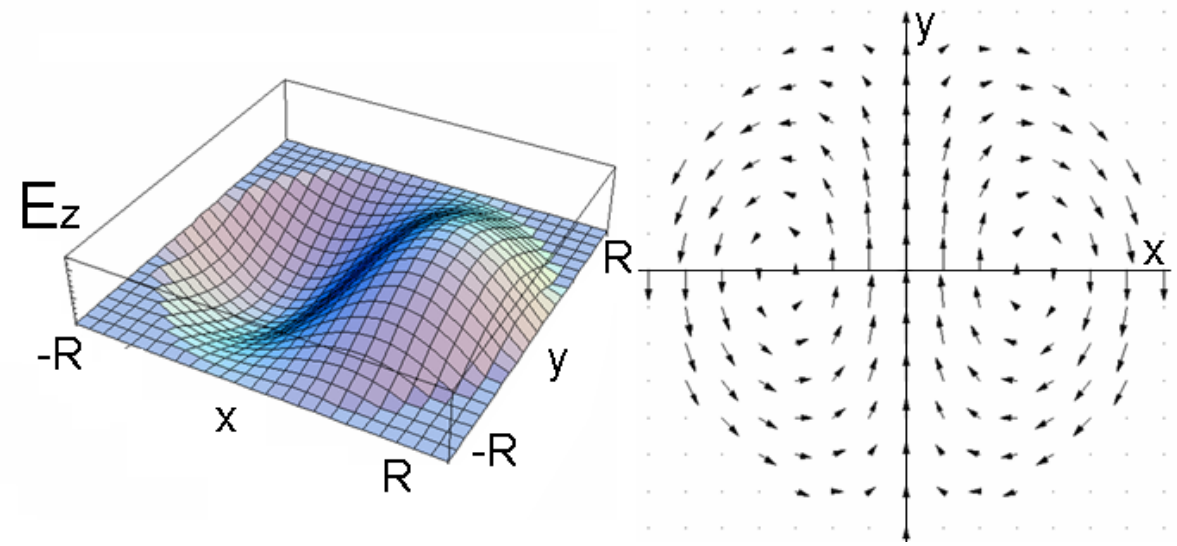

Figure 2.6: *Field distribution of a* TM_{110} *mode. The electric field magnitude in a plane with constant* z *is plotted on the left. The magnetic field is plotted as vectors in a plane (right). For different values of* z *the fields are the same.*

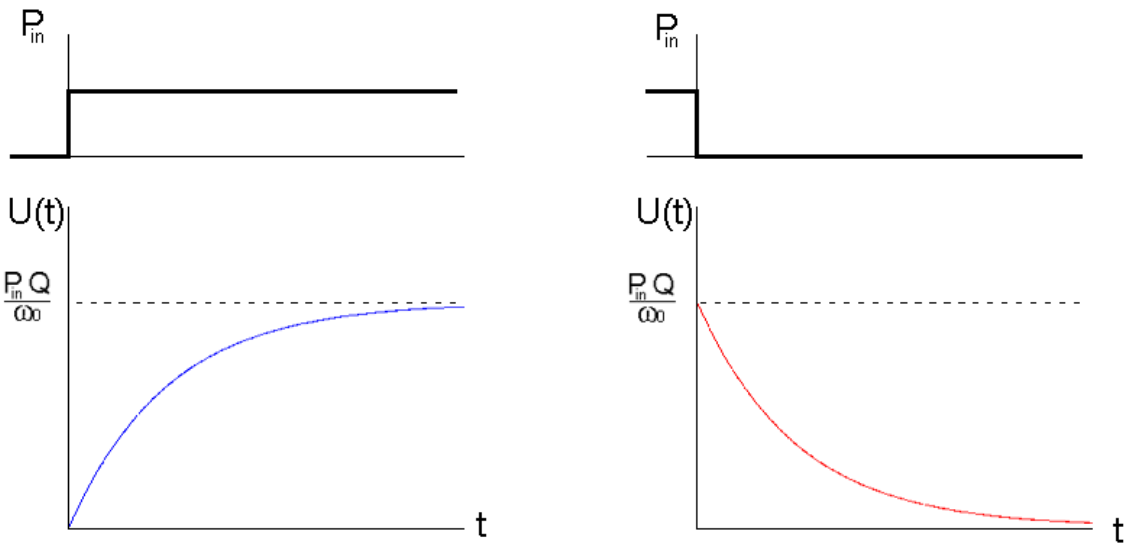

Figure 2.7: *Field energy as a function of time when external power source P_{in} is switched on at $t = 0$ (a) or switched off (b).*

A measure of the dissipation in the cavity is the quality factor Q defined as

$$Q = \omega_0 \frac{U}{P_{loss}} \tag{2.10}$$

Where ω_0 is the original resonance frequency, U is the energy stored in the cavity and P_{loss} the power dissipated in the cavity walls. If there is a power input P_{in} for $t > 0$ the energy change at any given time is

$$\frac{dU}{dt} = P_{in} - P_{loss} = P_{in} - \frac{\omega_0}{Q} U \tag{2.11}$$

Solving this differential equation gives the energy as a function of time

$$U(t) = P_{in} \frac{Q}{\omega_0} \left[1 - e^{-\omega_0 t/Q}\right] \tag{2.12}$$

Assuming there is no energy in the cavity at $t = 0$. As shown in figure 2.7a, U rapidly grows to a steady-state value of $P_{in}Q/\omega_0$. Now if we consider the decay of the field if P_{in} is switched to zero at $t = 0$ we find

$$U(t) = P_{in} \frac{Q}{\omega_0} e^{-\omega_0 t/Q} \tag{2.13}$$

which is sketched in figure 2.7b. Since

$$U(t) = \frac{1}{2} \epsilon_0 \left|E(t)\right|^2 \tag{2.14}$$

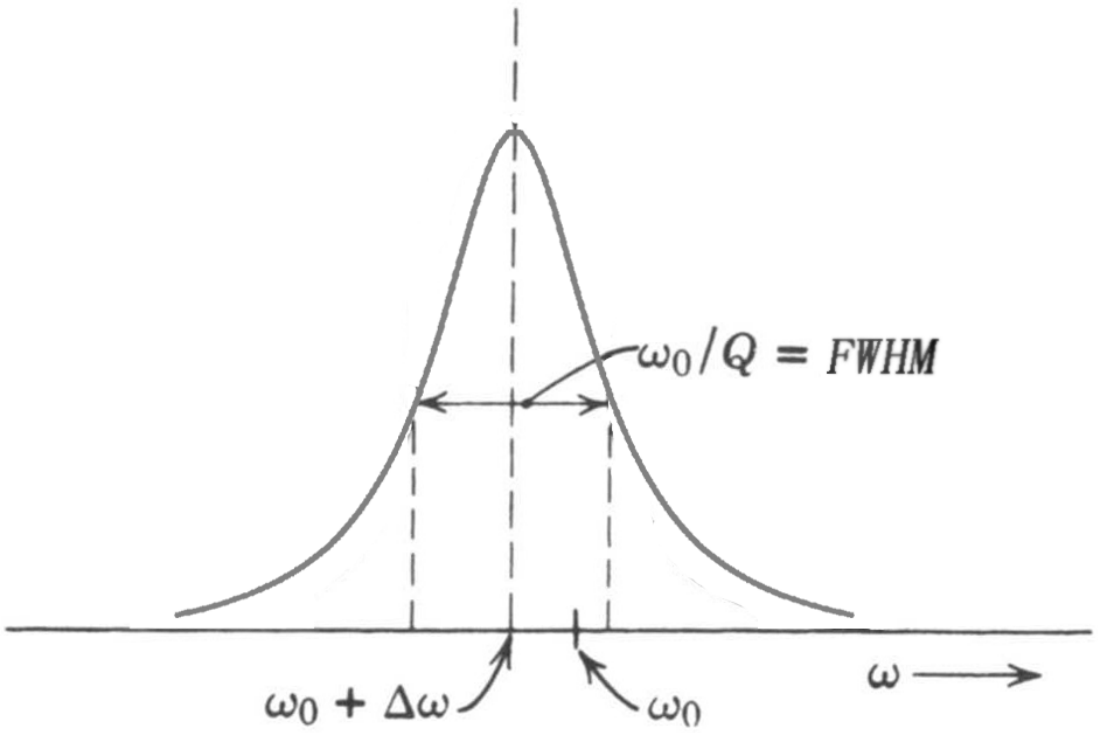

Figure 2.8: *Energy absorption follows a Lorentz curve around the resonance frequency* $\omega_0 + \Delta\omega$.

we can conclude that $E(t)$ behaves similar to $U(t)$. Off course $E(t)$ oscillates in time so that it becomes

$$E(t) = \sqrt{\frac{2P_{in}Q}{\epsilon_0\omega_0}} e^{-i\omega_0 t} e^{-\omega_0 t/2Q} \tag{2.15}$$

To find the frequency dependence of the fields in the cavity we take the Fourier transform of equation (2.15) which gives

$$\widetilde{E}(\omega) = \sqrt{\frac{P_{in}Q}{\pi\epsilon_0\omega_0}} \frac{1}{i(\omega - \omega_0) - \frac{\omega_0}{2Q}} \tag{2.16}$$

Then using equation (2.14) we find that the frequency dependence of the energy follows a Lorentz curve

$$\widetilde{U}(\omega) = \frac{P_{in}Q}{2\pi\omega_0} \frac{1}{(\omega - \omega_0)^2 + \left(\frac{\omega_0}{2Q}\right)^2} \tag{2.17}$$

This is shown in figure 2.8. The full width at half maximum (FWHM) of the Lorentz curve is equal to ω_0/Q. When power is applied to the cavity, the absorption of energy as a function of frequency will follow this curve. This can be used to determine Q of the cavity.

As a rule of thumb, Q is approximately equal to the ratio of the volume V of the pillbox to the volume of a thin shell of thickness $\delta/2$ surrounding this volume, $Q \approx 2V/\delta A$, where A is the surface area of the pillbox and δ the skin depth of the electromagnetic field inside the pillbox [11].

$$\delta = \sqrt{\frac{2}{\mu\omega_0\sigma}}, \tag{2.18}$$

where μ is the permeability and σ the conductivity of the wall material. Taking copper as wall material, with $\sigma = 5.8 \cdot 10^7\ \Omega^{-1}\mathrm{m}^{-1}$ and $\mu = 1.3 \cdot 10^{-6}$ H/m, the skin depth becomes 1.2 μm at 3 GHz. Assuming a cylindrically shaped cavity, $V/A \approx d/2$ for $R \gg d$ so that a cavity length $d \approx 10$ mm yields $Q \approx 10^4$.

Because the fields extend into the walls, the boundary conditions have changed, which will cause a shift $\Delta\omega$ in resonant frequency. As described in [8, p. 374] this shift can be calculated using the technique of perturbation of boundary conditions, which yields

$$\Delta\omega \approx -\frac{\omega_0}{2Q} \tag{2.19}$$

We intend to use a frequency of 3.00 GHz and a Q of the order of 10^4. Then the frequency shift is -0.15 MHz.

2.4 Applications of the TM_{010} mode

In this section three possible applications of the TM_{010} mode will be described. Firstly it can be used for accelerating electrons, secondly for electron bunch compression and thirdly as an electron lens.

2.4.1 Acceleration

Since the TM_{010} mode has an electric field component in the z-direction, it is commonly used for accelerating electrons. It is even possible to couple several cavities such that the electrons are accelerated all the way through. These cavities can have electric fields strengths of up to 100 MV/m [9].

2.4.2 Longitudinal focusing

The longitudinal electric field E_z accelerates or decelerates electrons. To a group or 'bunch' of electrons it imparts an energy spread. If a bunch of electrons passes through the cavity within a half period of the field variation, thus within 160 ps for the 3 GHz field, then the electric field can be used to shorten the bunch duration. If the entrance phase of the bunch is right then the first electrons are effectively slowed down during their passage through the cavity while the last electrons are accelerated. Consequently the last electrons will start catching up with the first so that the electron bunch becomes shorter. This extra-short electron bunch can then be used to do many interesting experiments. Since the energy difference applied by the cavity is much smaller than the forward kinetic energy, relatively small fields will suffice. For an electron energy of 100 keV a field strength of 5 MV/m suffices to focus a bunch of a few picoseconds duration to some tens of femtoseconds [7].

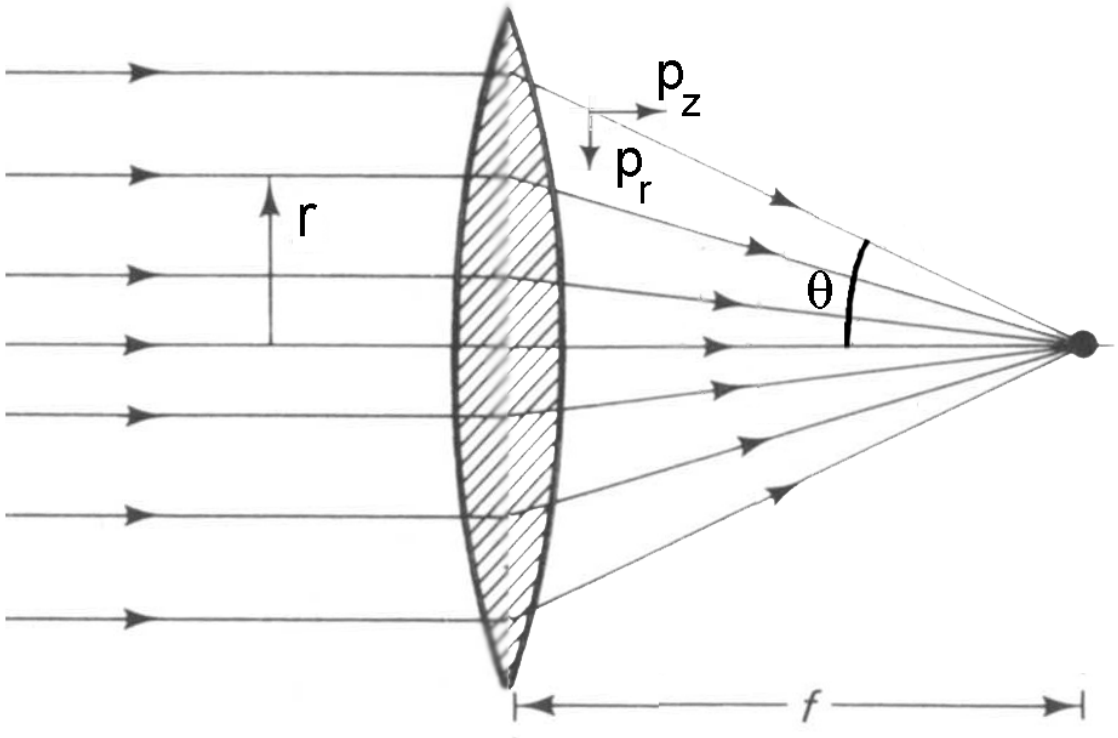

Figure 2.9: *Electron beam focusing.*

2.4.3 Transverse focusing

With a TM_{010}-mode field it is also possible to focus an electron beam or a bunch in the transverse direction. Figure 2.9 shows this kind of focusing with the relevant parameters, where f is the focal distance of the lens, θ the angle of deflection from the z-axis and r the distance from the axis. The momentum of the electron in the forward direction is p_z, the momentum in radial direction is p_r. The tangent of θ is equal to

$$\tan\theta = \frac{r}{f} = \frac{p_r}{p_z} \tag{2.20}$$

To calculate p_r we need to integrate the radial component of the Lorentz force F_L over the cavity.

$$p_r = \int F_L dt = \int -e\left(E_r - v_z B_\phi\right) dt \tag{2.21}$$

In the pillbox field description of section 2.1 we found a description of B_ϕ and found E_r to be zero. However, as a result of the holes which are inevitable to let electrons enter the cavity, a z-derivative of E_z is introduced, which results in a radial component E_r. $E_z(0,0,z)$, will look something like figure 2.10. In appendix B the fields are derived for the most general distribution, where they are written as a series expansion in r. Taking only the first term of the expansion, the linear part, we find

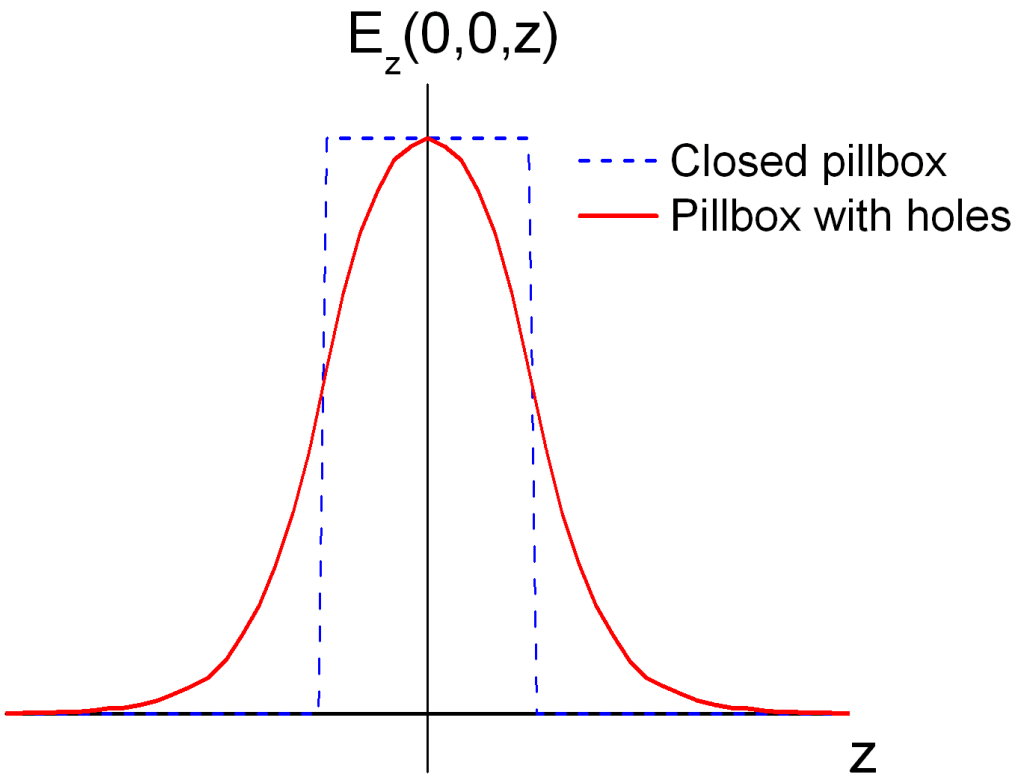

Figure 2.10: *The electric field component E_z along the z-axis for a pillbox cavity with holes and one without holes.*

$$E_r = -\frac{1}{2}\frac{\partial E_z(z)}{\partial z} r\cos(\omega t + \phi_0) \tag{2.22}$$

$$B_\phi = -\frac{\omega}{2c^2} E_z(z) r \sin(\omega t + \phi_0) \tag{2.23}$$

Where $E_z(z) \equiv E_z(0,0,z)$ is the electric field on the z-axis and ϕ_0 is the phase at $t = 0$. With this we can calculate p_r using equation (2.21) and assuming that r and v_z are constant. Furthermore we use $t = z/v_z$ and with $v_r \ll v_z$ we write $\gamma = \sqrt{\frac{1}{1-\beta^2}}$, the Lorentz factor, with $\beta = v_z/c$. Then we find, after partial integration

$$p_r = \frac{erv_z}{2\gamma^2\beta^2c^2} \int_{-\infty}^{\infty} \frac{\partial E_z(z)}{\partial z} \cos\left(\frac{\omega z}{v_z} + \phi_0\right) dz \tag{2.24}$$

If we assume the cavity to be thin, i.e. the electrons pass through in a time much shorter than the period of the field, we can use $\frac{\omega z}{v_z} \ll 1$, which gives

$$\begin{aligned} p_r &= \frac{erv_z}{2\gamma^2\beta^2c^2} \int_{-\infty}^{\infty} \frac{\partial E_z(z)}{\partial z} \left[\cos\left(\frac{\omega z}{v_z}\right)\cos(\phi_0) - \sin\left(\frac{\omega z}{v_z}\right)\sin(\phi_0)\right] dz \\ &= \frac{erv_z}{2\gamma^2\beta^2c^2} \int_{-\infty}^{\infty} \frac{\partial E_z(z)}{\partial z} \left[\cos(\phi_0) - \frac{\omega z}{v_z}\sin(\phi_0)\right] dz \\ &= \frac{er\omega}{2\gamma^2\beta^2c^2} \sin(\phi_0) \int_{-\infty}^{\infty} E_z(z) dz \end{aligned} \tag{2.25}$$

With this we can calculate the focal distance of the TM_{010} cavity using equation (2.20).

$$f = \frac{2m\gamma^3\beta^3c^3}{e\omega\sin(\phi_0)} \cdot \frac{1}{\int_{-\infty}^{\infty} E_z(z)dz} \tag{2.26}$$

A Copper pillbox resonant at 3 GHz with length $d = 6$ mm and field amplitude $E_0 = 5$ MV/m requires 4 kW input power and has a focal distance of 15 cm at $\phi_0 = 0$. With a good cavity design the power consumption can be reduced to 0.3 kW, while keeping the same focal distance [7].

The description above is linear in r. For an accurate description higher order terms have to be taken into account, such as the spherical aberration. Besides that, chromatic aberration has to be taken into account, which is an aberration resulting from a spread in velocity of the electrons.

To use the cavity as a lens the electrons have to arrive at the right phase in the cavity. This requires the use of short bunches of electrons, i.e. much shorter than the field period of 300 ps. Any finite bunchlength will however result in a 'phase'-aberration, a focusing error as a result of the difference in arrival phase.

The major advantage of using this RF field as a lens is that it can act both as a positive and a negative lens. Because of that its spherical aberration van be used to correct the spherical aberration of commonly used magnetostatic lenses. This correction probably requires strong focusing and thus large input power, which could become problematic. Alternatively, perhaps the aberration of the RF lens can be increased by changing the cavity shape to enable aberration correction at lower field strength.

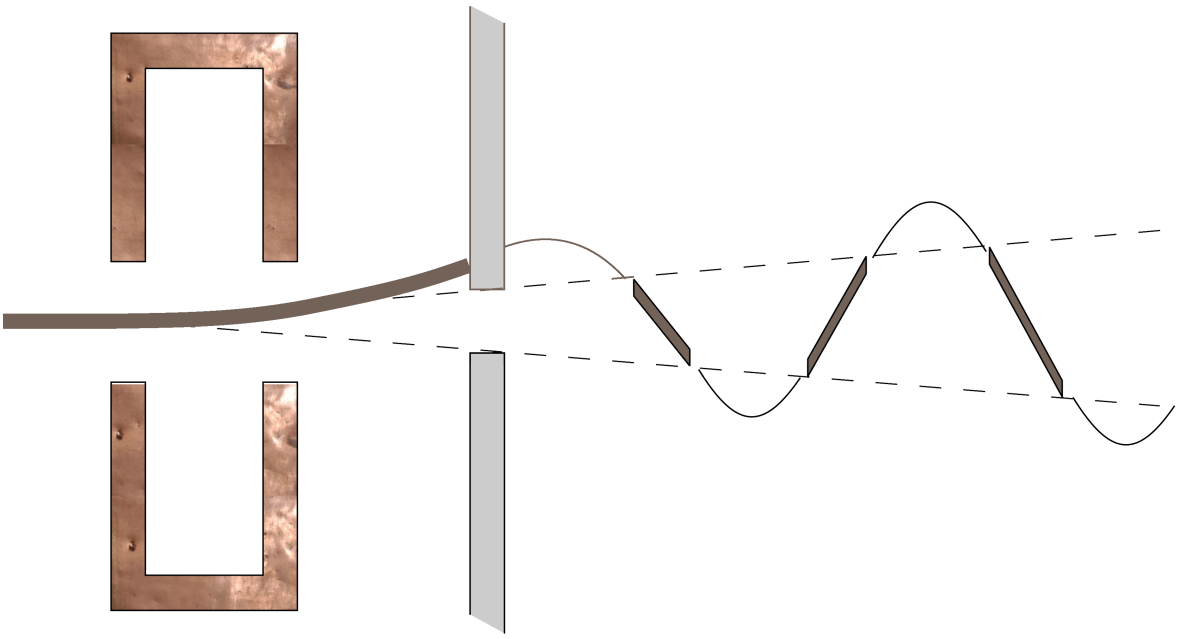

Figure 2.11: *Electron beam chopping with an aperture behind a resonant cavity.*

2.5 Applications of the TM_{110} mode

In this section one possible application of the TM_{110} mode is described. As was mentioned at the end of section 2.2 the cavity deflects an electron beam or bunch sideways. This can be used to chop the electron beam in an electron microscope into short bunches. Furthermore it can be used in a streak camera for measuring ultrashort bunch durations, which will be described in chapter 3.

2.5.1 Electron beam chopping

Electrons pass through the cavity in the z-direction with speed v_z. They experience a magnetic field in the y-direction.

$$B_y = B_0 \sin(\omega t + \phi_0) \tag{2.27}$$

This results in a momentum in x-direction p_x of

$$p_x \sim v_z B_0 \sin(\omega t + \phi_0) \tag{2.28}$$

If now an aperture is placed behind the cavity at some distance z, then only those electrons can pass through that did not get too much transverse momentum. This setup is drawn schematically in figure 2.11

The exact formulas will be given in the next chapters, but the result is that an aperture with diameter $a = 25\mu$m at a distance $z = 0.1$ m combined with $B_0 = 8 \cdot 10^{-3}$ T gives electron bunches of duration $t_b = 100$ fs. This field requires 3.1 kW RF power when using a pillbox-shaped cavity, but this can be reduced by using an energy-efficient shape as described

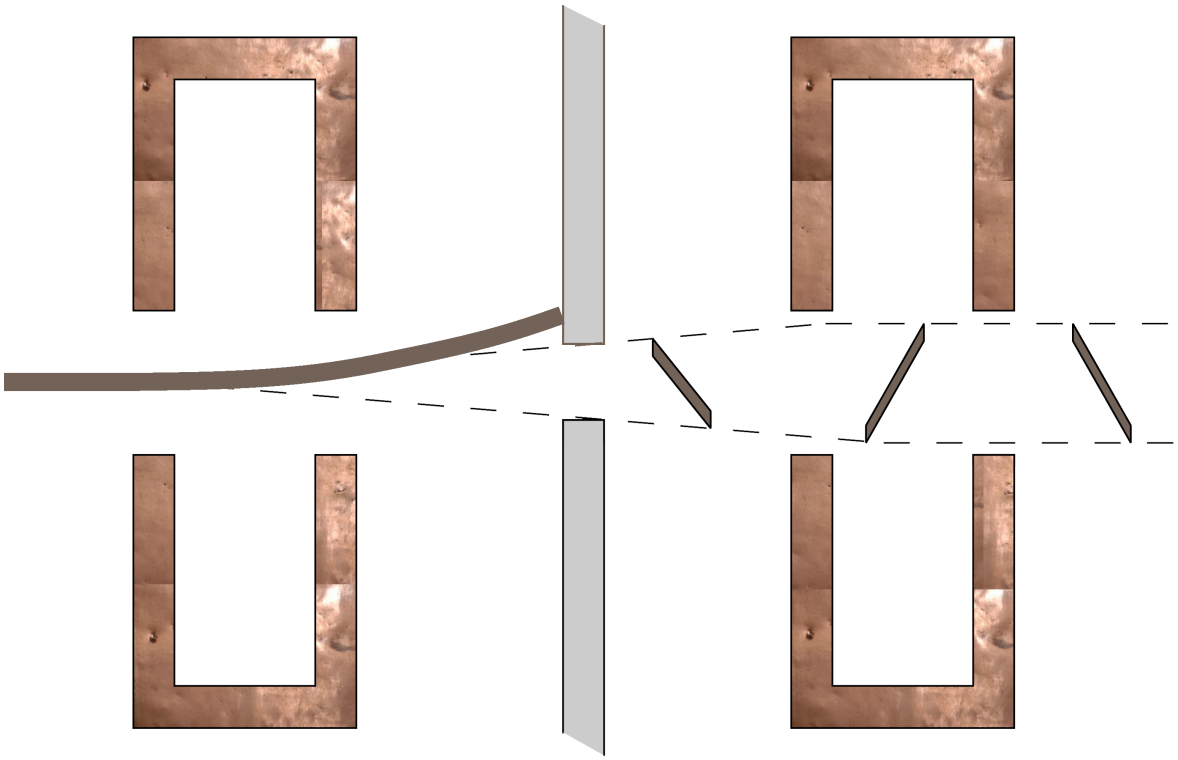

Figure 2.12: *Electron beam chopping produces a distorted electron puls, which can be corrected with a second cavity.*

in chapter 4. The bunch duration scales as

$$t_b \sim \frac{a}{zB_0} \tag{2.29}$$

The electrons that experience no net force go straight on along the axis and pass through the aperture. Electrons that arrive a bit earlier or later will get a small upward or downward momentum yet still be able to pass through the aperture. This produces a distorted puls, as illustrated in figure 2.11.

Putting a second cavity behind the aperture will stop the lateral expansion induced by the first cavity if the electrons arrive at this cavity when the field is in the opposite direction of the first cavity, as depicted in figure 2.12. This suffices if the chopping takes place at the top of the microscope. The resulting pulse will pass through the column and sample and create an image on the detector.

If the chopping is done at the bottom of the microscope it is essential that electrons that passed through a certain spot of the sample also arrive on one spot of the detector i.e. a horizontal line of the pulse at the left of figure 2.13 must be returned to a horizontal line at the right side. This requires a setup with three cavities where the second cavity (with a field twice as large as the others and in the opposite direction) reverses the transverse motion caused by the first and the third stops the transverse motion as all electrons are back in position. This is illustrated in figure 2.13.

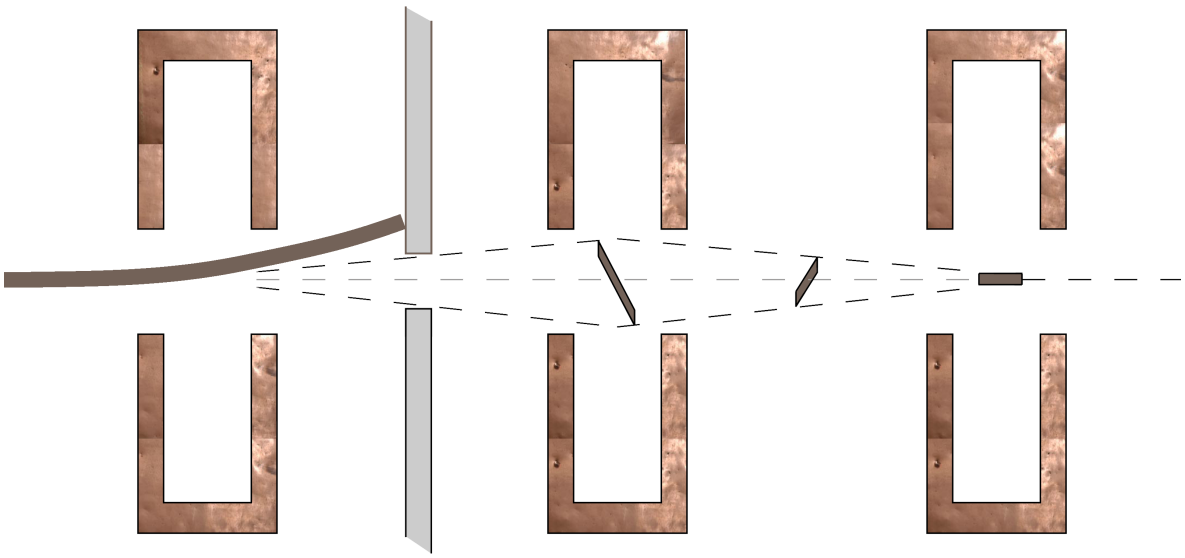

Figure 2.13: *Electron beam chopping produces a distorted electron puls. A second deflecting cavity reverses the transverse motion of the electrons and a third cavity stops the transverse motion as the electrons are back in their original position.*

Chapter 3

Streak camera

A streak camera is a common tool for measuring electron bunch durations. The principle of operation is quite simple. An electron bunch moves through a variable electric or magnetic field. While the bunch moves through the field, the field strength is increased (or decreased), for example linearly as shown in figure 3.1. The field is in a direction transverse to the motion of the electrons, so the electrons become deflected sideways. The angle of deflection of the electrons is proportional to the time integral of the field, which is the area under the graph in figure 3.1. The electrons at the front of the bunch arrive at $t = 0$ and leave the field after a transition time t_{tr}. The electrons at the back of the bunch arrive in the field region at $t = t_b$, where t_b is the bunch duration and have the same transition time t_{tr}. As can be seen from the graph, the front electrons become deflected less then the back electrons. If after some drift space the electrons are captured on a screen, then the front and back electrons will arrive on a different spot, as illustrated in figure 3.2. This way the bunch forms a line on the screen, a "streak". From the length of the line the original bunch duration can be calculated when the field properties are known.

In this chapter the variable field will be the time dependent magnetic field in the TM_{110} pillbox-cavity described in section 2.2. In section 3.1 the ideal streak will be described, i.e. the streak of a mono energetic bunch of zero transverse size and zero angular spread. In the remaining sections deviations from this ideal streak will be considered. In section 3.2 deviations caused by energy spread are described, in section 3.3 those caused by the finite dimension of the bunch. The effects due to finite angular spread are described in section 3.4. Next, all these calculations are compared with simulations in section 3.5 and finally all results are summarized in section 3.6.

In this chapter electron energies are assumed to be 100 keV, which is typical for many electron microscopes and our setup. For this energy the Lorentz factor is

$$\gamma = \left(1 - \frac{v^2}{c^2}\right)^{-1/2} = 1.20 \tag{3.1}$$

The calculations have been done non-relativistically, which therefore results in an error of approximately 20%. In order to compare the calculations with the simulations, which are done relativistically, the relevant relativistic calculation results are given in appendix C.

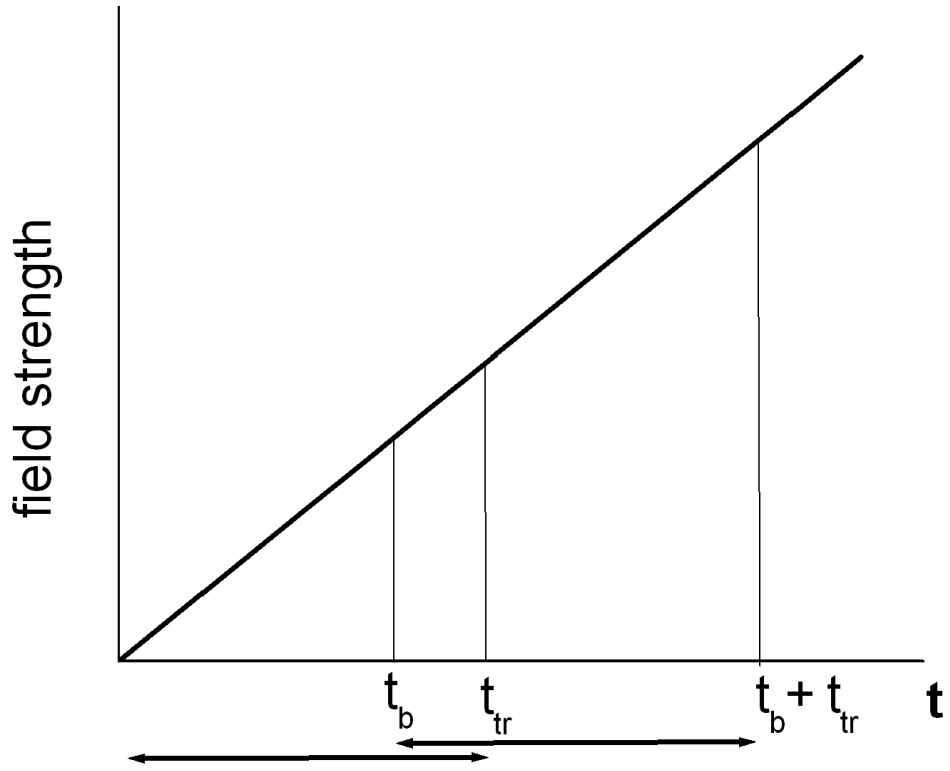

Figure 3.1: *A linearly increasing transverse field can be used for streaking an electron bunch. The back electrons, which arrive at $t = t_b$ are deflected more than the front electrons which arrive at $t = 0$.*

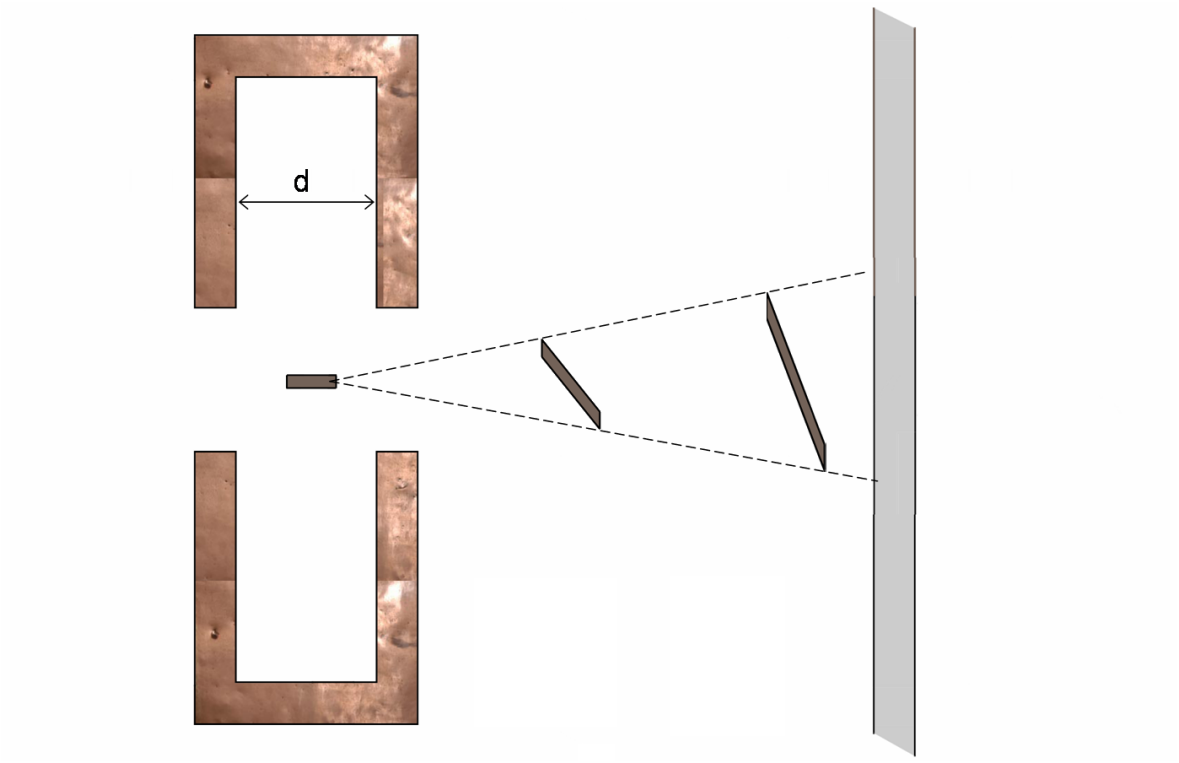

Figure 3.2: *A cavity can be used to streak an electron bunch.*

3.1 Ideal streak

Electrons moving along the z-axis or at a small distance $r \ll R$ from the axis, will experience a field as was given by equation (2.9)

$$B_y = B_0 sin(\omega t + \phi_0) \tag{3.2}$$

Here B_0 is the amplitude of the magnetic field in the cavity, which is equal to $\frac{E_0}{2c}$. When evaluating equations in this chapter we will assume a value of $E_0 = 10$ MV/m. Then $B_0 = 16.7 \cdot 10^{-3}$ T = 16.7 mT. The phase of the field at t=0 is ϕ_0. Now we calculate the angle of deflection of an electron after passing through the cavity. We assume its velocity v_z to be constant and its distance r from the z-axis to remain small inside the cavity. Then we find by integrating the force exerted by the magnetic field on the electron that

$$\theta = \frac{p_x}{p_z} = \frac{2eB_0}{m\omega} \sin(\omega t_c + \phi_0) \sin(\frac{1}{2}\omega t_{tr}) \tag{3.3}$$

where t_c is the time at which the electron is in the center of the cavity and t_{tr} is the transition time. When a bunch with duration t_b is deflected the difference in deflection angle between the first ($t_c = t_0 - \frac{1}{2}t_b$) and the last ($t_c = t_0 + \frac{1}{2}t_b$) electron is

$$\begin{aligned} \Delta\theta = \theta_l - \theta_f &= \frac{2eB_0}{m\omega} \left[\sin\omega(t_0 + \frac{1}{2}t_b) - \sin\omega(t_0 - \frac{1}{2}t_b) \right] \sin\frac{1}{2}\omega t_{tr} \\ &= \frac{4eB_0}{m\omega} \sin(\omega\frac{1}{2}t_b) \cos(\omega t_0 + \phi_0) \sin(\frac{1}{2}\omega t_{tr}) \end{aligned} \tag{3.4}$$

assuming t_{tr} is the same for all electrons and t_0 is the time when the center of the bunch is at the center of the cavity. To maximize $\Delta\theta$ the phase of the field ϕ_0 should be adjusted until $\omega t_0 + \phi_0 = 0$, so that the cosine term in equation (3.4) equals 1. Then t_0 is a zero-crossing of B_y. The transit time of the electrons is determined by their velocity and the interaction length d of the cavity.

$$t_{tr} = \frac{d}{v_z} \tag{3.5}$$

To maximize the second sine term in equation (3.4) ωt_{tr} should be taken equal to π. At an electron energy of 100 keV and a cavity resonant frequency of 2.9985 GHz this gives an interaction length of d=27 mm. For this optimization ωt_{tr} could be chosen equal to 3π as well, but this will not increase $\Delta\theta$ and only introduce more disturbance of the electron bunch. With these optimizations we find for values of t_b smaller than 10 ps so that we can write $\sin(\frac{1}{2}\omega t_b) \approx \frac{1}{2}\omega t_b$ and for B_0=16.7 mT

$$\Delta\theta \approx \frac{2eB_0 t_b}{m} \tag{3.6}$$

To measure the streak length we will use a CCD camera with a pixel size of the order of 10 μm. Thus if the camera is put at a distance of 100 mm from the cavity, a 20 fs streak can be resolved. The camera can be put farther away to resolve even shorter streak lengths, but in practice the resolution will be limited by other factors, which will be described in the next sections.

3.2 Energy spread

In the previous section t_{tr} was assumed to be the same for all electrons. However, any real bunch of electrons will have energy spread and thus velocity spread, so that the transit time differs between electrons. The momenta of the electrons will vary around the average as

$$p_z = p_{z_0} + \delta p, \tag{3.7}$$

where p_{z_0} is the electron momentum at 100 keV energy. Typical energy spread is of the order of 1%, so δp will typically be 0.5 % of p_{z_0}. The angle of deflection now becomes

$$\begin{aligned} \theta &= \frac{2eB_0}{m\omega} \sin(\omega t_c + \phi_0) \sin\left(\frac{1}{2}\omega t_{tr_0} \frac{p_{z_0}}{p_z}\right) \\ &\approx \frac{2eB_0}{m\omega} \sin(\omega t_c + \phi_0) \left[1 - \frac{1}{2}\left(\frac{\pi}{2}\frac{\delta p}{p_{z_0}}\right)^2\right], \end{aligned} \tag{3.8}$$

where t_{tr_0} is the transit time at 100 keV energy. In the last step $\frac{\delta p}{p_{z_0}} \ll 1$ is assumed as well as $\omega t_{tr_0} = \pi$.

With these assumptions θ varies with the square of δp. Thus both faster ($\delta p > 0$) and slower ($\delta p < 0$) electrons are deflected less than electrons with momentum p_{z_0}. As described in the previous section, the cavity phase should be adjusted such that the average deflection is zero. In that case all electrons with a nonzero δp produce a shorter streak, so that the streak length will not be influenced.

The low sensitivity to change in momentum is a result of the low sensitivity to change in t_{tr}. By choosing the optimal interaction length d the sine term with t_{tr_0} has a value near its maximum, where it is less sensitive to changes. If the average momentum of the bunch is not p_{z_0} or d is not optimal, then the sine term is not at its maximum and approximating it gives a linear dependence on δp.

An electron bunch with an energy spread has a varying bunch duration all the time, also inside the cavity. But because of high sensitivity to t_c and low sensitivity to t_{tr} we can say the cavity effectively produces a streak corresponding to the bunch duration exactly at the center of the cavity, with only small deviations as a result of differences in transit time.

3.3 Off-axis behavior

3.3.1 Magnetic field dependence

When a bunch moves through the cavity it does not move exactly on the axis. The bunch has some size in the x and y-direction. But away from the axis the field is not precisely as given in equation (3.2). A Taylor expansion of the field from section 2.2 around the axis to second order gives the following equation.

$$B_y = B_0 \sin(\omega t)\left[1 - \frac{1}{8}k^2y^2 - \frac{3}{8}k^2x^2\right] \tag{3.9}$$

where $k = \omega/c$. With this you can calculate that θ only deviates 0.5‰ for $y = 1$ mm and 1.5‰ for $x = 1$ mm. Since bunches will be used that are always smaller than this we can assume the magnetic field is the same for the entire bunch.

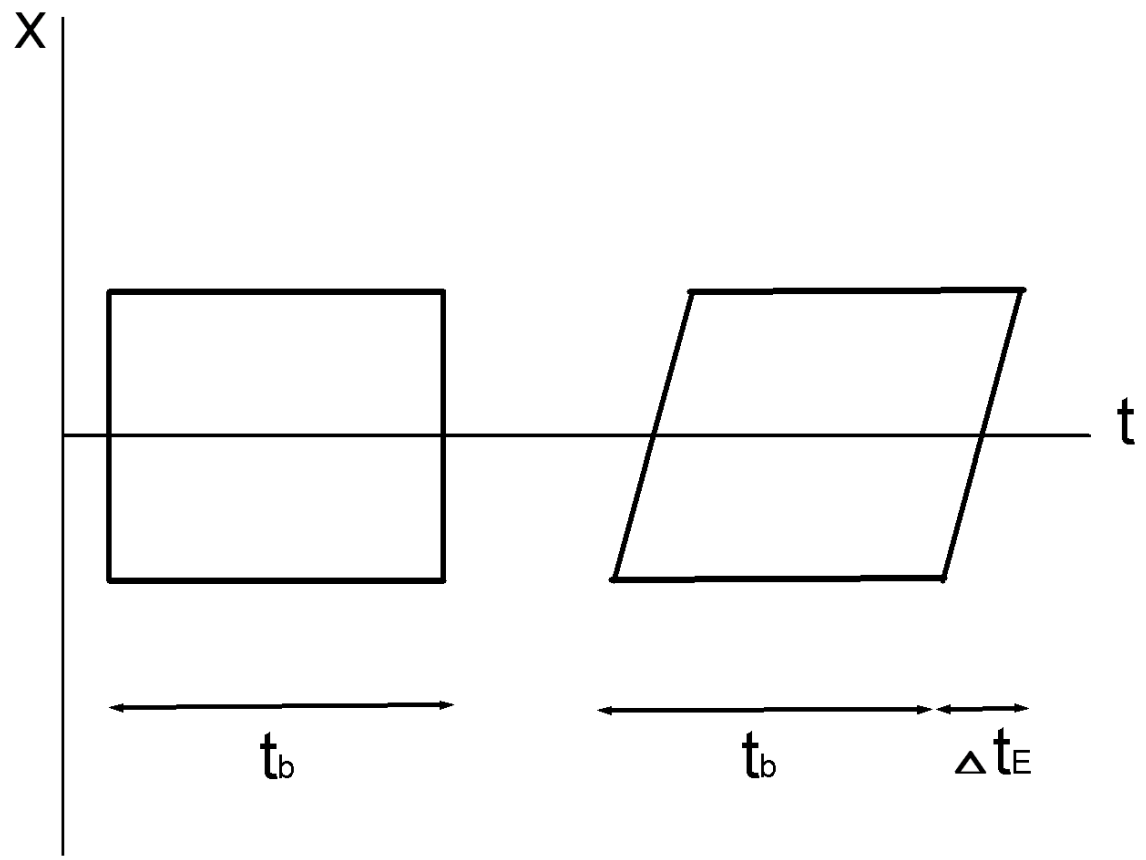

Figure 3.3: *An electron bunch with a size in x-direction becomes longer, because electrons at large x positions are somewhat accelerated or decelerated.*

3.3.2 Electric field dependence

The magnetic field given above is not the only field that should be taken into account. There is also a longitudinal electric field, as described in section 2.2 which scales to first order as

$$E_z = \frac{1}{2} E_0 k x \cos(\omega t + \phi_0) = \omega B_0 x \cos(\omega t + \phi_0) \tag{3.10}$$

Here it will be assumed that $\phi_0 = 0$. This electric field deforms the bunch as follows. Electrons that have a position some distance from the axis in the x-direction will become accelerated or decelerated by the electric field. This is sketched in figure 3.3. As a result the bunch is effectively lengthened, t_c is different for electrons at large x-positions. The total forward momentum, including that as a result of the electric field is

$$p_z(x,t) = p_{z_0} - \int_{-\frac{\pi}{2\omega}}^{t} eB_0 \omega x \cos(\omega t) dt = p_{z_0} - eB_0 x \left[sin(\omega t) + 1 \right] \tag{3.11}$$

With p_{z_0} the momentum before the electrons enter the cavity. It is assumed that the electrons enter the cavity exactly at $t = -\pi/2\omega$. Integrating equation (3.11) gives the position as a

function of time.

$$z(x,t) = v_{z_0}\left(t + \frac{\pi}{2\omega}\right) - \frac{eB_0x}{m}\left(t + \frac{\pi}{2\omega}\right) + \frac{eB_0x}{m\omega}\cos(\omega t) \tag{3.12}$$

Electrons that are unaffected by the electric field, those at x=0 , will arrive at the center of the cavity at t=0, so

$$z(0,0) = \frac{\pi v_{z_0}}{2\omega} = \frac{1}{2}d \tag{3.13}$$

Electrons that are affected by the electric field arrive at the center at $t = t_E$. Solving $z(x, t_E) = \frac{1}{2}d$ yields the following expression for t_E.

$$t_E = \frac{(\frac{\pi}{2} - 1)}{\omega}\left[\frac{p_{z_0}}{eB_0x} - 1\right]^{-1} \tag{3.14}$$

Here we assumed t_E small so we can write $\cos(\omega t_E) \approx 1$. Evaluating this expression with values as used before and assuming $x < 1$ mm we find that the bunch is effectively lengthened by an amount

$$\Delta t_E \approx (\frac{\pi}{2} - 1)\frac{eB_0\Delta x}{\omega p_{z_0}} \approx 4.5 \cdot 10^{-10}\Delta x \tag{3.15}$$

where Δx is the width of the bunch. Thus as sketched in figure 3.3, a bunch with a size in x-direction effectively becomes longer as a result of the electric field. Since the streak camera is very sensitive to changes in t_c and only little sensitive to changes in t_{tr}, it suffices for describing bunch lengthening to take into account t_E, which is the change in t_c. To keep the error on the bunch duration measurement small, the lengthening has to be minimized. This can be achieved by reducing the bunch size in x-direction before the cavity. To reduce bunch lengthening t_E to for example 20 fs, an aperture would have to be used to reduce the x-dimension of the bunch to 45 μm. Since t_E scales with B_0, reducing B_0 will decrease lengthening. Furthermore it is possible to perform streak length measurements with different aperture sizes and extrapolate results to zero size in x-direction.

3.3.3 Curved trajectory

In the previous sections it was assumed that the electrons follow a straight line. It is simple to see that this is not the case. The magnetic field around the axis has been described before in equation (3.2). This field causes a force and hence a velocity v_x in the x-direction.

$$\begin{aligned} v_x(t) = \int_{t_c - \frac{1}{2}t_{tr}}^{t} \frac{e}{m} v_z B_y(t) dt &= -\frac{ev_zB_0}{m\omega}\left[\cos(\omega t) - \cos(\omega t_c - \frac{1}{2}\omega t_{tr})\right] \\ &= -\frac{ev_zB_0}{m\omega}\left[\cos(\omega t) - \sin(\omega t_c)\right] \end{aligned} \tag{3.16}$$

Then assuming $\omega t_{tr} = \pi$, the x-position of the electrons is

$$\begin{aligned} x(t) &= x_0 - \frac{ev_zB_0}{m\omega}\int_{t_c - \frac{\pi}{2\omega}}^{t}\left[\cos(\omega t) - \sin(\omega t_c)\right] dt \\ &= x_0 - \frac{ev_zB_0}{m\omega^2}\left[\sin(\omega t) - \sin(\omega t_c - \frac{\pi}{2}) - \sin(\omega t_c)(\omega t - \omega t_c + \frac{\pi}{2})\right] \\ &\approx x_0 - \frac{ev_zB_0}{m\omega^2}\left[\sin(\omega t) + 1 - \omega t_c(\omega t + \frac{\pi}{2})\right] \end{aligned} \tag{3.17}$$

Where t_c is assumed small, so the terms with t_c can be approximated to first order in t_c. For B_0=16.7 mT and $t_c = 0$ the electrons will move as much as 2.7 mm from their original position x_0. Probably the biggest disadvantage of this displacement is the fact that the streak will not be at the center of the capturing screen. Furthermore this displacement will result in a net acceleration of the electron bunch because they will experience more E_z field as they move off-axis. For $B_0 = 16.7$ mT, the electrons leave the cavity with 3% more momentum on average, so 6% extra energy. This momentum increases with the square of B_0. The lengthening of the bunch by the E_z field will not be different, since the bunch will stay in the area where E_z scales linearly with x.

3.4 Angular spread

If the variable field in the streak camera is off, the electron bunch forms a spot on the screen. When the field is on, the bunch forms a line on the screen and the length of the line will depend on the bunch duration as described before. The width of the line will be equal to the diameter of the spot. In order to properly determine the length of the line, the length should be substantially larger than the width. The diameter of the spot and thus the width of the line can be decreased by using an aperture in front of the deflection cavity. However, after the aperture the bunch size will gradually increase. This is a consequence of the angular spread in the bunch. In any real electron bunch or beam, the electrons will have some transverse momentum, though much smaller than the forward momentum. As a result they move at small angles with the z-axis.

The angular spread has several causes. One is the process of creation of the bunch. When the electrons are extracted from the electron source they always have momentum in a random direction as a result of the temperature of the source and the process of extraction. After acceleration the transverse part of the momentum spread shows as angular spread. Next, the angular spread can increase as a result of the repulsive Coulomb force between electrons or external fields such as magnetic lenses.

From simulations of our setup we expect the bunch to diverge with an angle of approximately 1 mrad between the streak cavity and the screen. For $B_0 = 16.7$ mT a bunch with a duration of 170 fs is deflected over an angle $\Delta\theta = 1$ mrad. Such a bunch will produce a line with a length to width ratio of 2, as is shown in figure 3.4. A shorter bunch will produce a line with a smaller length to width ratio. This will become increasingly hard to measure in practice. If the bunch duration is 20 fs, then the length of the line will be only 10% larger than the width. This may still be measurable, although the accuracy will be low. To measure more accurately and thus to be able to measure even shorter bunches or measure at lower values of B_0, the angular spread has to be reduced. This can be done by placing an aperture in front of the streak cavity, which will remove the outside of the bunch, the electrons with the biggest angular spread. The aperture only needs to remove the outside electrons in x-direction, but a circular aperture will probably be more convenient than a rectangular one. We expect that the angular spread depends linearly on x, with 1 mrad divergence for $x_0 = 1$ mm. The spot size on the screen becomes

$$x_s = x_0 + Zx_0 \tag{3.18}$$

Here x_0 is the transverse size of the bunch at the cavity and Z is the distance from cavity to screen.

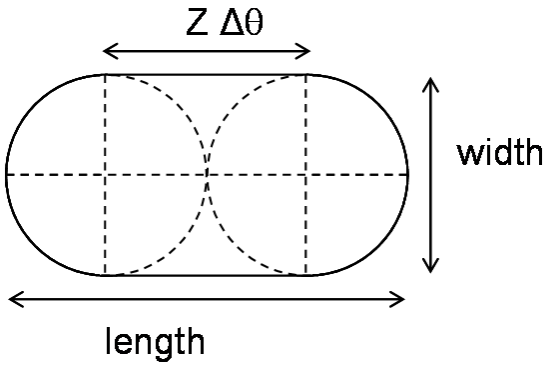

Figure 3.4: *Example of electron bunch streak. The width of the line is determined by the aperture size and angular spread in the bunch. The length of the line is equal to the width plus the length of the streak $Z\Delta\theta$.*

3.5 Simulations

Next to the analytical calculations of the previous sections, the particle tracking simulation programme General Particle Tracer [2] has been used to calculate the motion of electron bunches in the streak camera setup. The calculation uses several starting values, which can be chosen freely. These include the x and y dimensions of the bunch, the energy and energy spread of the electrons and the external fields in the setup. In this section the simulation results will be given and be compared to the analytical calculations of the previous sections. To make this comparison, the pillbox fields of section 2.2 have been used in the simulation, so without the holes that disturb the fields.

Next, the simulations can be done with more realistic and complicated fields. This more realistic field has been taken from the simulations in chapter 4, which have been checked by on-axis field measurements (chapter 5) In order to keep data files manageable the field is exported with a mesh size of 2 mm. This will cause some error but we expect to obtain reasonable results nonetheless. The GPT simulation results with this 'real' field will be included in the relevant graphs and values will be given at the end of this chapter.

The simulations are most clear when they start from one dimensional bunches. These bunches have no angular spread, or energy spread and we will use bunches with some size in either z or x-direction. The size in z direction will be given as a duration in time. With these bunches all aspects from the previous sections can be studied more or less separately.

3.5.1 Bunch duration

Firstly the bunch duration dependence of the streak length is studied. For this purpose the starting values for x and y are taken to be zero and all particles have the same initial energy of 100 keV exactly. The bunch is created at point $z = 0$ during a time t_b. This time t_b is varied from 10 fs to 10 ps. The bunch passes through the pillbox fields with frequency 3.00 GHz and amplitude $B_0 = 16.7$ mT, over a distance $d = 25$ mm. Figure 3.5 shows the simulation results. Plotted is the size in x-direction at a distance of $z = 100$ mm from the cavity center

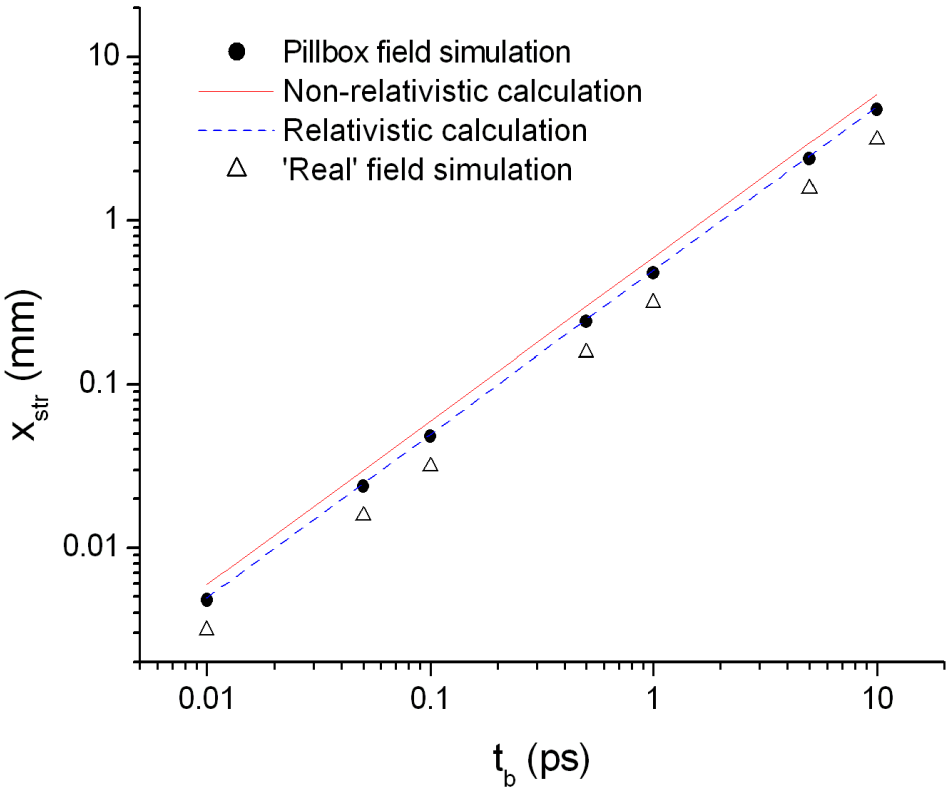

Figure 3.5: *A plot of simulated and calculated streak length versus bunch duration.*

as a function of bunch duration. The solid line is the analytical result from section 3.1, equation (3.4). The main quantitative discrepancy between calculation and simulation lies in the classical approximation in the calculation. A proper relativistic calculation using $p = \gamma mv$, as done in appendix C shows that the classically calculated deflection angle θ should be divided by γ which equals 1.20 for 100 keV electrons. Furthermore a different interaction length d has been used, which gives a difference of almost 1%. With these adaptations the calculation gives the result shown as the dashed line. The remaining difference of approximately 3% may result from combinations of the effects described in this chapter (higher order effects) and from a variation of t_0 which can be a few ps because the phase of the cavity is not exactly correct. The cavity phase ϕ_0 has been adjusted until the average deflection angle $\theta = 0$. Then $\omega t_0 + \phi_0$ will be zero. Limited accuracy in ϕ_0 gives an offset in the deflection angle of a few mrad. We therefore conclude that for a pillbox cavity the streak is given by $\Delta\theta = 4.9 \cdot 10^9 t_b$ (SI units). The 'real' field simulations give $\Delta\theta = 3.1 \cdot 10^9 t_b$.

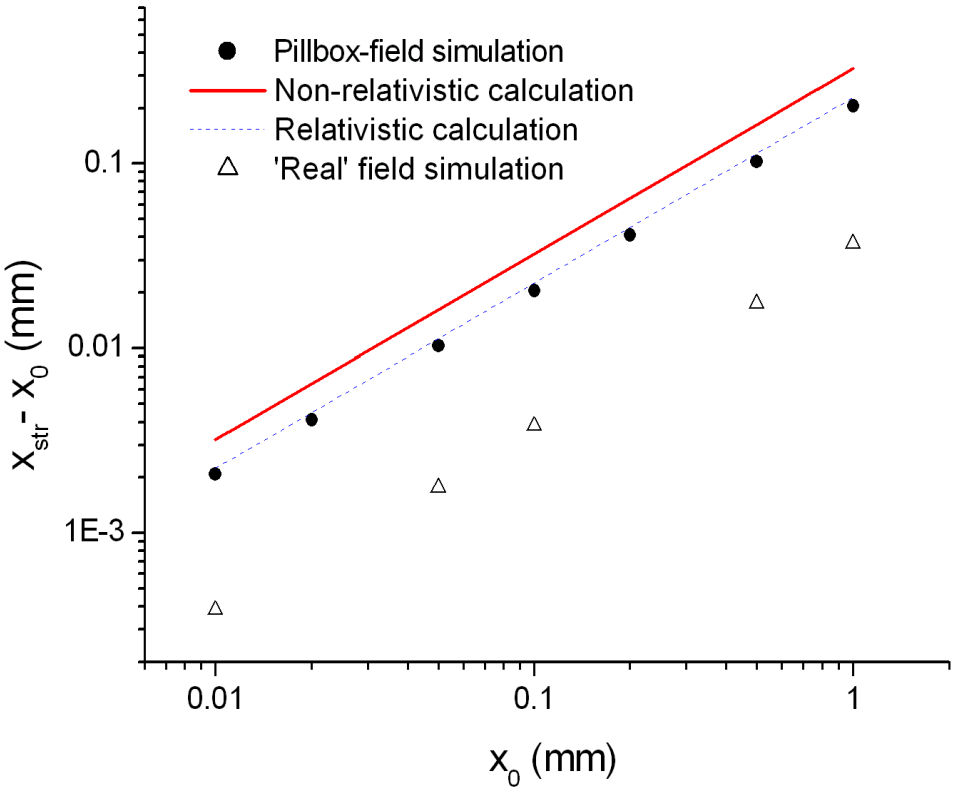

Figure 3.6: *This graph shows the change in size in the x-direction of an electron bunch as a function of the original size.*

3.5.2 x-Direction

Next the streak length dependence on the bunch size in x-direction is studied. Therefore a line bunch is created with no length in y- or z-direction, so created at one point in time. The rest is the same as before. Figure 3.6 shows the simulation results. The streak length x_{str} minus the starting size x_0 is plotted against the bunch's starting size x_0. The solid line represents the non relativistically calculated values. These have been calculated by substituting Δt_E of equation 3.14 as bunch duration t_b into equation 3.4. They differ only quantitatively with the simulation results. A relativistic calculation as given in appendix C and presented by a dashed line in figure 3.6 differs only 9% from simulations. This difference may be ascribed to a variation of t_0 and higher order effects, as in the previous section.

As these simulations show, the extra length of the bunch is $\Delta t_E = 4.2 \cdot 10^{-10} x_0$ for the pillbox cavity and $\Delta t_E = 1.2 \cdot 10^{-10} x_0$ for the 'real' field. Then the change in streak length $\delta\theta$ due to x_0 is given by $\delta\theta = 2.05 x_0$ for a pillbox cavity and by $\delta\theta = 0.37 x_0$ for the real field (all in SI units).

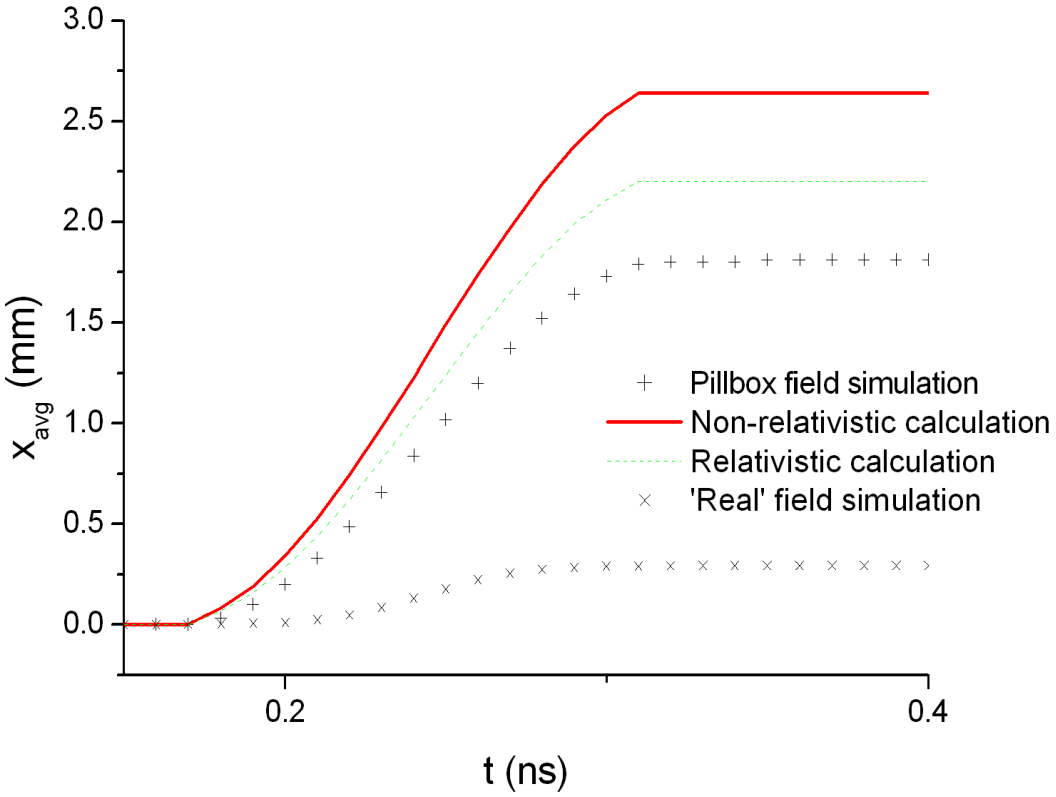

Figure 3.7: *Calculated and simulated electron trajectories in the streak cavity.*

3.5.3 Curved trajectory

As described before in section 3.3.3, the bunch follows a curved trajectory. In figure 3.7 the average x-position of the bunch in the simulation is plotted against time. The solid line represents the trajectory as calculated non-relativistically in equation (3.17) for $t_c = 0$ and $B_0 = 16.7$ mT. The dashed line shows the trajectory for a relativistic calculation. Even for this calculation there is a large difference (more than 20%) with the simulation. In both calculations $t_c = 0$ is assumed, but from the simulation results we can see that after passing through the cavity the bunch has a small but non-zero average deflection angle θ. This means that t_c is not exactly zero, and from θ we find $t_c = 0.2 \pm 0.05$ ps, which gives only a small deviation. The remaining difference will be a result of higher order effects such as acceleration of the bunch in the cavity.

The simulations for the 'real' field show only 0.3 mm sideways displacement in the cavity.

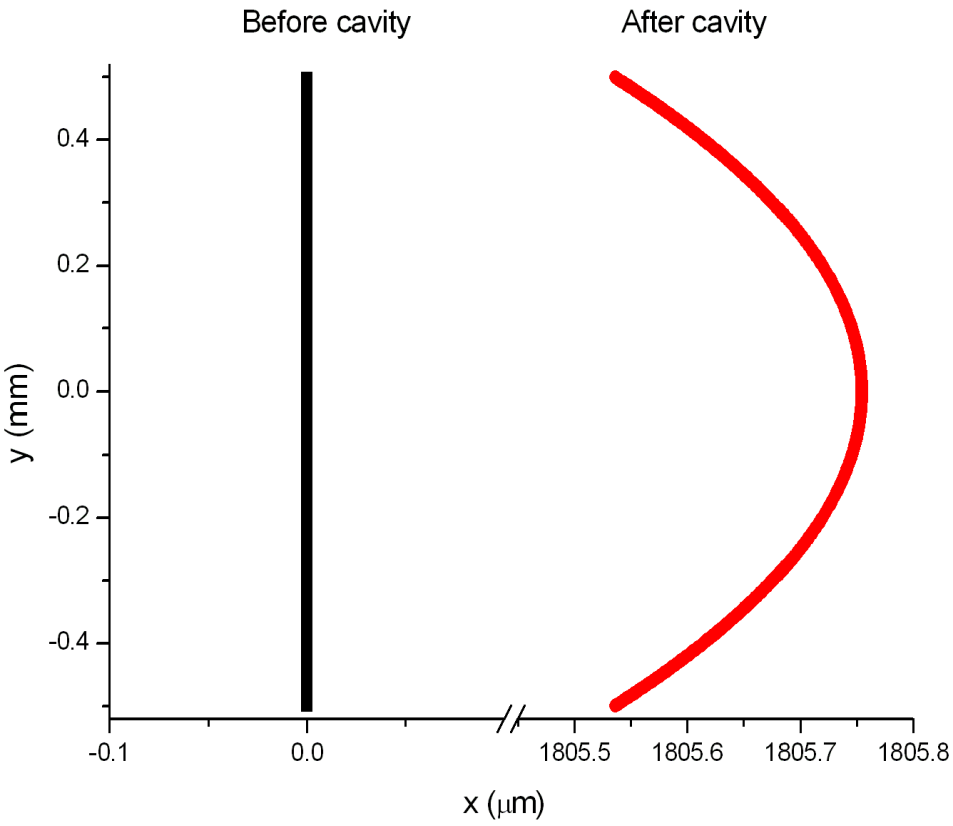

Figure 3.8: *Front view of the bunch before it has passed the cavity (left) and after it has passed the cavity (right).*

3.5.4 y-Direction

Equation (3.9) shows that B_y decreases with the square of y. To show this dependence we use the curved trajectory of the previous section. The simulation now starts with a bunch with a length only in y-direction. This bunch follows a curved trajectory while in the cavity, but a bit less sideways for large y values. Figure 3.8 shows a front view of the bunch before and after passing the cavity. It shows the y^2 dependence and it shows that for values of y smaller than 1 mm, as we expect to use, B_y can be assumed to be independent of y.

3.5.5 Momentum spread

In order to study the influence of a change in momentum, several simulations have been done with different momentums. Bunches are simulated with a size in z-direction of 0.5 ps, no transverse size and momentum is the same for each electron in the bunch. The results of these simulation runs are give in figure 3.9, where the streak length is plotted against the starting momentum of the bunch. The solid line gives the calculated result of section 3.2, i.e. equation (3.8) multiplied with the z-position at which the streak length is measured. For the

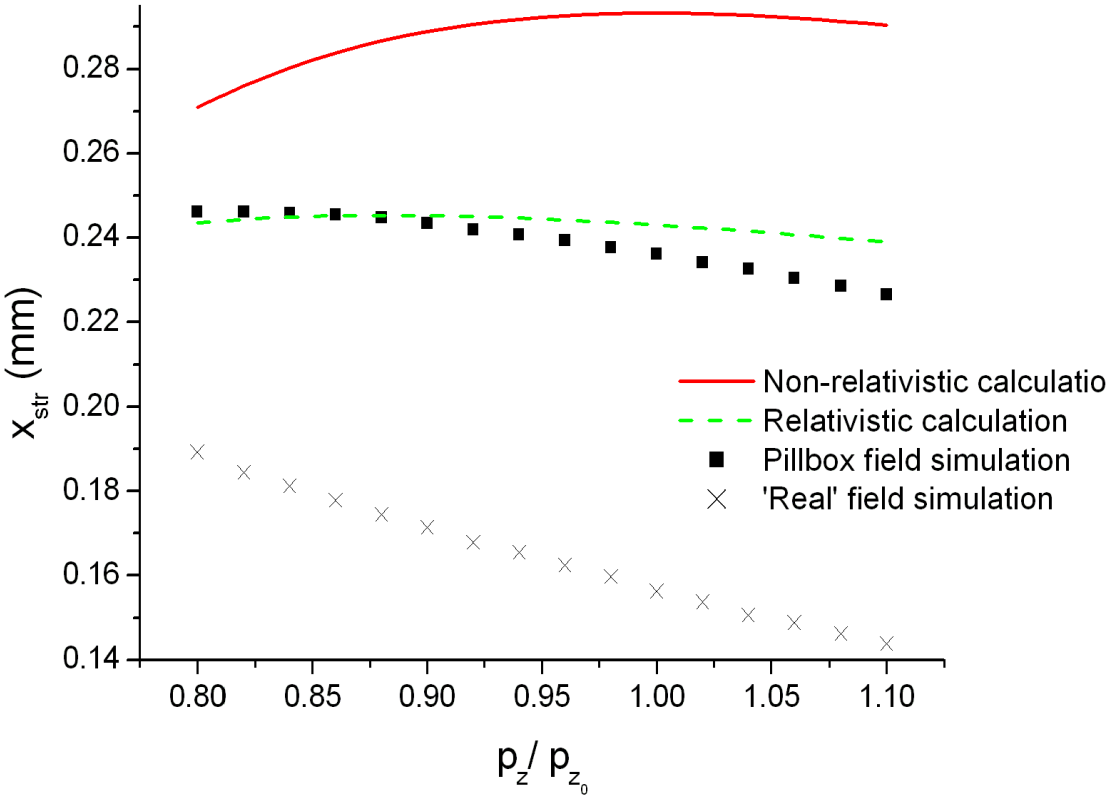

Figure 3.9: *This plot shows the streak length as a function of the momentum of the electron bunch.*

simulation that is 100 mm, measured from the cavity center. The calculation is off at two points. Firstly it gives a 20% larger streak length than the simulation, just like in section 3.5.1. The relativistically calculated dashed line is more accurate in that respect. Secondly the calculation shows that electrons with either smaller or larger momentum than p_{z_0} will be streaked less than electrons with momentum p_{z_0}. After all, the pillbox cavity was designed to have the optimal momentum to be p_{z_0}, by optimizing the cavity length. The dashed line is calculated with the same cavity length as the simulations, $d = 25$ mm, which is slightly less than the optimal 27.4 mm. This shifts the optimal momentum to a lower value. The simulation appears to give an optimal momentum which is even lower than expected. This is bound to be a result of the net acceleration that the bunch experiences. We are thus no longer operating the cavity with electron momentum around the optimal value. Therefore the streak length depends more or less linearly on electron momentum. As the simulations show, we can approximate the change in streak length $\delta\theta$ due to δp with $\delta\theta = -0.37\delta p_z \frac{\Delta\theta}{p_{z_0}}$ for the pillbox cavity. So 1% momentum change causes 0.4% change in streak length. For the real field this is $\delta\theta = -0.95\delta p_z \frac{\Delta\theta}{p_{z_0}}$.

For a bunch with momentum spread the streak length will depend on momentum distribu-

tion. Typically the streak length will be determined by the slowest electrons. However, when the fastest electrons are at the front of the bunch and the slower ones at the back, the front half of the bunch will produce a shorter streak and the back half a longer streak. This way the streak length of the bunch will be nearly the same as if it had no momentum spread.

3.6 Conclusion

From the calculations and simulations described in this chapter it can be concluded that measuring electron bunch durations from tens of femtoseconds to tens of picoseconds is possible. Table 3.1 summarizes the results of this chapter for both the classical and the relativistic calculation as well as for the simulation. The y-dependence is left out, because it is negligible. Values we expect in our measurements are given in table 3.2. From this can be concluded that effects from momentum spread can be neglected. In the following two sections we will substitute the values of table 3.2 into the equations of table 3.1, for 8 different combinations of the parameter values, and discuss the results. Tables 3.3 and 3.4 finally summarize these results.

Table 3.1: *Equations describing the performance of the streak cavity, in SI units. The equations are derived from a classical calculation, a relativistic calculation and (relativistic) simulations all for $B_0 = 16.7$ mT. The calculations concern the pillbox fields.*

	Classical calculation	Relativistic calculation	Pillbox simulation	'Real' field simulation	Field strength dependence
streak length $\Delta\theta$	$5.9 \cdot 10^9 t_b$	$4.9 \cdot 10^9 t_b$	$4.9 \cdot 10^9 t_b$	$3.1 \cdot 10^9 t_b$	$\sim B_0$
Δt_E	$5.4 \cdot 10^{-10} x_0$	$4.5 \cdot 10^{-10} x_0$	$4.2 \cdot 10^{-10} x_0$	$1.2 \cdot 10^{-10} x_0$	$\sim B_0$
$\delta\theta(x_0)$	$3.2 x_0$	$2.2 x_0$	$2.05 x_0$	$0.37 x_0$	$\sim B_0^2$
$\delta\theta(\delta p_z)$	-	-	$-0.37 \delta p_z \frac{\Delta\theta}{p_{z_0}}$	$-0.95 \delta p_z \frac{\Delta\theta}{p_{z_0}}$	

Table 3.2: *Expected values for experimental quantities.*

Quantities in experiment	expected values
bunch duration	10 fs - 10 ps
momentum spread $\delta p/p_{z_0}$	1%
angular spread	1 mrad
transverse bunch size x_0	10 μm - 1 mm
distance from cavity to capturing screen	100 - 500 mm
magnetic field amplitude B_0	0 - 8 mT

3.6.1 Discussion of pillbox cavity performance

10 ps bunch, $B_0 = 16.7$mT

When measuring long bunches we can put the screen at $Z = 100$ mm from the cavity. Then the spot size due to angular spread is $x_s = 1.1$ mm. The streak length will be $x_{str} = 4.9$ mm, so much larger than the spot size and easy to measure.

Since transverse size is approximately 1 mm, lengthening due to the electric field gives an extra streak length $x_E = 0.2$ mm, only 4%. Thus, the bunch duration can be easily measured with 4% accuracy.

10 ps bunch, $B_0 = 8$ mT

With the screen still at 100 mm spot size is 1.1 mm, streak length will be 2.3 mm. Lengthening will be only 0.05 mm. Now the streak length change of 0.4% due to energy spread has to be taken into account. All together, the bunch duration can be measured easily with an accuracy of 2%.

10 fs bunch,$B_0 = 16.7$ mT

To measure this tiny bunch duration we put the screen as far away as possible, $Z = 500$ mm. Even then the streak length will be only 25μm, thus hard to measure. The spot size is 1.5 x_0 and lengthening is equal to x_0, where we can choose x_0 with an aperture. To have a streak length of 10% of the spot size so we can just measure it, we need an aperture size $x_0 = 170\mu$m. To get only 10% lengthening the aperture has to be 3 μm. Since this is impossible, we will need to measure with different apertures and extrapolate to zero aperture size.

10 fs bunch, $B_0 = 8$ mT

Again we use $Z = 500$ mm, to find a streak length of just 12 μm. Thus for a reasonable spot size we need $x_0 = 80\mu$m. To get 10% lengthening an aperture of 5μm is required, so we will need to extrapolate to that.

Measuring 10 fs bunch duration clearly is a challenge, but not impossible.

3.6.2 Discussion of 'real' field cavity performance

10 ps bunch, $B_0 = 16.7$mT

When measuring long bunches we can put the screen at $Z = 100$ mm from the cavity. Then the spot size due to angular spread is $x_s = 1.1$ mm. The streak length will be $x_{str} = 3.1$ mm, so much larger than the spot size and easy to measure.

Since transverse size is approximately 1 mm, lengthening due to the electric field gives an extra streak length $x_E = 0.04$ mm, only 1%. Now the streak length change of 1% due to energy spread has to be taken into account. All together, the bunch duration can be measured easily with an accuracy of 2%.

10 ps bunch, $B_0 = 8$ mT

With the screen still at 100 mm spot size is 1.1 mm, streak length will be 1.5 mm. Lengthening will be only 0.01 mm. Now the streak length change of 1% due to energy spread has to be taken into account. All together, the bunch duration can be measured easily with an accuracy of 2%.

10 fs bunch,$B_0 = 16.7$ mT

To measure this tiny bunch duration we put the screen as for as possible, $Z = 500$ mm. Even then the streak length will be only 15μm, thus hard to measure. The spot size is 1.5 x_0 and lengthening is equal to $0.19x_0$, where we can choose x_0 with an aperture. To have a streak length of 10% of the spot size so we can just measure it, we need an aperture size $x_0 = 100\mu$m. To get only 10% lengthening the aperture has to be 8 μm. Since this is impossible, we will need to measure with different apertures and extrapolate to zero aperture size.

10 fs bunch, $B_0 = 8$ mT

Again we use $Z = 500$ mm, to find a streak length of just 7 μm. Thus for a reasonable spot size we need $x_0 = 50\mu$m. To get 10% lengthening an aperture of 18μm is required, so we will need to extrapolate to that.

Table 3.3: *Summary of the performance of the pillbox cavity.*

Bunch duration	10 ps	10 ps	10 fs	10 fs
B_0	16.7 mT	8 mT	16.7 mT	8 mT
Z screen-cavity	100 mm	100 mm	500 mm	500 mm
streak length x_{str}	4.9 mm	2.3 mm	25 μm	12 μm
spot size x_s	1.1 x_0	1.1 x_0	1.5 x_0	1.5 x_0
streak lengthening x_E	0.2 x_0	0.05 x_0	1.03 x_0	0.24 x_0
streak length accuracy	4%	2%	(10%)	(10%)
transverse bunch size /aperture x_0	1 mm	1 mm	0.17 mm / 2.5 μm	80 μm/ 5 μm

Table 3.4: *Summary of the performance of the 'real' field cavity as designed in this thesis.*

Bunch duration	10 ps	10 ps	10 fs	10 fs
B_0	16.7 mT	8 mT	16.7 mT	8 mT
Z screen-cavity	100 mm	100 mm	500 mm	500 mm
streak length x_{str}	3.1 mm	1.5 mm	15 μm	7 μm
spot size x_s	1.1 x_0	1.1 x_0	1.5 x_0	1.5 x_0
streak lengthening x_E	0.04 x_0	0.01 x_0	0.185 x_0	0.04 x_0
streak length accuracy	2%	2%	(10%)	(10%)
transverse bunch size / aperture x_0	1 mm	1 mm	0.1 mm / 8 μm	47 μm/ 18 μm

Chapter 4

Cavity design

To get the required field mode, a right cylinder will suffice, which is simple to design. This right cylinder cavity or pillbox cavity was the basis for the calculations in the previous chapter. This was useful for gaining understanding of the operation of the streak camera. It was assumed that in the cavity the magnetic field along the z-axis is constant, of magnitude B_0 and pointing in the y-direction. This is correct for a closed pillbox, but introducing holes in the top and bottom to let electrons pass through changes this magnetic field profile. The profiles are shown in figure 4.1. for both profiles we will define B_0 as the magnetic field amplitude in the center of the cavity, thus as the maximum field on the z-axis. This is no longer the maximum magnetic field in the cavity.

The holes in the cavity also cause an electric field $E_x(0, 0, z)$ along the z-axis, which is shown in figure 4.2. Its maximum will be called E_{max}, even though there may be a higher E_x field elsewhere in the cavity.

To get a field amplitude of $B_0 = 16.7$ mT in a pillbox cavity, as was used in the previous chapter, 13.4 kW is required. For half the field amplitude, $B_0 = 8$ mT, we need 3.1 kW. Applying that much power to a small component in an electron microscope is bound to cause large disturbances. Furthermore we want to keep the power supply to the cavity compact. We want to use a compact solid-state amplifier and coaxial cables with a small loop antenna for coupling the 3 GHz signal into the cavity. The amplifier can deliver up to 1 kW of power. For larger power a larger setup is required with a big klystron for power generation and rectangular wave guides for incoupling.

In order to decrease the power consumption of the cavity, an alternative shape has been designed. To calculate the power usage simulations have been done with CST Microwave Studio [1]. Because the required field is not rotationally symmetric, it cannot be calculated with a two-dimensional solver such as SUPERFISH [3], which is commonly used for cavity design. The final energy-efficient cavity shape is shown in figure 4.3. With this shape only 860 W is required for a field amplitude $B_0 = 8$ mT. Although this is only half the field amplitude of that used in the calculations of the previous chapters, it still is sufficient for the desired application. This chapter describes the design process of the energy-efficient cavity.

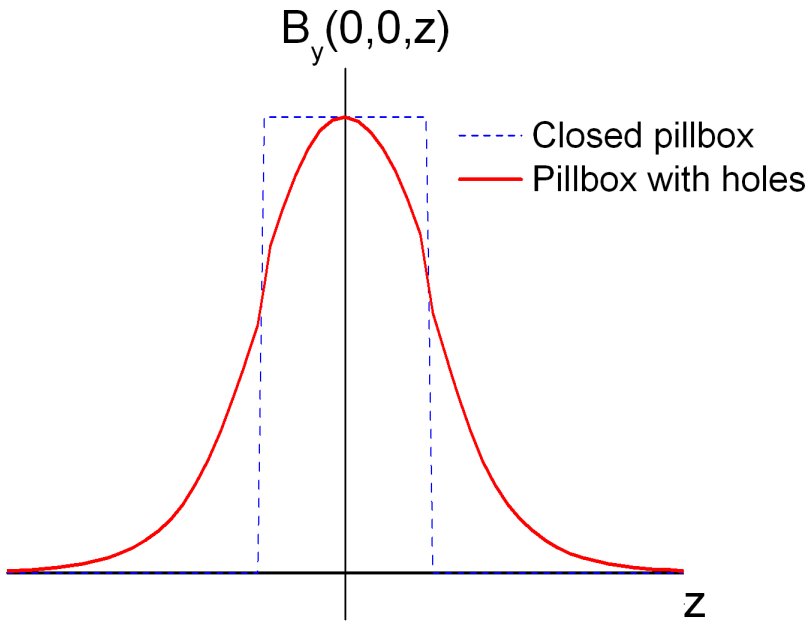

Figure 4.1: *Magnetic field profile for pillbox cavity with and without holes.*

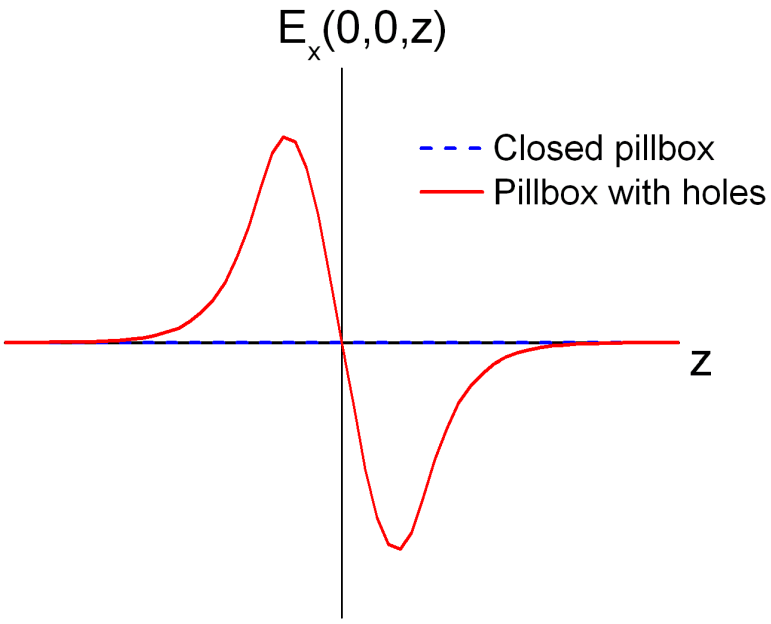

Figure 4.2: *Electric field profile for pillbox cavity with holes.*

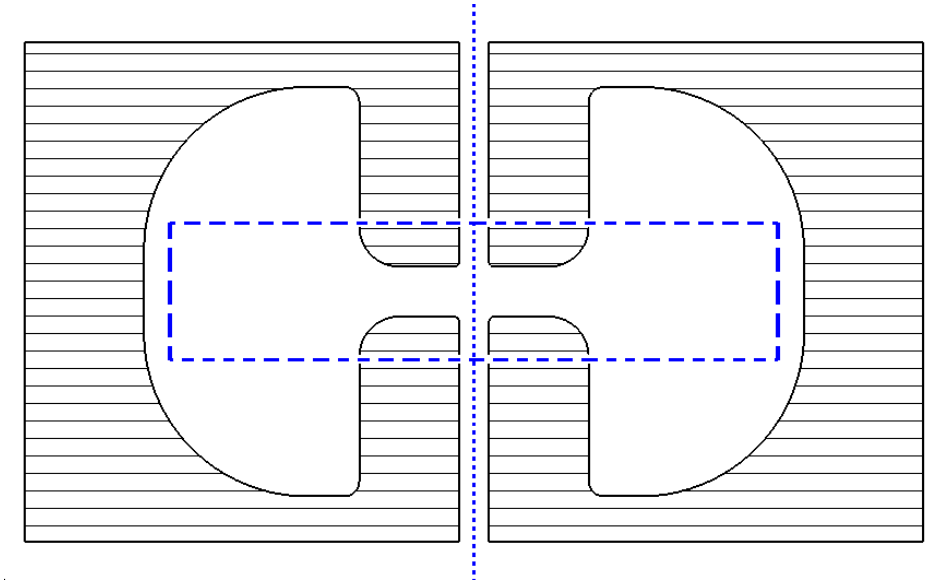

Figure 4.3: *This cross-section of the rotationally symmetric cavity shows the efficient shape. The dashed line indicates the size of the pillbox cavity as used for the calculations of chapter 3.1. The electrons pass through along the dotted line, the z-axis.*

4.1 Design starting point

The starting point for the simulations is a hollow cylinder. From the calculations of section 2.2 follows that the radius R should be 61 mm to get the cavity at the correct resonance frequency. By choosing a length $d \approx 25$ mm, the region with a significant magnetic field strength B_y can be made such that electrons pass through in approximately half the period of the RF field. One other requirement is that electrons can pass through along the z-axis. Therefore an entrance and an exit hole of 6 mm diameter are required.

Figure 4.4 shows the cylinder with the above mentioned dimensions. In the simulation the cavity material is assumed to be a perfect electric conductor. The space inside the cavity is assumed to be perfect vacuum. The holes in the top and bottom of the cavity are closed at $z = \pm 50$ mm. Since at this point the field strength is nearly zero, this will not affect the simulation results. With the shape of the cavity as an input, the program calculates the resonance frequencies ω of the cavity and the corresponding field distributions. To calculate the quality factor Q from these results, the conductivity of the cavity wall is assumed to be that of copper. Then the energy dissipation due to surface currents in the cavity wall can be calculated rewriting equation (2.10)

$$P_{loss} = \frac{\omega U}{Q} \tag{4.1}$$

Where U is the total stored energy in the electromagnetic field. For a pillbox cavity as used for calculations, so with radius $R = 61$ mm and a thickness $d = 25$ mm, at a field strength $B_0 = 8 \cdot 10^{-3}$ T, P_{loss} and thus the required input power is 3.4 kW.

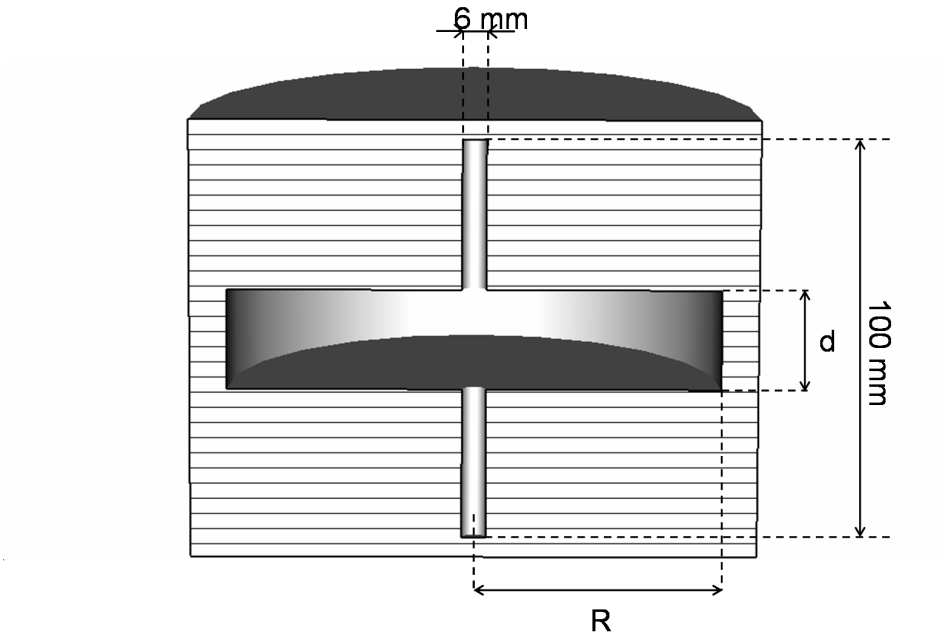

Figure 4.4: *Starting point for the cavity design is a right cylinder.*

4.2 First variation

Now the dimensions and the shape of the cavity will be varied. For that purpose the vacuum inside the cavity is simulated as three concentric cylinders. The inner cylinder has a radius of 3 mm and a length of 100 mm, it represents the holes in the cavity for electron passage. The inner cylinder is kept the same for all simulations. The middle cylinder has outer radius R_2 and inner radius 3 mm. It has a length d_2. The outer cylinder has inner radius R_2, outer radius R_3 and length d_3. The starting values are chosen $R_2 = 30$ mm, $R_3 = 60.9$ mm, $d_2 = 15$ mm and $d_3 = 50$ mm. These parameters are varied one by one and the resulting power requirement is calculated. The result is plotted in figure 4.6. To get the lowest power consumption the following values are taken $R_2 = 23$ mm, $d_2 = 10$ mm and $d_3 = 55$ mm from now on. This change in dimensions naturally has its effect on the resonant frequency. To get the frequency right the dimensions can be changed somewhat around the chosen optimal values. This will be done later. R_3 is kept constant for now at 60.9 mm, changing it has little effect on the power consumption but a rather large effect on frequency. The resulting shape after this optimization step is shown in figure 4.5. These chosen values for the three parameters R_2, d_2 and d_3 are not the best possible values. As described above, they were varied independently. To find the optimal values the entire 3D parameter space should be investigated, which requires much calculation time. The chosen values give a result which is good enough though, since with this shape approximately 1.1 kW is needed for $B_0 = 8$ mT.

Its efficiency can more or less understood as follows. The power loss scales as

$$P_{loss} \sim B^2 A \delta \tag{4.2}$$

Where B is the field strength in the cavity (actually the field at the cavity wall), A is the wall area and δ is the skindepth, the distance the fields extend into the wall, which is typically of

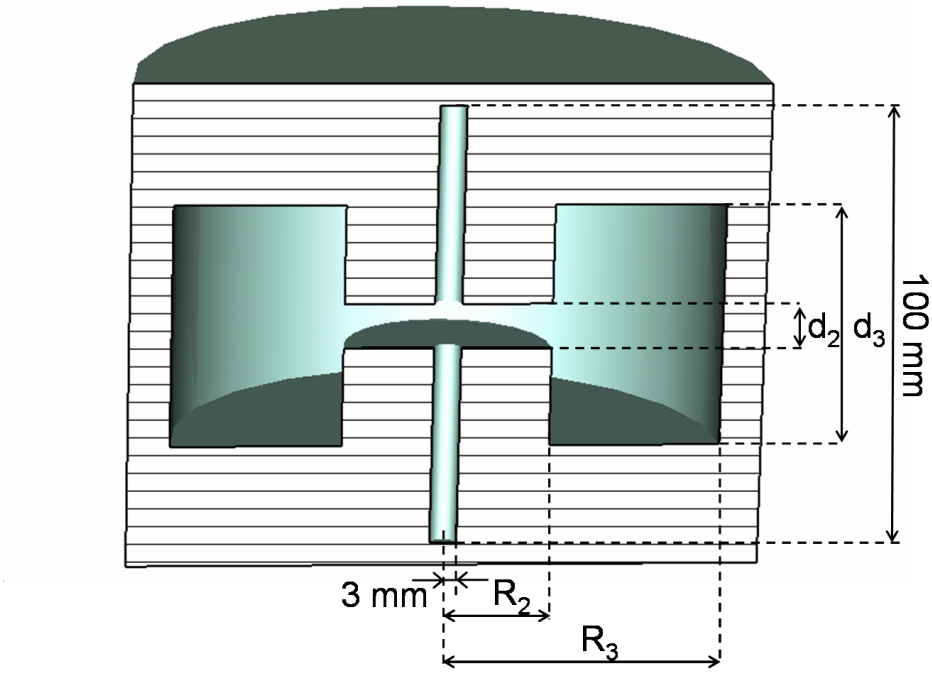

Figure 4.5: *The first changes for decreasing the power usage of the cavity are done by dividing the cavity into three parts and varying their sizes.*

the order of micrometers. The energy U stored in the cavity scales as

$$U \sim B^2 V \tag{4.3}$$

With V the cavity volume. Assuming U constant and a simple cylindrical cavity geometry we find

$$P_{loss} \sim \frac{A}{V} \sim \frac{1}{d} \tag{4.4}$$

So to decreases losses the cavity length should be increased, but this also decreases field strength. To obtain large field strength around the axis we keep d small there, while making it large otherwise.

4.3 Rounding

The next step in optimizing the cavity is rounding off the edges. Instead of a 90° angle circular edges are made with radii c_0 through c_3. This is illustrated in figure 4.7, which shows the cavity cross-section with optimal radii. As the graphs in figure 4.8 show, the optimal values are $c_1 = 8$ mm and $c_3 = 25$ mm, while the edges c_0 and c_2 are best kept right, so zero radius. Because a right edge is hard to machine, c_0 is chosen 1 mm and $c_2 = 3$ mm radius. With these rounded edges, power demand for the cavity has come just under 1 kW for $B_0 = 8$ mT.

To get the cavity at the intended frequency of 2997.9 MHz some dimensions have been varied to get most frequency shift at the least cost of increased power usage. This gives the final cavity dimensions of $R_3 = 66.20$ mm, $c_3 = 32.7$ mm, $h_3 = 82$ mm and the rest as given before. The choice for exactly this frequency will be explained in section 4.6.

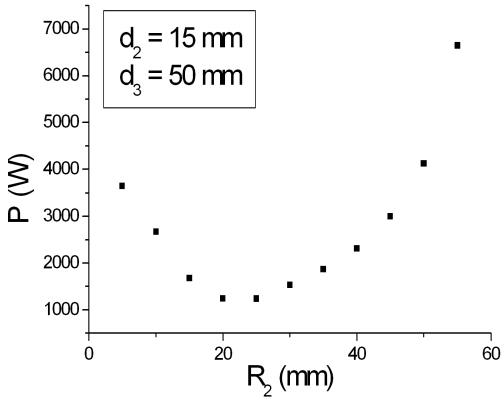

(a)

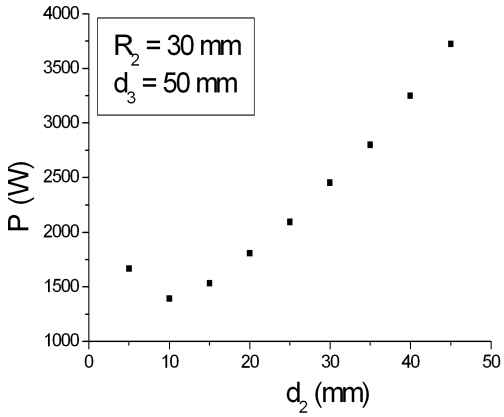

(b)

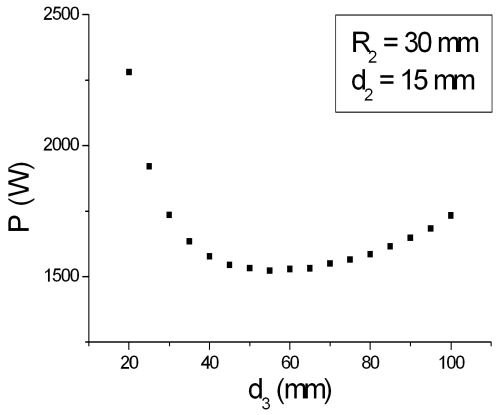

(c)

Figure 4.6: *These graphs show the power usage as a function of several cavity dimensions.*

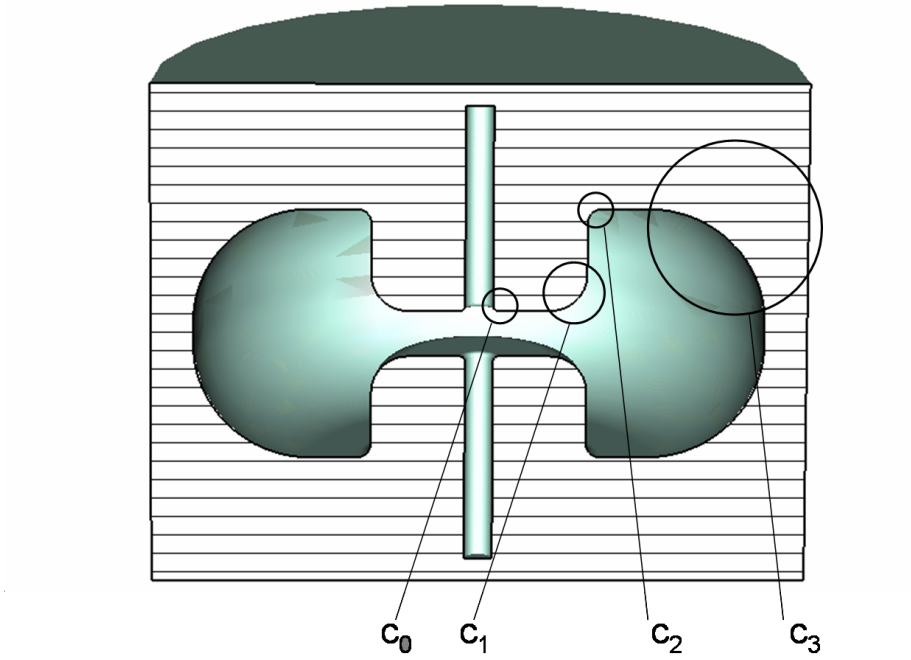

Figure 4.7: *Cavity cross-section with rounded edges.*

4.4 Further optimization

Although the result from the previous section is the cavity that has actually been built, further improvements are possible. One way to reduce the power usage of the cavity even further is to abandon rotational symmetry. As a simple example of this, the cavity can be "squeezed" in one direction while otherwise keeping all sizes the same as shown in figure 4.9. When we adapt the same coordinate system as used to describe the field mode in section 2.2, the on-axis magnetic field points in y-direction. If we then reduce the cavity size in y-direction, we reduce the volume where the magnetic field is large, without affecting magnetic field along the z-axis. This should result in reduced power losses. As figure 4.10 shows, a substantial reduction in power loss can indeed be achieved this way, up to 30% for a ratio $y/x = 0.4$. This looks very promising, but since it is not possible to construct a non-rotationally symmetric cavity to within the required accuracy of 10 μm, such cavities are not investigated any further here.

Other optimizations that may be conceivable concern the goals of optimization. While here the goal was to use as little power as possible for an on-axis maximum field strength of 8 mT, other goals may yield different cavity shapes. For example the magnetic field B_y integrated along the z-axis could be considered instead of simply its maximum along the z-axis, or the electric field E_x along the axis. Alternatively, an other cavity shape could give a certain preferred field aberration, a certain profile along the z-axis or a less disturbing electric field distribution around the z-axis.

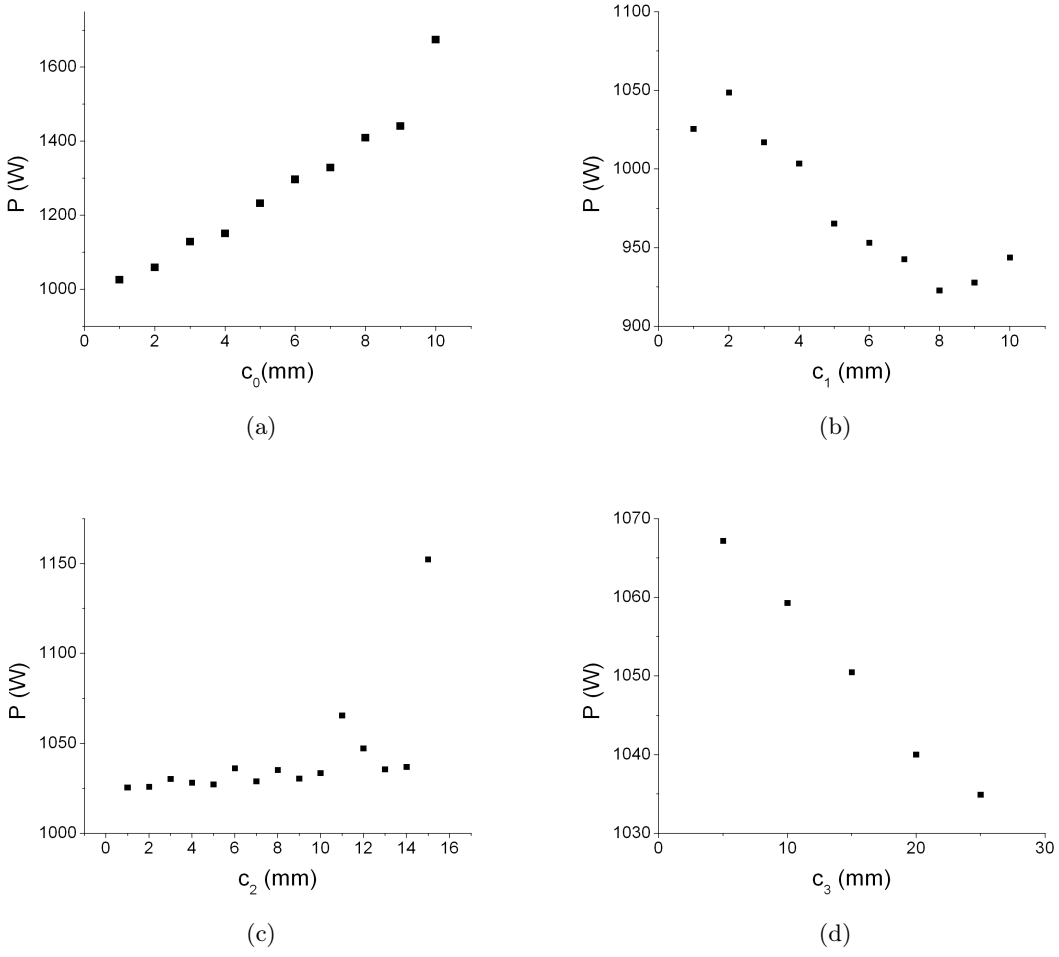

Figure 4.8: *These graphs show the power usage as a function of edge radius.*

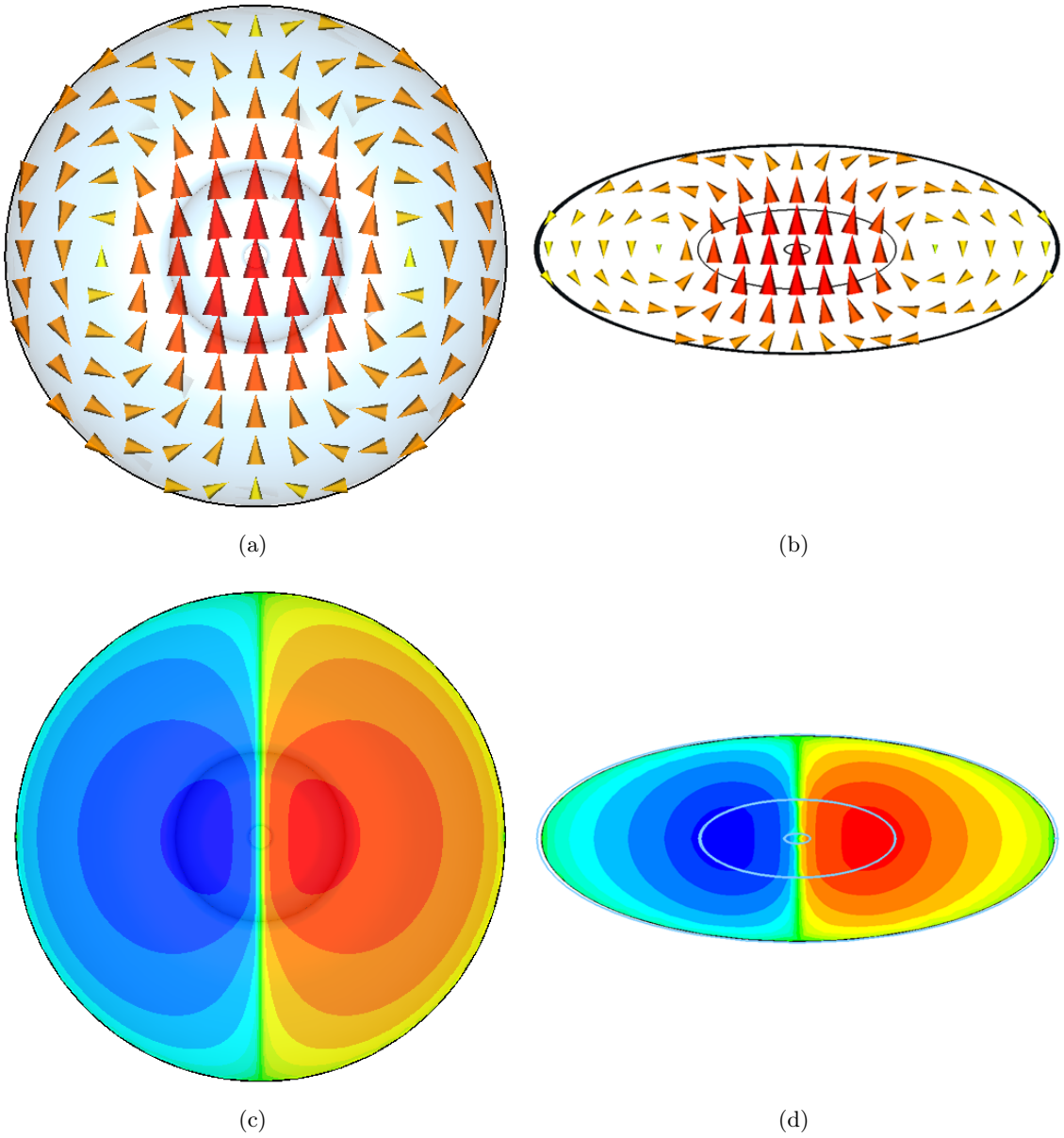

(a) (b)

(c) (d)

Figure 4.9: *The magnetic field distribution for $z = 0$ in a cylindrically symmetric cavity (a) and in a cavity which is "squeezed" (b) so its size in y and x direction differs. The magnitude of the longitudinal electric field E_z of both is given in (c) and (d) respectively. For a ratio of $y/x = 0.4$, up to 30 % power reduction can be achieved relative to the $y/x = 1$ ratio in (a).*

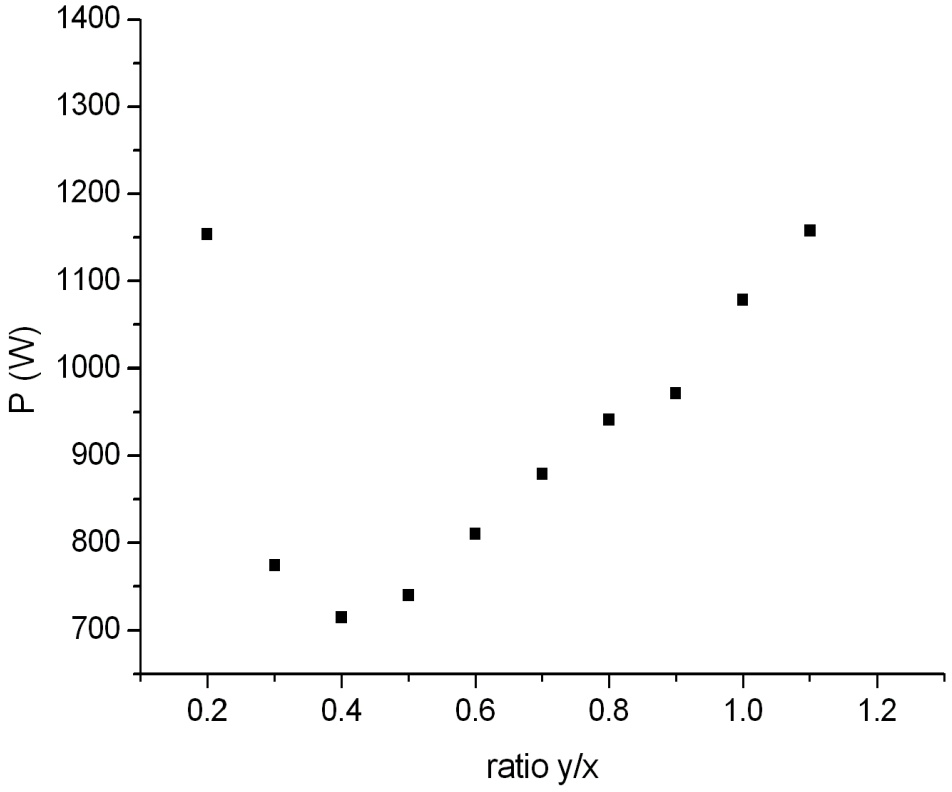

Figure 4.10: *A graph of the power usage as a function of the ratio y/x.*

4.5 Accuracy

To calculate the field distribution for any cavity shape the electromagnetic field simulation program CST Microwave Studio has been used, which features an eigenmode solver to calculate field modes in a closed cavity. To perform the calculations the cavity shape is subdivided into small cells that form a mesh, a three dimensional grid. Although some error may originate from the field calculation itself, the main source of inaccuracy is the finite resolution of the mesh. Because of limited computing capacity and to keep computation times workable, the field and power loss calculations during cavity shape optimization have been done with some ten thousand mesh cells. With this mesh density the resonant frequency of the mode can be off by as much as 5% and the power loss can have an error of up to 10% or even 20%. This error is so large because the power loss is calculated from the frequency, quality factor and field strength, so that simulation errors will add up.

While the magnitude of the power loss is rather inaccurate, the dependence of power loss on cavity shape variations is not expected to differ so much. Therefore optimizing power consumption of the cavity is expected to work out fine even for low mesh quality.

A high accuracy of the resonant frequence of the cavity is required when it is used together with another cavity. This will be described in the next section. To calculate the frequency of the final design to within an accuracy of 0.1 MHz, a long series of simulations has been done with an increasing number of mesh cells. The result of this series is shown in figure 4.11, where the calculated frequency is plotted against the number of mesh cells used.

To verify the accuracy of the simulation an aluminium prototype cavity has been constructed before the final copper cavity. The aluminium prototype cavity had somewhat different dimensions, giving a calculated frequency of 3002.06 ± 0.01 MHz. The measured resonant frequency of the aluminium cavity, after correction for the air pressure, is 3002.4 ± 0.2 MHz in vacuum. The final copper cavity has a calculated resonant frequency of 2997.75 ± 0.05 MHz. The measured frequency is 2998.0 ± 0.2 MHz. The difference between simulated and measured values is approximately 0.3 MHz. Other types and shapes of cavities have been constructed in a similar way, where differences were of the order of 1 MHz. The differences between simulated and calculated values can have several causes.

- Machining errors. Simulations show that varying R_3 over 10 μm, which is the machining accuracy, gives a variation of 0.3 MHz in resonant frequency.

- Cavity deformation during brazing. The cavity is made from two parts which are soldered together at high temperature (up to 700°C)in vacuum during 8 to 12 hours. Stress in the material, introduced during manufacturing, which relaxes during heating, may deform the cavity. To prevent this effect the cavity described in this thesis has been heated before the last, most accurate machining step. Probably as a result of this, the frequency shift during soldering was only 0.2 MHz.

- Volume change from antenna. To drive the field inside the cavity a small loop antenna (ca. 120 mm^3) is inserted into the cavity. The cavity volume will decrease as a result, but the frequency difference will be of the order of 10 kHz.

- CST Microwave Studio simulation error. Although simulations appear to converge quite well, to within 0.05 MHz of the final value, there might still be some remaining systematic

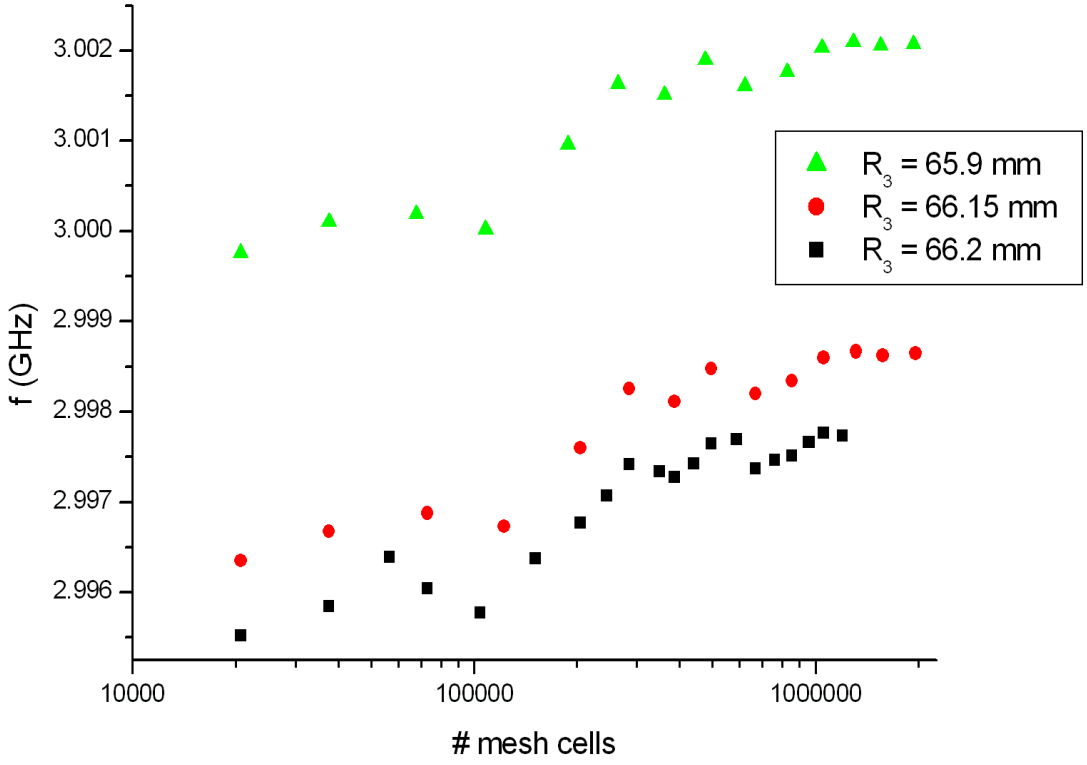

Figure 4.11: *The calculated resonant frequency of the cavity depends on the number of mesh cells used in the calculation. For a large number of cells, the frequency converges to a final value. The rightmost result required 5 hours calculation time.*

error. This could be investigated by comparing simulation results on a pillbox with analytical results.

- Finite conductivity. For frequency calculations in the simulations perfect conductivity of the cavity wall material is assumed. Since conductivity is in practice finite, boundary conditions differ resulting in a frequency shift. As was mentioned in section 2.3 this will be approximately -0.3 MHz.

It can be concluded that the simulations give a good frequency calculation, with an error of less than 10^{-4}, as long as the mesh is chosen dense enough.

4.6 Tuning

In the setup where we want to use the cavity as a streak camera, we will use it together with another cavity. It is important to note that in order to use two or more cavities simultaneously, they have to be excited at exactly the same frequency. This is necessary because for both cavities the phase of the RF field at the moment the bunch passes the center of the cavity is crucial for its proper operation. To ensure that the phases of both cavities are locked, the RF fields of both cavities are derived from a single source.

As equation (2.17) shows, the cavities have a certain bandwidth of frequencies they can absorb. Since the designed cavity has a quality factor of approximately 9000, its absorption spectrum has a FWHM of approximately 0.3 MHz. Thus if the resonant frequencies of the cavities differ 0.3 MHz and they are driven at their average frequency, they both absorb 50% of the signal they receive. That means that 50% of the total power is reflected to the amplifier. This requires a setup that can handle so much reflection and it limits the amount of power you can deliver to the cavities. Reducing reflection to 10% requires a frequency difference of 0.1 MHz or less between cavities. With the design method described before and a machining accuracy of 10 μm cavities can be designed with an accuracy of 0.3 MHz. Clearly, this is not sufficient for using two cavities simultaneously. For fine-tuning the resonant frequency a few options exist.

- Temperature change. By heating or cooling the copper of the cavity its volume and therefore its frequency will change, at approximately 0.05 MHz/K. Controlling the temperature of the cavity is troublesome work, however, which we hope to avoid.

- Tuning plunger. By introducing a metal plunger into the cavity, its frequency will increase because of the change in cavity volume. By choosing a proper width and length of the plunger, 1.5 MHz change is possible. Such a tuning stub has been implemented in the cavity, so its frequency can be varied over this range easily. This will be described in more detail in section 5.3. From simulations is concluded that the plunger does not significantly influence the fields near the z-axis.

4.7 Design results

In this section the simulated results of the designed cavity will be given. The main goal of the design was to reduce the power usage of the cavity. Figure 4.12 shows the magnetic

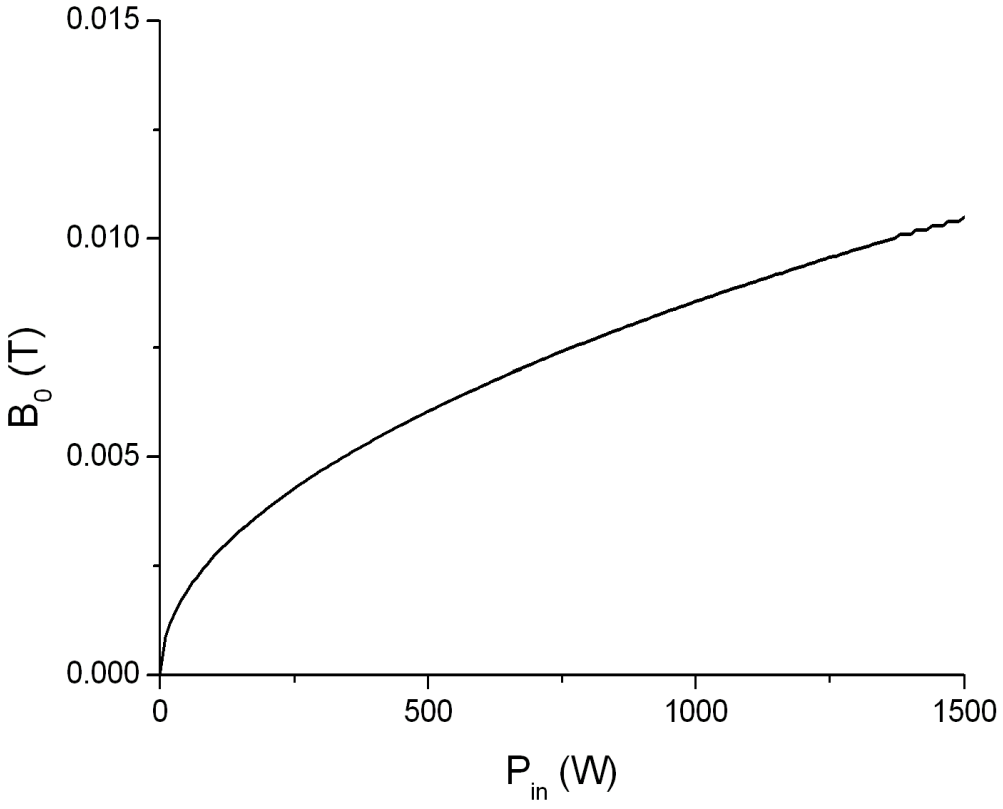

Figure 4.12: *Peak magnetic field on the central axis of the final cavity as a function of power input.*

field amplitude B_0 at the center of the cavity as a function of power input P_{in}. A magnetic field with $B_0 = 8$ mT requires 880 ± 25 W and furthermore $P_{in} \sim B_0^2$. The magnetic field amplitude on the z-axis is given in figure 4.13a, figure b gives the electric field. Off course the field strength depends on the amount of power input, but if $B_0 = 8$ mT then $E_{x,max} = 7.9 \cdot 10^4$ V/m. To compare the effect of the electric and magnetic field, the magnetic field has to be multiplied with the electron velocity at 100 keV, which gives $v_z B_0 = 1.31 \cdot 10^6$ V/m. Thus we can conclude that the effect of E_x on the streak length can be neglected; the effect of B_y is much larger. Table 4.1 summarizes the main properties of the cavity.

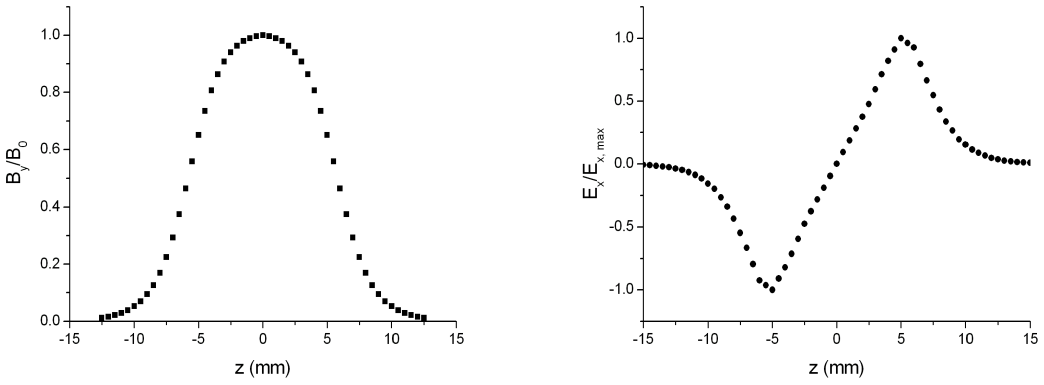

(a) (b)

Figure 4.13: *The magnetic (a) and electric (b) field profile along the z-axis.*

Table 4.1: *Cavity properties as derived from simulation, for* $B_0 = 8\ mT$.

Parameter	value
$2\pi\omega$	2997.75 ± 0.05 MHz
Q	11630 ± 20
P_{in}	860 ± 20 W
$E_{x,max}$	$7.9 \cdot 10^4$ V/m

Chapter 5

Cavity characterization

After the more efficient cavity shape had been designed as described in the previous chapter, a prototype was constructed. With this prototype the simulations could be validated and the construction method could be tested before the final cavity was constructed. The prototype was made for operation at normal air pressure, so without vacuum seals or flanges. Furthermore a hole was made in the side of the cavity, after the first measurements were finished, to test the tuning of the cavity by inserting a tuning plunger into it. The prototype was made from aluminium with a machining accuracy of 10 μm.

With the measurement results on the prototype, the cavity dimensions for the final design were slightly altered to obtain the correct resonant frequency. Furthermore the optimal tuning plunger size was implemented. The final cavity has been constructed from copper with vacuum seals to enable operation at low pressure. Before any measurements could be performed, an antenna had to be inserted into the cavity. The antenna is a small loop wire, inserted into the cavity as shown in figure 5.1, through a hole that enables rotation of the antenna. A radio frequency current through the wire will create a varying magnetic field through the loop antenna. This will create the desired TM_{110} field mode in the cavity. By rotating the antenna, the magnetic flux component parallel to the TM_{110} field can be changed. This way the absorption of the cavity can be optimized. Several measurements have been performed, both on the aluminium prototype cavity and the final copper cavity. First the absorption by the cavity of an RF signal as a function of its frequency will be described in section 5.1. From this measurement the resonant frequency of the cavity can be determined. Next, the fields on the z-axis of the cavity have been measured, as will be described in section 5.2. Then, in section 5.3 the tuning of the cavity to the correct frequency will be considered and finally its behavior when used at maximal desired power is described in section 5.4.

5.1 Absorption

To measure the absorption of RF power by the cavity, we have used a network analyzer. This sends a low-power RF signal into the cavity through a coaxial cable with a loop antenna and measures the amplitude and phase of the reflected signal. The network analyzer sweeps the signal frequency through a given range and displays a plot of the amplitude or phase of the reflected signal as a function of frequency. Measuring the absorption with the network analyser gives the result shown in figure 5.2. The measurement is fitted with a Lorentzian.

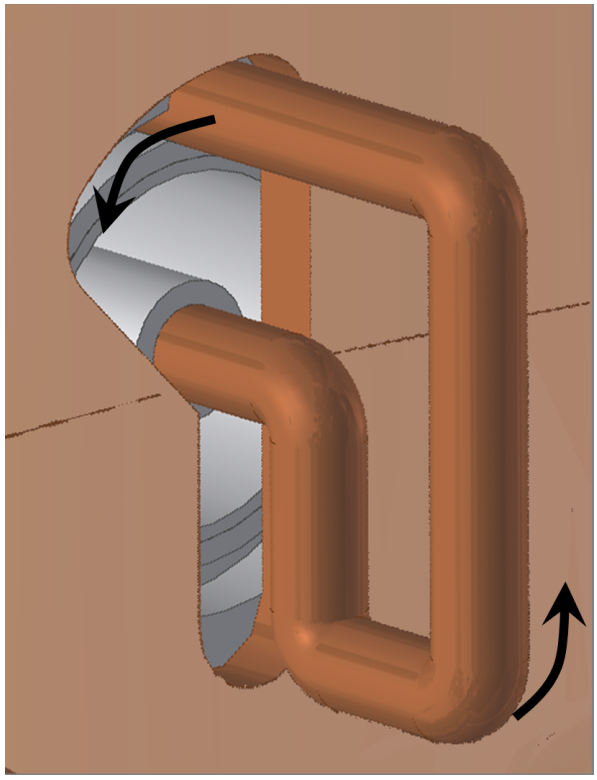

Figure 5.1: *Loop antenna, inserted into the cavity through a small hole in the wall. The antenna transfers RF power from the coaxial transmission line to the cavity.*

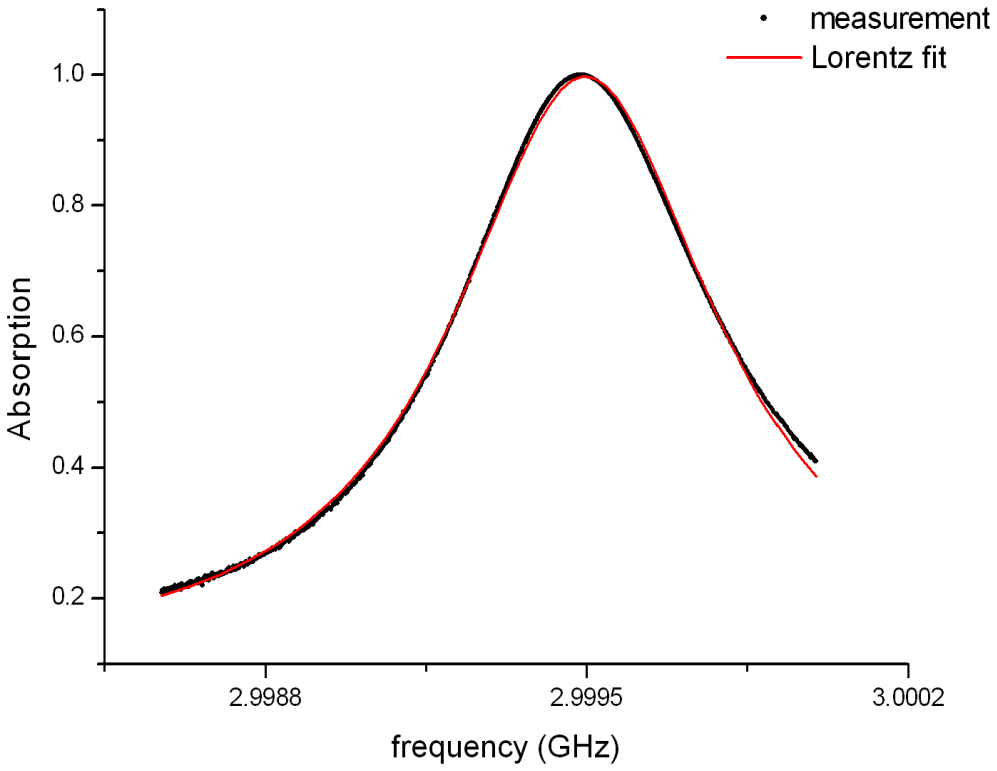

Figure 5.2: *RF signal absorption by the copper cavity. The measurement result is fitted with a Lorentzian as described in section 2.3*

Using equation (2.17) we can then find the resonant frequency of the cavity and its quality factor Q. The measurement on the copper cavity of figure 5.2 gives a resonant frequency of 2.99950 GHz and $Q_L = 4.3 \cdot 10^3$.

This measured Q_L is in fact the quality factor of the entire setup of cavity and power supply, which in this case is the network analyser. It is called the loaded Q_L and is approximately half the unloaded Q_0 of the cavity itself. So the unloaded Q_0 of the cavity is $8.6 \cdot 10^3$. The simulations of chapter 4 gave $Q_0 = 11630 \pm 20$.

The resonant frequency is usually just read from the network analyser as the point with maximum absorption. This gives a difference of only 0.01 MHz from fitting the entire curve.

5.2 Field profile

In order to verify that the field in the cavity is indeed as the simulations of section 4.7 suggest, the field strength on the z-axis has been measured. This has been done by placing a small object on various positions along the axis and measuring the resulting shift in resonant frequency ω_0 of the cavity. This frequency shift is caused by the change in volume of the cavity and is given by [11]

$$\frac{\Delta\omega}{\omega_0} = -\frac{3\epsilon_0 \Delta V}{4W}\left(\frac{\epsilon_r - 1}{\epsilon_r + 2}E^2 + \frac{\mu_r - 1}{\mu_r + 2}B^2c^2\right) \tag{5.1}$$

Here W is the total stored energy in the cavity, ΔV is the volume of the small object introduced into the cavity, its relative dielectric constant is ϵ_r and its relative magnetic permeability is μ_r. E and B are the unperturbed electric and magnetic fields strength at the position of the introduced object.

From simulations of section 4.7 we know that Bc is at least 10 times E on the z-axis, so measuring the magnetic field profile is relatively easy. For this purpose we glued a small piece of iron to a 0.05 mm diameter fishing line, to move it through the cavity. The line is suspended from an electric micrometer to measure the displacement of the iron piece. Iron has a large μ_r as well as ϵ_r, so that we can write

$$\Delta\omega \sim E^2 + B^2c^2 \sim B^2 \tag{5.2}$$

and measuring the frequency shift allows us to calculate the on-axis magnetic field profile. The result is shown in figure 5.3 as well as the simulation result. The difference between these two is less than 2 % except at the ends, where the measurement is less accurate because of the small fields there.

Measuring E on the axis with this method was unsuccessful. The maximum frequency shift when measuring B with the piece of iron was 400 kHz. For E this will not be more than 1 kHz if you use a material with high ϵ_r and μ_r very close to unity. If μ_r is more than 1.01, B already has a larger effect on frequency shift than E. Besides, temperature variations disturb the measurements. The resonant frequency depends linearly on cavity diameter, so using the thermal expansion coefficient of copper $k_T = 17 \cdot 10^{-6}\mathrm{K}^{-1}$ we can calculate that 1 K temperature change causes a frequency change of 50 kHz.

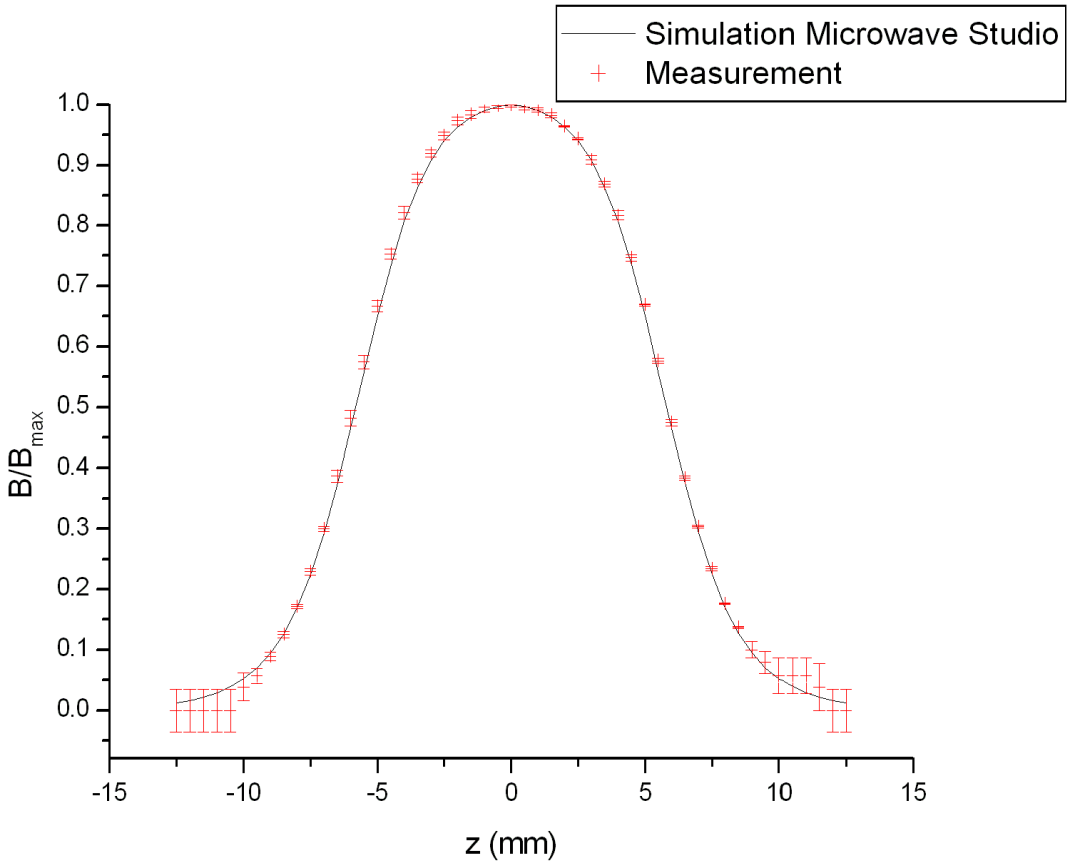

Figure 5.3: *The measured and simulated magnetic field amplitude on the z-axis. With the axial fields known, the fields in the entire cavity are known.*

5.3 Cavity tuning

The cavity described in this thesis will be used in a streak camera setup. Therefore we shall refer to it as streak cavity. Eventually, it will be used together with another cavity, a focusing cavity [7]. The cavities were designed and machined nearly simultaneously. First a prototype of both cavities was constructed, after which both designs were adjusted and the final cavities were constructed.

When operating the cavities together we want to drive them at the same frequency. To have enough absorption in the cavity they have to be tuned to within 0.1 to 0.3 MHz of each other, depending on absorption requirements. Therefore the streak cavity is fitted with a tuning plunger which can increase its resonant frequency. Thus the streak cavity has to be designed at a frequency somewhat below the design frequency of the focus cavity.

When the aluminium prototype cavities were constructed it was measured that the resonant frequency of the focus cavity was 0.2 ± 0.1 MHz lower than the simulated resonant frequency. For the streak cavity the resonant frequency was 0.3 ± 0.2 MHz higher than simulated. Now it was assumed that this difference was at least partly due to the used simulation program, since a different program has been used for each cavity. Therefore the difference between measurement and simulation is taken as a correction on the simulated frequency for the final cavity. So if simulations give a resonant frequency of 2997.75 ± 0.05 MHz for the streak cavity, we expect that after construction we will measure 2998.1 ± 0.3 MHz. The large error results mainly from the measurement. Although the frequency is measured quite accurately, it varies between measurements, most likely due to temperature variation. This gives a range of expected frequencies. Now we want to make sure that the range of the streak cavity is below the range of the focus cavity. Then using the tuning plunger the frequencies can be made equal. This requires a plunger which can increase the frequency at least 0.8 MHz. Different plungers have been tested on the aluminium prototype cavity. In figure 5.4 the frequency shift has been plotted against the length L of the plunger inside the cavity. A negative length means the stub is retracted into the cavity wall, resulting in a hole with depth $-L$. Also in this figure are some simulation results from CST Microwave Studio [1] where plungers were simulated in a broader range of length and radius.

There can be some offset in the measured data, because it is difficult to say when exactly the plunger has no length in the cavity. The error will be 1 mm at most. Otherwise, the measurements and simulations are in good agreement. After this test we decided to use a plunger of 14 mm diameter and up to 10 mm length, which allows tuning over a comfortable 1.5 MHz. Figure 5.5 shows the simulated frequencies for the final cavities as well as the expected frequencies. Also shown in this figure are the actual frequencies of the cavities as measured after construction. Before brazing, these indeed lie in the expected range. However, the cavities are constructed in several parts which have to be brazed together at high temperatures. When this was done with the focus cavity its resonant frequency appeared to have increased 0.9 MHz probably as a result of deformation due to annealing during brazing. To prevent or at least decrease this change for the streak cavity, it was heated and thus annealed before the last, very accurate machining step. This way stresses in the material could relax without changing the resonant frequency. Indeed, the resonant frequency of the streak cavity changed very little during brazing. Screwing the tuning plunger as far as construction allowed into the cavity turned out to be just enough to get the streak cavity to the same frequency as the focus cavity. Figure 5.6 shows the frequency shift as a function of the length L of the plunger inside

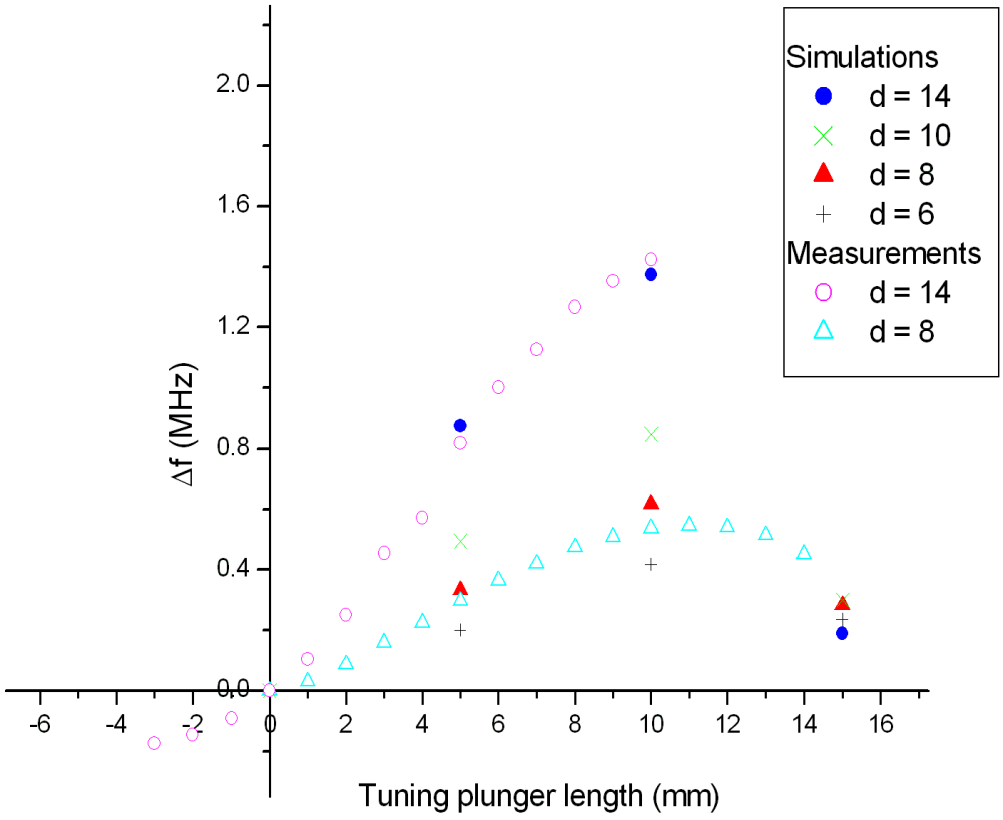

Figure 5.4: *Cavity tuning with a tuning plunger. The resonant frequency can be increased, to a maximum, or slightly decreased. A negative length means the plunger is retracted into the cavity wall, creating a hole. Measurements have been performed on the aluminium prototype.*

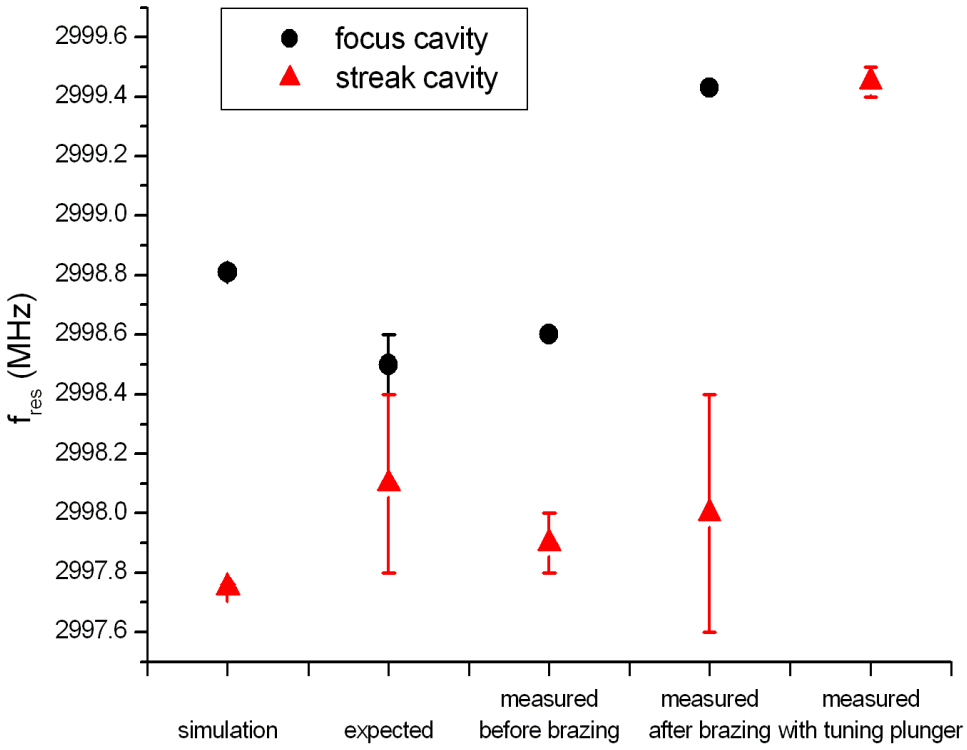

Figure 5.5: *Resonant frequency of focus cavity and streak cavity for different steps in design and production process. Starting on the left are shown the frequencies from simulations and then, derived from the simulations, the frequency range in which the frequency is expected to lie after construction. When this frequency was measured after construction, before brazing, it was found to lie in this range indeed. The frequency changed substantially during brazing, in particular for the focus cavity, but the frequencies can still be made equal with the tuning plunger.*

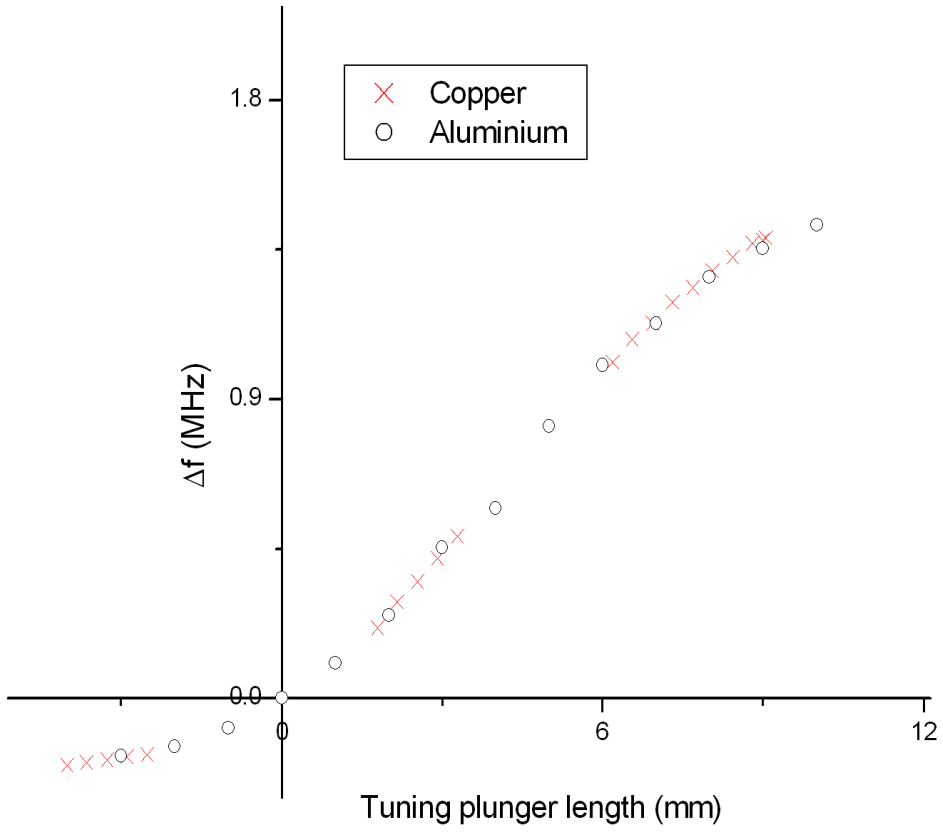

Figure 5.6: *Resonant frequency for different plunger lengths in the aluminium prototype and final copper cavity.*

the cavity. Because of some solder leaking into the screw thread during brazing the plunger can only be moved over a short range. Therefore three plungers of different lengths were used. Again it is hard to determine the point where $L = 0$, so there is some offset remaining on both axes. In the figure the offset is chosen to best fit the measurement on the aluminium cavity. It is possible to use a longer plunger to increase the frequency further if required. However, the frequency will probably increase only some 0.2 MHz before decreasing as in figure 5.4.

5.4 High-field operation

When operating the cavity for electron manipulation the setup as shown in figure 5.7 is used. An RF signal is generated by a Rohde&Schwarz SM300 signal generator. It can be tuned from 9 kHz to 3 GHz and delivers 10 mW of output power. This signal is amplified using a 3 GHz 1 kW solid state high power amplifier model AM 84-3S2-50-60R from Microwave Amps Ltd. It can be operated at a frequency of 2.998 ± 0.02 GHz, delivering up to 850 W of output power to the cavity through a coaxial cable with a loop antenna. The amplifier has to be operated in pulsed mode, so it has to be enabled with block pulses of 10 μs duration at a frequency of 1 kHz. With this setup supplying power to the cavity we can measure the absorption in the cavity by placing a directional coupler between the amplifier and the cavity. Then the forward and reflected signal can be measured with an oscilloscope. The 3 GHz signal is too fast to be sampled by the oscilloscope, but it does show the envelope of the RF pulse.

When the reflected power is minimal the applied frequency is the resonant frequency of the cavity. Thus, when the frequency of the applied signal is varied the amount of reflected power changes. By constantly monitoring the applied and reflected power it is found that the resonant frequency gradually decreases (presumably by heating of the cavity) while the setup is running. The resonant frequency as a function of the duration of the measurement is shown in figure 5.8 The frequency decrease is most likely a result of the increasing cavity size which is due to heating by energy dissipation in the cavity wall. Since nearly all the RF energy is absorbed by the cavity a time-averaged 9 W is dissipated in the cavity walls. The frequency decreases approximately 0.3 MHz, which corresponds with a temperature increase of 6 K.

A similar thing will happen with the focus cavity. In fact, because it is smaller it heats up more and faster than the streak cavity, so its frequency decreases more. With a power input of 850 W it decreases 0.8 MHz in resonant frequency. It does not need that much power for normal operation, though. The plan is to operate both cavities with the same power supply, so the power will be split between them, probably using 200 W for focusing and 600 W for the streak cavity. This will result in a frequency decrease of around 0.2 MHz for both cavities, although the exact value will have to be measured. If they should end up at different frequencies the tuning plunger length has to be adjusted. The current plunger probably has enough range to allow this. The design of the streak cavity is such that to move the tuning plunger, the vacuum has to be broken. This is somewhat inconvenient, but once the frequency is tuned correctly, it should not require any further tuning.

To calculate the field strength B_0 in the center of the cavity, we use equations (2.10) and (4.3) with the simulation result that for $U = 1$ J, B_0=0.3467 T. This gives

$$B_0 = 0.3467\sqrt{\frac{P_{in}Q}{\omega_0}}(T) \tag{5.3}$$

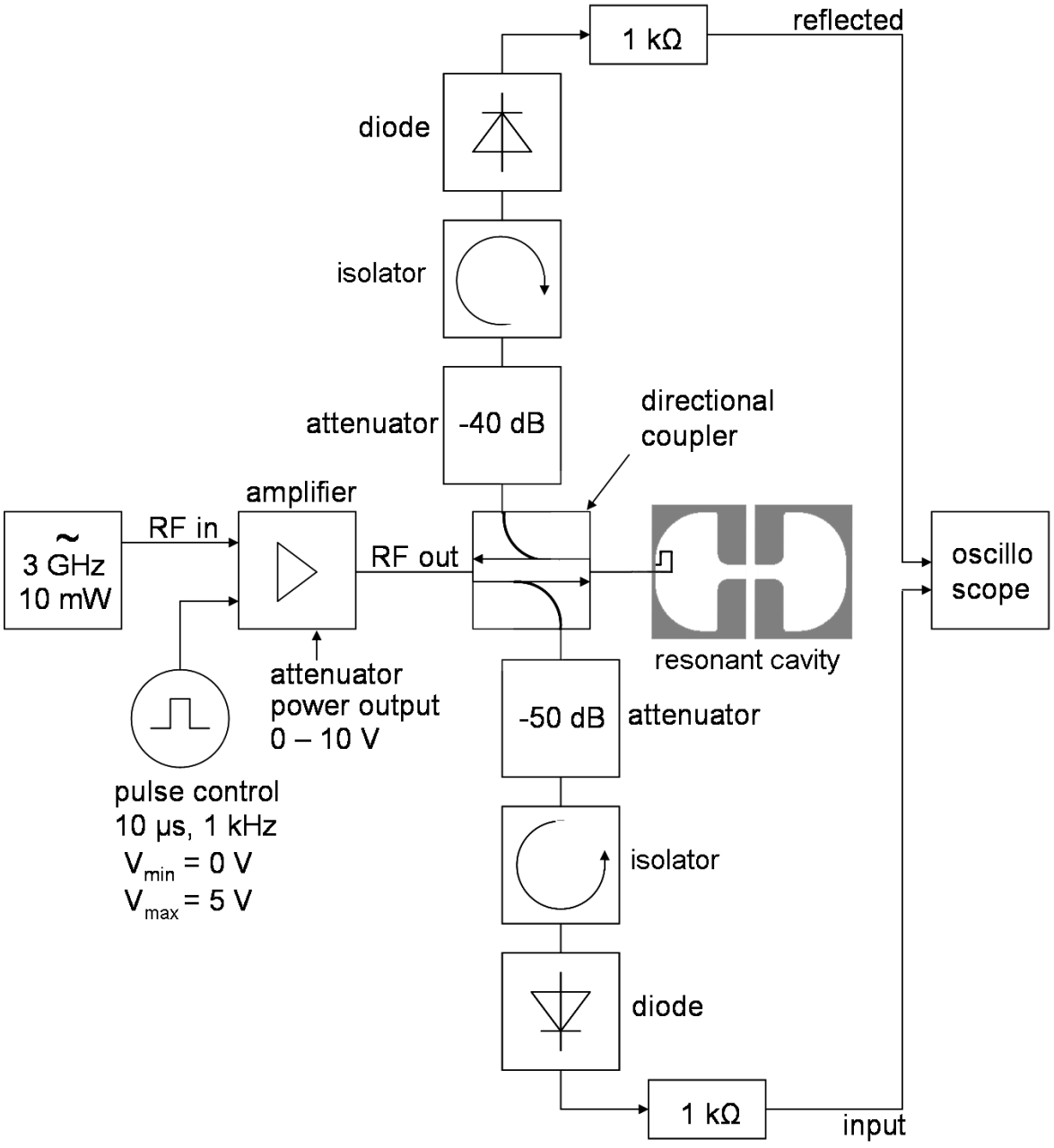

Figure 5.7: *A schematic of the 1 kW setup as used for driving the cavity with up to 1 kW RF power. The power applied to and reflected from the cavity are measured with an oscilloscope.*

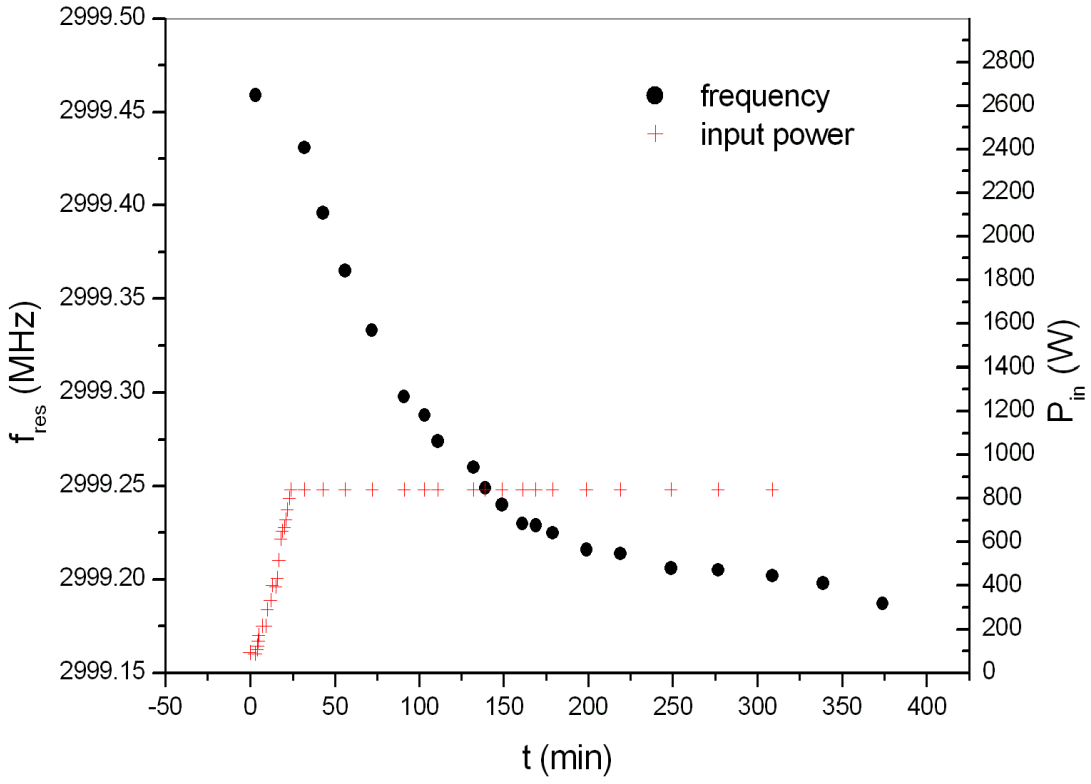

Figure 5.8: *As power is applied to the cavity it heats up, expands and its frequency decreases.*

If we substitute measured values into this equation, $P_{in} = 840 \pm 10$ W and $Q = 8800 \pm 400$, we get $B_0 = (6.8 \pm 0.3)10^{-3}$ T.

5.5 Discussion and conclusion

As the measurement results in this chapter show, the process of designing a cavity using CST Microwave Studio and machining it with an accuracy of at least 10μm is very accurate.

- The resonant frequency of 2998.0 ± 0.4 MHz after construction differs only -0.15 to $+0.65$ MHz from simulations, no more then 0.02%.
- The magnetic field profile on the cavity axis is equal to the simulation, within the measurement accuracy.

Having validated simulation results we can reasonably assume that the entire field description from simulations is correct, in particular the on-axis electric field, which is virtually impossible to measure. Because we need to set the resonant frequency even more accurately then can be realized with this design method, a plunger is inserted into the cavity for additional tuning, which allows tuning up to $+1.5$ MHz with an accuracy of 0.01 MHz. This plunger can also be used to correct for frequency variation caused by heating during operation.

Chapter 6

Conclusion

In this thesis three applications of RF cavities for electron microscopy have been described. Application as a streak camera has been the main part. Further, the application as an electron beam chopper and electron lens have been considered.

6.1 Streak camera

The calculations and simulations described in this thesis show that measuring bunch durations from 10 fs to 10 ps should be possible. Several deviations from the ideal streak have been analyzed, showing that only two factors cause some disturbance when measuring streak length; transverse bunch dimension and energy spread in the bunch. Energy spread causes an error of approximately 1% in the streak length measurement, transverse bunch size causes lengthening of the bunch in the cavity. A transverse size of 1 mm causes approximately 100 fs lengthening. When measuring much larger bunch durations this is not a big problem, but for short bunch duration an aperture is required to reduce the transverse size and thereby the lengthening.

The energy-efficient cavity has a required input power of 0.9 kW for a field amplitude $B_0 = 8$ mT. As a comparison, the pillbox cavity as used for calculations requires 3.1 kW input power for $B_0 = 8$ mT. However, to produce similar streak lengths the pillbox cavity can be operated at $B_0 = 5$ mT, which requires only 1.3 kW. The error due to energy spread for the pillbox cavity is approximately half that of the energy-efficient cavity; bunch lengthening due to the transverse size of the bunch is approximately twice as much for the pillbox cavity as it is for the energy-efficient cavity. Since lengthening seems to be the limiting factor when measuring bunch duration, the energy-efficient cavity will have a better resolution than the pillbox cavity.

Characterization measurements show that the resonant frequency of the cavity differs no more than 0.02% from the design and the on-axis magnetic field profile is in good agreement with the design. With the tuning plunger the frequency can be adjusted to within 0.01 MHz from the desired frequency. The cavity has been driven with 1 kW RF power without breakdown, so it is ready for implementation in the streak camera setup.

6.2 Electron beam chopper

If the streak cavity is used for electron beam chopping the capturing screen has to be replaced with an aperture. The calculations will be basically the same, so when using the energy-efficient cavity with 0.9 kW input power the beam can be chopped into 1 ps bunched with a 150 μm aperture at $Z = 100$ mm from the cavity.

Many aspects require further investigation however, such as the influence of disturbance of the beam by the cavity. The calculations on the streak cavity will provide a good basis for this investigation. Finally, a new cavity design may deliver a cavity which better satisfies the need for low disturbances in an electron microscope.

Bibliography

[1] Cst microwave studio 2006. http://www.cst.com.

[2] General particle tracer. http://www.pulsar.nl/gpt.

[3] Superfish. http://laacg1.lanl.gov.

[4] M.R. Armstrong. Practical considerations for high spatial and temporal resolution dynamic transmission electron microscopy. *Ultramicroscopy*, 2006.

[5] O. Bostanjoglo and T. Rosin. Ultrasonically induced magnetic reversals observed by stroboscopic electron microscopy. *Optica acta: international journal of theoretical and applied optics*, 24(6):657–664, June 1977.

[6] FEI Company. Titan 80-300. http://www.feicompany.com/Products/Families/Titan/, 2006.

[7] E.F. de Jong. Rf compression cavity for single-shot ultra-fast electron diffraction. Master's thesis, Eindhoven University of Technology, June 2007.

[8] J.D. Jackson. *Classical Electrodynamics*. John Wiley & Sons, Inc., 3rd edition, 1999.

[9] F.B. Kiewiet. *Generation of ultra-short, high-brightness relativistic electron bunches*. PhD thesis, Eindhoven University of Technology, June 2003.

[10] V.A. Lobastov, R. Srinivasan, and A.H. Zewail. Four-dimensional ultrafast electron microscopy. *Proceedings of the National Academy of Sciences*, 102(20):7069–7073, May 2005.

[11] L. Maier and J. Slater. Field strength measurements in resonant cavities. *J.Appl.Phys.*, 23(1):68–77, 1952.

[12] O. Scherzer. Sphärische und chromatische korrektur von elektronenlinsen. *Optik*, 2:114–132, 1947.

Appendix A

Cavity field derivation

In this chapter the electromagnetic field distribution in a cylinder-shaped or 'pillbox'-shaped resonant cavity with radius R and thickness d will be derived. In the cavity there exist no charges or currents and the walls will be assumed to be perfectly conducting. The electric (E) and magnetic (B) fields always satisfy Maxwell's equations, which are as follows, for the case of no charges or current.

$$\vec{\nabla} \cdot \vec{E} = 0, \tag{A.1}$$

$$\vec{\nabla} \times \vec{E} = -\frac{\partial \vec{B}}{\partial t}, \tag{A.2}$$

$$\vec{\nabla} \cdot \vec{B} = 0, \tag{A.3}$$

$$\vec{\nabla} \times \vec{B} = \frac{1}{c^2}\frac{\partial \vec{E}}{\partial t} \tag{A.4}$$

For a perfectly conducting wall the boundary conditions for the fields are that E must be perpendicular to the wall and B must be parallel to the wall. The fields will be described in cylindrical coordinates (r, ϕ, z) and a sinusoidal time dependence is assumed.

$$\begin{aligned} \vec{E}(r,\phi,z,t) &= \vec{E}_0(r,\phi,z)\cos(\omega t) \\ &= [E_r(r,\phi,z)\vec{e}_r + E_\phi(r,\phi,z)\vec{e}_\phi + E_z(r,\phi,z)\vec{e}_z]\cos(\omega t) \end{aligned} \tag{A.5}$$

$$\begin{aligned} \vec{B}(r,\phi,z,t) &= \vec{B}_0(r,\phi,z)\sin(\omega t) \\ &= [B_r(r,\phi,z)\vec{e}_r + B_\phi(r,\phi,z)\vec{e}_\phi + B_z(r,\phi,z)\vec{e}_z]\sin(\omega t) \end{aligned} \tag{A.6}$$

To obtain an equation with only the electric field we take the rotation of equation (A.2).

$$\begin{aligned} \vec{\nabla} \times (\vec{\nabla} \times \vec{E}) &= \vec{\nabla}(\vec{\nabla} \cdot \vec{E}) - \vec{\nabla}^2\vec{E} = -\vec{\nabla}^2\vec{E} \\ &= -(\vec{\nabla} \times \frac{\partial \vec{B}}{\partial t}) = -\frac{\partial}{\partial t}(\vec{\nabla} \times \vec{B}) = -\frac{1}{c^2}\frac{\partial^2 \vec{E}}{\partial t^2} \end{aligned} \tag{A.7}$$

Thus

$$(\vec{\nabla}^2 + k^2)\vec{E}_0 = 0, \tag{A.8}$$

with

$$k^2 = \frac{\omega^2}{c^2}. \tag{A.9}$$

And similarly, by taking the rotation of a equation (A.4)

$$(\vec{\nabla}^2 + k^2)\vec{B}_0 = 0, \tag{A.10}$$

Equations (A.8) and (A.10) are called the wave equations.

It is important to note that $\vec{\nabla}^2$ operating on a vector is the vector Laplacian. In cylindrical coordinates this is

$$\vec{\nabla}^2\vec{A} = \begin{pmatrix} \left[\frac{\partial^2}{\partial r^2} + \frac{1}{r}\frac{\partial}{\partial r} + \frac{1}{r^2}\frac{\partial^2}{\partial \phi^2} + \frac{\partial^2}{\partial z^2} - \frac{1}{r^2}\right] A_r - \frac{2}{r^2}\frac{\partial}{\partial \phi}A_\phi \\ \left[\frac{\partial^2}{\partial r^2} + \frac{1}{r}\frac{\partial}{\partial r} + \frac{1}{r^2}\frac{\partial^2}{\partial \phi^2} + \frac{\partial^2}{\partial z^2} - \frac{1}{r^2}\right] A_\phi + \frac{2}{r^2}\frac{\partial}{\partial \phi}A_r \\ \left[\frac{\partial^2}{\partial r^2} + \frac{1}{r}\frac{\partial}{\partial r} + \frac{1}{r^2}\frac{\partial^2}{\partial \phi^2} + \frac{\partial^2}{\partial z^2}\right] A_z \end{pmatrix}$$

For a TM (Transverse Magnetic) field distribution the only field component in the longitudinal direction is the electric field E_z. It satisfies the wave equation, which yields for a sinusoidal dependence in ϕ- and z-direction

$$\left[\frac{\partial^2}{\partial r^2} + \frac{1}{r}\frac{\partial}{\partial r} - \frac{m^2}{r^2} - \left(\frac{l\pi}{d}\right)^2 + k^2\right] E_z(r)\cos(m\phi)\cos\left(\frac{l\pi z}{d}\right) = 0 \tag{A.11}$$

When we change variables to $\rho = k_c r$ with $k_c^2 = k^2 - \left(\frac{l\pi}{d}\right)^2$, the equation becomes Bessel's equation, so that $E_z(r)$ must be

$$E_z(r) = E_0 J_m(k_c r) \tag{A.12}$$

A field distribution can be TM, as described above, or TE (Transverse Electric). For a TE field distribution the only field component in the longitudinal direction is the magnetic field B_z, but this mode will not be considered here.

There are many different types or modes of TM field distribution. These are indicated with an index: TM_{mnl}. Here m is the number of periods in the azimuthal or ϕ-direction and l the number of half periods in the longitudinal or z-direction. Indexes m and l have already been used in the description above. The index n relates the cavity radius to k_c, because on the cylinder wall, so for $r = R$, the longitudinal electric field has to be zero and thus $k_c R$ has to be equal to x_{mn}, the n-th root of the m-th order Bessel function.

From the longitudinal field distribution the other field components' distribution can be derived using equations (A.2) and (A.4). For example, using the ϕ-component of (A.2) and the r-component of (A.4) we get two equations with E_z, E_r and B_ϕ. This enables us to eliminate one of the transverse fields e.g. B_ϕ and express E_r as a function of E_z. This can be done for all transverse components.

Thus, in general the TM fields are given by

$$E_z = E_0 J_m(k_c r)\cos(m\phi)\cos\left(\frac{l\pi z}{d}\right) \tag{A.13}$$

$$E_r = -\frac{l\pi}{k_c^2 d}E_0\frac{\partial}{\partial r}J_m(k_c r)\cos(m\phi)\sin\left(\frac{l\pi z}{d}\right) \tag{A.14}$$

$$E_\phi = \frac{ml\pi}{k_c^2 d}E_0\frac{1}{r}J_m(k_c r)\sin(m\phi)\sin\left(\frac{l\pi z}{d}\right) \tag{A.15}$$

$$B_r = \frac{k^2 m}{k_c^2\omega}E_0\frac{1}{r}J_m(k_c r)\sin(m\phi)\cos\left(\frac{l\pi z}{d}\right) \tag{A.16}$$

$$B_\phi = \frac{k^2}{k_c^2\omega}E_0\frac{\partial}{\partial r}J_m(k_c r)\cos(m\phi)\cos\left(\frac{l\pi z}{d}\right) \tag{A.17}$$

The frequency of the field can be calculated using

$$\omega^2 = c^2\left[\left(\frac{x_{mn}}{R}\right)^2 + \left(\frac{l\pi}{d}\right)^2\right]. \tag{A.18}$$

Appendix B

Field expansion

To derive the fields in a resonant cavity of any given shape, the fields can be written as a series expansion in r, the distance from the axis. When substituting this in Maxwell's equations, it is found that the fields are fully described if the fields on the z-axis are known. This will be done first for the TM_{010} mode and next for the TM_{110} mode. Although it is disputable whether the modes can still be called 'Transverse Magnetic' with their respective indices, this still is a useful way of discerning different modes.

B.1 TM_{010} expansion

To describe the field for a generalized TM_{010} mode the following assumptions are made:

$$\frac{\partial \vec{E}}{\partial \phi} = 0 \tag{B.1}$$

$$E_\phi = 0 \tag{B.2}$$

$$\vec{E} = E_0 \cos(\omega t) \tag{B.3}$$

This leads to

$$E_z = \sum_{n=0}^{\infty} a_n(z) r^n \cos(\omega t) \tag{B.4}$$

$$E_r = \sum_{n=0}^{\infty} b_n(z) r^n \cos(\omega t) \tag{B.5}$$

$$B_\phi = \sum_{n=0}^{\infty} c_n(z) r^n \sin(\omega t) \tag{B.6}$$

The components B_r and B_z are zero, as follows from equation (A.2), the rotation of $\vec{E}$. Substituting the above expansions in equation (A.1), the divergence of $\vec{E}$, we can write b_n as a function of a_n. With the wave equation (A.8) we can write any a_n as a function of a_0 and

with the rotation of $\vec{B}$, equation (A.4), c_n can be related to a_n. The resulting coefficients are

$$b_{n+1}(n+2) = -a_n' \tag{B.7}$$
$$a_{n+2}(n+2)^2 = -a_n'' - k^2 a_n \tag{B.8}$$
$$c_{n+1} = \frac{-1}{n+2}\frac{\omega}{c^2}a_n \tag{B.9}$$

Where ' means $\frac{\partial}{\partial z}$. Since the wave equation also shows that $a_1 = 0$ we can write the fields as

$$E_z = \sum_{n=0}^{\infty} a_{2n} r^{2n} \cos(\omega t) \tag{B.10}$$
$$E_r = \sum_{n=0}^{\infty} -\frac{a_{2n}'}{2n+2} r^{2n+1} \cos(\omega t) \tag{B.11}$$
$$B_\phi = \sum_{n=0}^{\infty} -\frac{\omega a_{2n}}{c^2(2n+2)} r^{2n+1} \sin(\omega t) \tag{B.12}$$

From this description it is clear that the only field on the z-axis ($r = 0$) is

$$E_z(0) = a_0(z) cos(\omega t) \tag{B.13}$$

If this field is known from measurement of simulations, the field at any position in the cavity is known.

B.2 TM_{110} expansion

The most general expansion for a field distribution is

$$A(r,\phi,z) = \sum_{m=0}^{\infty}\sum_{n=0}^{\infty} \alpha_{mn}(z) r^n \cos(m\phi) + \beta_{mn}(z) r^n \sin(m\phi) \tag{B.14}$$

where A is some field component. From the calculation of section 2.2 it can be deduced that the TM_{110} mode can be described with only the $m = 1$ terms. We will choose E_z to behave as $\cos(\phi)$, then the axial magnetic field will be in the y-direction as we assumed in this work. With already a glance at Maxwell's equations to see which component behaves as $\sin(\phi)$ and

which as $\cos(\phi)$ we define the field components as

$$E_r = \sum_{n=0}^{\infty} a_n(z) r^n \cos(\phi) \tag{B.15}$$

$$E_\phi = \sum_{n=0}^{\infty} b_n(z) r^n \sin(\phi) \tag{B.16}$$

$$E_z = \sum_{n=0}^{\infty} c_n(z) r^n \cos(\phi) \tag{B.17}$$

$$B_r = \sum_{n=0}^{\infty} d_n(z) r^n \sin(\phi) \tag{B.18}$$

$$B_\phi = \sum_{n=0}^{\infty} f_n(z) r^n \cos(\phi) \tag{B.19}$$

$$B_z = \sum_{n=0}^{\infty} g_n(z) r^n \sin(\phi) \tag{B.20}$$

When substituting this series expansions into Maxwell's equations we find that

$$c_0 = g_0 = 0 \tag{B.21}$$

$$a_0 = -b_0 \tag{B.22}$$

$$d_0 = f_0 \tag{B.23}$$

and writing all coefficients as a function of a_n and f_n

$$a_{2n+2}\left[(2n+3)^2 - 1\right] = -k^2 a_{2n} - \frac{2n+3}{2n+1} a''_{2n} - \frac{2\omega}{2n+1} f'_{2n} \tag{B.24}$$

$$b_{2n+2}(2n+3) = k^2 a_{2n} - a_{2n+2} - \omega f'_{2n} \tag{B.25}$$

$$c_{2n+1}(2n+1) = a'_{2n} + \omega f_{2n} \tag{B.26}$$

$$d_{2n+2}(2n+3) = f_{2n+2} - f''_{2n} + \frac{\omega}{c^2} a'_{2n} \tag{B.27}$$

$$f_{2n+2}\left[(2n+3)^2 - 1\right] = -\frac{2n+3}{2n+1} k^2 f_{2n} - f''_{2n} - \frac{\omega}{c^2} \frac{2}{2n+1} a'_{2n} \tag{B.28}$$

$$g_{2n+1} = -\frac{\omega}{c^2} a_{2n} + f'_{2n} \tag{B.29}$$

On the z-axis, for $r = 0$ we can write the fields as

$$E_r = a_0 \cos(\phi) \qquad B_r = f_0 \sin(\phi) \tag{B.30}$$

$$E_\phi = -a_0 \sin(\phi) \qquad B_\phi = f_0 \cos(\phi) \tag{B.31}$$

When we calculate from these the field components in cartesian coordinates we find

$$E_x = a_0(z) \qquad B_x = 0 \tag{B.32}$$

$$E_y = 0 \qquad B_y = f_0(z) \tag{B.33}$$

From this we can conclude that if the electric and magnetic fields on the axis are known, the fields in the entire cavity can be described.

Appendix C

Relativistic streak camera calculations

In the calculations of chapter 3, relativistic effects were neglected. Since this can give an error of approximately 20%, the main calculation results of that chapter are given here including relativistic effects. Starting point is the equation for the momentum p of the electrons.

$$p = \gamma m v \tag{C.1}$$

Where $\gamma = \left[1 - \frac{v^2}{c^2}\right]^{-1/2}$, m the electron mass, v the electron velocity and c the speed of light. The magnetic field working on the electrons is still

$$B_y = B_0 \sin(\omega t + \phi_0) \tag{C.2}$$

The resulting momentum p_x is still the integral of the field, but p_z is now according equation (C.1), so that θ becomes

$$\theta = \frac{p_x}{p_z} = \frac{2eB_0}{\gamma m \omega} \sin(\omega t_c + \phi_0) \sin\left(\frac{1}{2}\omega t_{tr}\right) \tag{C.3}$$

The changed factor in this equation stays in all subsequent equations, so $\Delta\theta$ for a bunch with duration t_b becomes

$$\Delta\theta = \frac{4eB_0}{\gamma m \omega} \sin\left(\omega \frac{1}{2} t_b\right) \cos(\omega t_0 + \phi_0) \sin\left(\frac{1}{2}\omega t_{tr}\right) \tag{C.4}$$

When considering energy spread in section 3.2 it was assumed that

$$\frac{v_{z_0}}{v_z} = \frac{p_{z_0}}{p_z} \tag{C.5}$$

Relativistically, however

$$\frac{p_{z_0}}{p_z} = \frac{\gamma_0 m v_{z_0}}{\gamma m v_z} \approx 1 - \gamma_0^2 \frac{\delta v}{v_{z_0}} \tag{C.6}$$

Where $\gamma_0 = \left[1 - \frac{v_{z_0}^2}{c^2}\right]^{-1/2}$ and $\delta v = v_z - v_{z_0}$, the variation in velocity,is assumed much smaller than v_{z_0} so that only linear terms in δv have to be considered. Consequently, the angle of

deflection becomes

$$\theta \approx \frac{2eB_0}{\gamma m\omega}\sin(\omega t_c+\phi_0)\left[1-\frac{1}{2}\left(\frac{\pi}{2}-\frac{1}{2}\omega t_{tr_0}\right)^2 - \left(\frac{\pi}{2}-\frac{1}{2}\omega t_{tr_0}\right)\frac{1}{2}\omega t_{tr_0}\frac{1}{\gamma_0^2}\frac{\delta p}{p_{z_0}}-\frac{1}{8}\left(\omega t_{tr_0}\frac{1}{\gamma_0^2}\frac{\delta p}{p_{z_0}}\right)^2\right] \tag{C.7}$$

The longitudinal electric field E_z changes electron momentum as described in section 3.3.2

$$p_z(x,t) = p_{z_0} - eB_0x\left[\sin(\omega t)+1\right] \tag{C.8}$$

Now we use

$$p = \gamma m v_z \approx \gamma_0 m v_z \tag{C.9}$$

Since

$$\gamma = \gamma_0\left[1+\frac{\delta v}{v_{z_0}}\left(\gamma_0^2-1\right)\right] \tag{C.10}$$

Then we integrate v_z to find

$$z(x,t) = v_{z_0}\left(t+\frac{\pi}{2\omega}\right)-\frac{eB_0x}{\gamma_0 m}\left(t+\frac{\pi}{2\omega}\right)+\frac{eB_0x}{\gamma_0 m\omega}\cos(\omega t) \tag{C.11}$$

Electrons with $x=0$ still arrive at the cavity center $t=0$. Then we find that t_E is, just like equation (3.14)

$$t_E = \frac{(\frac{\pi}{2}-1)}{\omega}\left[\frac{p_{z_0}}{eB_0x}-1\right]^{-1} \tag{C.12}$$

Special thanks to: Jeroen, Nick, Raymond, Tijs, Wendy, Wouter, Zineb & Willemijn.